THE INFLUENCE OF TUTT CELLS ON

TROPICAL CYCLONE MOTION IN THE NORTHWEST PACIFIC OCEAN

A DISSERTATION SUBMITTED TO THE GRADUATE DIVISION OF THE
UNIVERSITY OF HAWAI'I IN PARTIAL FULFILLMENT OF THE
REQUIREMENTS FOR THE DEGREE OF

DOCTOR OF PHILOSOPHY

IN

METEOROLOGY

AUGUST 2008

By

Jason E. Patla

Dissertation Committee:

Duane Stevens, Chairperson
Gary Barnes
Pao-Shin Chu
Yi-Leng Chen
Niklas Schneider

DTIC DEFENSE TECHNICAL INFORMATION CENTER

Information for the Defense Community

DTIC® has determined on `09` `09` `2008` that this Technical Document has the Distribution Statement checked below. The current distribution for this document can be found in the DTIC® Technical Report Database.

☑ **DISTRIBUTION STATEMENT A.** Approved for public release; distribution is unlimited.

☐ © **COPYRIGHTED.** U.S. Government or Federal Rights License. All other rights and uses except those permitted by copyright law are reserved by the copyright owner.

☐ **DISTRIBUTION STATEMENT B.** Distribution authorized to U.S. Government agencies only. Other requests for this document shall be referred to controlling office.

☐ **DISTRIBUTION STATEMENT C.** Distribution authorized to U.S. Government Agencies and their contractors. Other requests for this document shall be referred to controlling office.

☐ **DISTRIBUTION STATEMENT D.** Distribution authorized to the Department of Defense and U.S. DoD contractors only. Other requests shall be referred to controlling office.

☐ **DISTRIBUTION STATEMENT E.** Distribution authorized to DoD Components only. Other requests shall be referred to controlling office.

☐ **DISTRIBUTION STATEMENT F.** Further dissemination only as directed by controlling office or higher DoD authority.

Distribution Statement F is also used when a document does not contain a distribution statement and no distribution statement can be determined.

☐ **DISTRIBUTION STATEMENT X.** Distribution authorized to U.S. Government Agencies and private individuals or enterprises eligible to obtain export-controlled technical data in accordance with DoDD 5230.25.

We certify that we have read this dissertation and that, in our opinion, it is satisfactory in scope and quality as a dissertation for the degree of Doctor of Philosophy in Meteorology.

DISSERTATION COMMITTEE

Duane Stevens
Chairperson

Gay M. Barnes

ii

ACKNOWLEDGEMENTS

ABSTRACT

Eleven tropical cyclones (TCs) are examined using the latest ECMWF reanalysis (ERA-40) and JTWC best track data to determine how tropical upper tropospheric trough (TUTT) cells influence TC tracks. This type of interaction has led to enormous TC track forecast errors at 72 hour (2000+ km) in the northwest Pacific and are often overlooked and under-forecast frequently due to poor numerical model TUTT cell forecasts. Cases are selected because a TC exhibited a "non-standard" track, a TUTT cell was the sole large-scale transient feature within 2000 km of the TC's center, and the TC intensity was >17 m s^{-1}. Analysis shows that the circulations' separation distance, orientation, intensity, and the depth and breadth of the TUTT cell's closed circulation are critical characteristics in determining the likelihood of a TUTT cell influencing a TC's track. Interactions occur at distances greater than 1700 km, continue for periods ranging from 24 to 48 hours and happen 2-3 times per year in this active TC basin.

Examination of the TC's deep layer mean (DLM), upper, middle and lower layers along with various quadrants of the upper layer (100-500 hPa) demonstrate a link between the TUTT cell's wind field and the non-standard TC tracks. The TC's 5°-7° mass-weighted DLM steering environment is found to be closest to actual TC motion in most cases. TC intensity variations and circulation proximity sometimes results in the DLM's 3°-5° radial band being closer to actual TC motion.

A conceptual model of how a TUTT cell can influence TC track is presented. The model provides quantified, decision-grade operational guidance for TC forecasters using pattern recognition scenarios. Application of the conceptual model at the JTWC is currently underway.

iv

TABLE OF CONTENTS

vi

LIST OF TABLES

LIST OF FIGURES

LIST OF ABBREVIATIONS

ATCR	Annual Tropical Cyclone Report
CLIPER	Climatology and Persistence forecast model
CPHC	Central Pacific Hurricane Center
DLM	deep layer mean
ECMWF	European Center for Medium Range Weather Forecast
ERA-40	European Center for Medium Range Weather Forecast ReAnalysis
ESL	Environmental Steering Layer
GFDN	Geophysical Fluid Dynamics Laboratory model
GMS	Geostationary Meteorological Satellite
GrADS	Grid Analysis and Display System
hPa(s)	hectopascal(s)
hr(s)	hour(s)
JTWC	Joint Typhoon Warning Center
K	Kelvin
kg	kilograms
km(s)	kilometer(s)
kts	knots (nautical miles per hour)
m(s)	meter(s)
mb(s)	millibar(s)
M_{TC}	tropical cyclone motion vector
NCAR	National Center for Atmospheric Research
NCEP	National Center for Environmental Prediction

NE	northeast
NHC	National Hurricane Center
NOGAPS	Navy Operational Global Atmospheric Prediction System
NW	northwest
P_{TC}	tropical cyclone propagation
PV	Potential Vorticity
PVU	Potential Vorticity Unit (1PVU= 1×10^{-6} m^2 K s^{-1} kg^{-1})
RHS	right hand side
s	second
SE	southeast
SST(s)	Sea Surface Temperature(s)
SW	southwest
TC(s)	Tropical Cyclone(s)
TDO	Typhoon Duty Officer
TS(s)	Tropical Storm(s)
T_{TC}	tropical cyclone translation
TUTT	Tropical Upper Tropospheric Trough
UCAR	University Corporation for Atmospheric Research
VSHW	Vertical Shear of the Horizontal Wind

CHAPTER 1

INTRODUCTORY DISCUSSION

1.1 Introduction

Accurate tropical cyclone (TC) track forecasts provide a much more valuable piece of information to the end-user than TC intensity forecasts. Even if an intensity forecast is poor, an accurate forecast position can at least indicate where and when *some* effects of the TC may be expected so that preparations could be made for a range of possible intensities. Understanding TC motion in order to accurately forecast its track requires a comprehension of the interaction between the TC and its environment.

A large-scale environmental feature commonly associated with a TC's environment is the subtropical ridge. Other features known to influence TC motion include mid-latitude troughs, other TCs and transient highs. Upper-level cold-core lows embedded within the Tropical Upper Troposphere Trough (TUTT), or TUTT cells, are a less well-known phenomena also believed to influence TC motion and are of considerable interest in the most active TC basin in the world, the northwest Pacific Ocean.

Research has been devoted to the large scale analysis of both TC (e.g., Haurwitz 1935, Frank 1977, Weatherford and Gray 1988, Willoughby 1995) and TUTT cell (Sadler 1967, Kelley and Mock 1982, Whitfield and Lyons 1992, Chen and Chou 1994) structure and dynamics in the Pacific and Atlantic Oceans. Since the geographic domains of each circulation largely overlap during typhoon season, it is reasonable to expect that the two phenomena would occasionally interact with one another.

TUTT cell influences on TC formation and intensification have been well documented (Ramage 1959, Sadler 1976 and 1978, Molinari et al. 1995 and 1998, Chan

and Kwok 1999, Hanley et al. 2001), but little research has been devoted to an influence on TC motion. A number of investigators, however, have made a call for such a study. Hodanish and Gray (1993), Holland and Lander (1993), Chen and Chou (1994), Fitzpatrick et al. (1995), Elsberry (1995), and Wu and Kurihara (1996) are a few examples. Some authors point to the data-sparseness of the TUTT cell's domain and lament a lack of understanding of how the two circulations interact. With improved satellite technology and state-of-the-art atmospheric computer reanalysis, these regions of data-sparseness have become less daunting.

This research investigates the influence of TUTT cells on TC motion, an often overlooked and under-forecast interaction that has been only speculated to actually occur. I perform this observational case study in an attempt to determine *how, when* and *why* TUTT cells influence TC motion and to delineate criteria for determining the likelihood and outcome of such an interaction. My methods result in the first-ever operational guidance for TC forecasters to use during TC/TUTT cell interactions and, with a better understanding of these interactions, provides a foundation for future studies.

1.2 The TUTT and TUTT Cells

1.2.1 The TUTT

TUTTs are sharply elongated, narrow, cyclonic shear zones (Whitfield and Lyons 1992) located in the northern and southern Pacific and Atlantic Oceans. The North Pacific TUTT, or mid-oceanic trough, is a semi-permanent feature that extends east-northeast to west-southwest from ~35°N in the eastern Pacific to ~15°N in the western Pacific. The TUTT was first identified by Sadler (1963, 1972, 1975) on his monthly 200

- 2 -

and 300 hPa wind climatology as a induced trough between the boreal subtropical and subequatorial ridges that extend in the upper-levels from eastern Asia and western North America, respectively. The TUTT appears as smoothed depiction of the paths taken by the transient TUTT cells discussed in the next section but may also reflect the large-scale flow (Fig. 1.1a). The TUTT develops primarily from June through October but reaches peak intensity during July, August and September. An example of a well formed TUTT using water vapor imagery is provided in Figure 1.1b.

Fitzpatrick et al. (1995) proposed that the TUTT helps to balance the enhanced boreal summertime convection and associated latent heat transport into the atmosphere over Asia. Increased radiative cooling over the subtropical oceans (~35°N over the central/east Pacific Ocean) in the vicinity of the TUTT during this climatological period of reduced precipitation leads to more subsidence (descending branch of the Hadley Cell). This dries the air aloft and permits more long-wave radiation loss to space. An overall balance is then maintained between the increased summertime warming over Asia and the enhanced cooling in the upper levels above the subtropical oceans.

1.2.2 TUTT Cells

Colton (1973) and Thorncroft (1993) suggested that TUTT cells form within the TUTT due to barotropic instability associated with mid-latitude troughs penetrating into the sub-tropics. Eddies eventually "cut off" from the trough and move as independent circulations which retrograde toward the west inside the TUTT (Kelly and Mock 1982). Similarly, eddy formation north of the subtropical jet provides another source of TUTT cells. Nieto and Schubert (1999) presented TUTT cell formation as a by-product of a

TC's outflow, broadening of the trough to the east of the TC due to environmental shear and the eastward dispersion of short Rossby wave energy. In general, though, there is no clear consensus on how TUTT cells form.

Composite analysis by both Kelley and Mock (1982) and Chen and Chou (1994) indicate North Pacific TUTT cells generally track toward the west-southwest at ~4.3 m s^{-1}, approximately with the phase speed of Rossby waves, and sometimes with highly erratic tracks (e.g., loops, variable speed). They have a mean wavelength of ~3000 km and a mean lifetime of about a week. Individual TUTT cells vary significantly in size, shape, and intensity during their life cycle but are considered synoptic scale phenomena. Their circulation is typically confined between 100 to 600 hPa with the strongest horizontal circulation near 200 hPa. At this level, the circulation's maximum horizontal winds are ~10 to ~20 m s^{-1} which occur at ~850 km radius. Figure 1.2 shows a relative vorticity cross-section of an actual TUTT cell and a TC (~46 m s^{-1}) from this study along with composites of their associated meridional or tangential wind fields. Notice the inverted appearance of the two circulations compared to the structure of two TCs.

TUTT cell winds can be enhanced if their circulation meshes with the flow of other upper-level large-scale features. Chen and Chou (1994) found that most (87%) TUTT cells contain "jet streaks" (20-30 m s^{-1}) within their outer circulation either to the northwest or south of the centers. These jet streaks correlated well with larger, more intense and longer-lived TUTT cells. Winds along the southeastern periphery of the TUTT cell are generally strongest relative to the rest of the circulation primarily due to the cell's tendency to mesh with strong upper-level westerlies to the south of the TUTT.

TUTT cells are most easy identified using water vapor imagery but are distinguished in infrared and visible satellite imagery by their nearly cloud-free center and comma-like appearance (Fig. 1.1c). Cloudiness reaches a maximum in the southeast half of the circulation, with a distinct minimum to the north through southwest. Maximum mass divergence occurs across the southern and eastern regions of the TUTT in the upper levels (125 – 400 hPa) with convergence at the lower levels (below 600 hPa) (Kelly and Mock 1982). Not surprisingly, the southeast quadrant consists of a TUTT cell's greatest upward vertical motion and convection with compensating downward motion near the center and to the northwest.

1.2.3 TUTT Cell Influence on Tropical Cyclone Intensity

Enhanced TC outflow channels, in response to TUTT-related upper level flow, are important for early and mid-season TC development and intensification in the North Pacific (Sadler 1976, 1978). The north to northwest positioning of TUTT cells relative to TC outflow channels allow TCs to maintain at least minimal typhoon intensity even after the TUTT cell had moved away or dissipated. Based on the upper level divergence structure and with no other factors considered (SST, shear), the southeast quadrant of a TUTT cell is an area favorable to either TC development (with a pre-existing disturbance) or intensification. Koteswaram (1967) and Kimball and Evans (2002) performed similar work centered on the modification of the environmental upper level outflow patterns (outflow channels) by the TUTT cell and the effect on TC mass continuity. Their results suggested that the enhancement of TC outflow caused by the juxtaposition of either the peripheral jet or an upper level low's divergent region typically

led to TC intensification. If no intensification or a weakening of the TC occurred, then another factor, such as vertical shear of the horizontal wind (VSHW) or significantly cooler sea surface temperatures, was responsible.

Molinari et al. (1995, 1998) studied the interaction of potential vorticity (PV) anomalies (troughs in the westerlies) with a couple TC cases. Their results suggested the VSHW induced by the PV anomalies typically inhibited TC intensification. Though a TUTT cell was not explicitly referenced, their upper level PV "anomalies" were similar in scale and intensity to that of an average TUTT cell.

A composite observational study by Hanley et al. (2001) focused on TC intensification resulting from various juxtapositions and distances between a TC and upper tropospheric positive PV anomalies (troughs). Their results indicated TCs over warm water and away from land intensified more often than they weakened during interactions. Their composite study involved relatively small PV anomalies ($\approx$ 1.5 PV units (1 PVU = 1 x 10^{-6} m^2 K s^{-1} kg^{-1}) in proximity (< ~1000 km) to their TC centers. Some TUTT cells from my study, however, yield higher PVU values (~2 to 6 PVUs), have larger sizes and are often further away (~1700 km) from the TC's center.

Wu and Cheng (1999) considered the upper level PV environment above and adjacent to Typhoons Flo and Gene (1990). Typhoon Flo (and similarly with Typhoon Gene) rapidly intensified as a large PV anomaly (a TUTT cell) provided a more effective outflow channel and contributed to upper level eddy flux convergence. Eddy flux convergence is believed to intensify TCs through the inward flux of cyclonic angular momentum (DeMaria et al. 1993). McBride (1981) used a composite study of intensifying TCs and demonstrated this inward flux in the TC's outflow layer. Merrill

(1988), however, suggested a balance must be considered between an intensifying effect and the weakening effect of increased VSHW that is often associated with PV anomalies.

1.2.4 TUTT Cell Influence on Tropical Cyclone Motion

There has been no previous research that directly addresses the influence of a TUTT cell on TC motion. This excludes implied effects resulting from TC intensification. An area of somewhat *related* research, however, was an observational study by Hodanish and Gray (1993) that correlated environmental winds located to the northwest of westward tracking TCs in the northwest Pacific to TC motion. A distinct relationship was found between TC motion and the state of the upper-level environmental winds (distance, depth, magnitude and sign of the zonal wind component) to the TC's northwest. TUTT cells could play a role by directly influencing a region's upper to middle tropospheric environmental winds and, consequently, affect the track of TCs.

Citations about the appearance of a TUTT cell's influence on TC motion do exist within the operational community. The Joint Typhoon Warning Center (JTWC) has numerous references to TC–TUTT cell "interactions" in their Annual Tropical Cyclone Report (ATCR) which caused a TC to slow, move in an unexpected direction or weaken. Typically, no outright explanation of the TUTT cell's role is provided. The National Hurricane Center (NHC) has also made references to TC motion-related interactions with upper level lows and is explicit in their discussion. One preliminary report for Hurricane Erin in 1995 described a TC's interaction with an upper level low as the significant reason downtown Miami was spared a direct hit by the category 1 hurricane. The report stated, "...the upper-level low near Florida affected (Hurricane) Erin's

movement…associated steering currents accelerated Erin from 2.5 to 7.7 m s^{-1} and diverted the cyclone around the northeast side of the low" (Rappaport 1995). Claims like this may adequately describe the appearance of the event but are quantitatively unsubstantiated. Hurricane Erin is discussed further in Chapter 3.

1.3 Applicable Tropical Cyclone Motion Characteristics

This study will introduce the large-scale mechanisms relative to the interaction of a TC and a TUTT cell. TC motion (M_{TC}), or the average vector displacement a TC moved during 6-hours (between two JTWC best track positions), is divided into two primary components; TC *translation* (T_{TC}) and TC *propagation* (P_{TC}), and is represented by:

$$M_{TC} = T_{TC} + P_{TC} \qquad (1.1)$$

Some sub-components could arguably be interchanged between either TC translation or propagation. In this case, the distinction is between those sub-components able to influence TC motion in a quiescent environment and those sub-components that rely on the surrounding environmental flow.

1.3.1 Tropical Cyclone Translation

TC translation is attributed to the TC following the environmental flow associated with large scale synoptic features, such as the subtropical ridge and mid-latitude troughs. An analogy to this concept is that of a "cork in a stream" which oversimplifies the complicated process of a TC being pushed along by larger scale flow. The ability to forecast the future state of these larger scale features from a barotropic perspective is critical to our ability to forecast TC track.

- 8 -

Mean TC steering flows, typically defined by various tropospheric layers, have been studied extensively over the past few decades. This includes work by Kasahara (1960), George and Gray (1976), Holland (1984), Carr and Elsberry (1990), and Figueroa (2003). The environmental steering flow is responsible for about 50-80% of TC motion (Elsberry 1995) and, in some cases, up to ~90% (Neumann 1992). The steering layer that is most influential to TC motion is believed to be directly related to TC intensity (George and Gray 1976, Carr and Elsberry 1990, and Wu and Kurihara 1996). A more intense TC (typhoon, hurricane) is expected to follow a deeper mean layer compared to a weaker TC (tropical storm or depression) (Dong and Neumann 1986, Velden and Leslie 1991).

Some numerical modeling studies suggest VSHW can cause a TC to tilt downshear. This tilt may lead to an interaction between the TC's lower cyclone and upper level anticyclone and is considered another translation component. Wu and Emanuel's (1993) used a 2-layer quasi-geostrophic model of an idealized TC and found the influence of even weak shear is at least as strong as the beta effect. They determined Northern Hemisphere (NH) TCs have a component of drift relative to the mean flow but to the left of the background vertical shear. A numerical model used by Flatau et al. (1994) focused on the downshear tilting effects of VSHW on a TC and the resulting interaction (mutual steering) between the TC's upper level anticyclone and its mid to lower level cyclone. Wang and Holland (1996) went on to incorporate the influence of upper level anticyclonic PV anomalies displaced downshear and, as with Wu and Emanuel (1993, 1995a), found TCs track to the left of the mean environmental VSHW vector.

Linear wind shear involves non-uniformity in the surrounding environmental flow at a specific level. Horizontal wind speed variations across a TC's environment can

cause a downshear tilt of the TC outer wind field. Wang and Li (1995) determined anticyclonic meridional shear (i.e. associated with a subtropical ridge) would feed kinetic energy to the beta gyres. As a result, the beta drift would be faster in anticyclonic meridional shear compared to cyclonic (e.g., associated with a mid-latitude trough).

1.3.2 Tropical Cyclone Propagation

This component of TC motion occurs even if the background flow vanishes. The beta effect is the most prominent TC propagation component. Beta (β) refers to the change in Coriolis (f) with latitude (y) and is how this component of TC propagation received its name. Beta is represented by:

$$\beta = {}^{df}/_{dy} \tag{1.2}$$

This theory of TC "self-advection" develops due to the interaction between the TC's circulation and the Earth's vorticity gradient. The barotropic vorticity equation is:

$$D\zeta_r/Dt = -v\,\beta \tag{1.3}$$

$$\zeta_a = (\zeta_r + f) = \text{const} \tag{1.4}$$

where ζ_r is relative vorticity and v is the velocity component. Equation 1.3 is used to demonstrate the principle of the conservation of absolute vorticity (ζ_a in Eqn. 1.4). Southward (northward) flow to the west (east) of the TC leads to positive (negative) value on the RHS of Equation 1.3 (y is negative for southward flow and f decreases toward the equator). To balance this change, a positive (negative) relative vorticity tendency develops. The TC then tends to move westward toward the area of positive relative vorticity tendency (Elsberry 1995). The positive/negative relative vorticity tendencies to the west/east of the TC induce anomalous circulations that result is a

- 10 -

wavenumber one beta gyre (Fig. 1.3). The result is a secondary cyclonic circulation to the west of the TC, anticyclonic circulation to the east and northward flow over the TC center (Holland 1983). The TC's own inner circulation distorts/rotates this gyre cyclonically (Fiorno and Elsberry 1989). The result is a combined poleward and westward advection ($\sim$ 1 to 3 m s^{-1}) with a greater influence on radially larger and more intense TCs located at higher latitudes (Carr and Elsberry 1994). The beta drift is defined as the overall influence of the beta gyres on TC motion. Wang and Li (1992) utilized a baroclinic primitive equation model and yielded similar beta drift as the baro9tropic models. They found the vertical structure of a vortex circulation has a similar effect on TC translation as the horizontal structure does.

Diabatic heating contributions is important to the distribution of PV. A definition of barotropic PV, conserved in adiabatic and frictionless flow, is:

$$PV = -g(\zeta_\Theta + f)^{d\Theta}/_{dp} \qquad (1.5)$$

where g is gravity, ζ_Θ is relative vorticity on an isentropic surface and $^{d\Theta}/_{dp}$ is static stability. Asymmetric convection results in the asymmetric release of latent heat. This, in turn, can modify the TC's PV distribution that alters the vorticity distribution (maximum vorticity tendency) and affect TC motion (Elsberry, 1995). Wu and Emanuel (1993) researched the high variability of PV in the troposphere. They suggested a TC's own upper level anticyclone (lower positive to negative PV values) could substantially affect TC motion. A TUTT cell has a similar scale and comparable wind magnitude as a TC's outflow anticyclone but with higher positive ζ_Θ values (cyclonic) resulting in greater PV. Chan et al. (2002) emphasized PV tendency based on a small number of cases in the northwest Pacific. They found a TC with steady motion is dominated by

horizontal PV advection, but a TC with significant convective asymmetries will lead to a "non-smooth" or irregular TC track. Since TUTT cell interactions can influence TC intensity (i.e. increase convection) (Sadler 1976), convective asymmetries are monitored.

1.3.3 Binary Tropical Cyclone Interaction

There has been significant research in understanding how two vortices interact since the pioneering work of Fujiwhara (1923). Brand (1970), Dong and Neumann (1983), Carr et al. (1997), Carr and Elsberry (1998), Prieto (2003) and Wu et al. (2003) have all observationally discussed binary TC interaction characteristics. Their results yielded various critical separation distances, interaction types (one-way, mutual) and stages (approach, orbit, escape, and merger). Operational guidance was developed as a result called the Systematic Approach to TC Forecasting by Carr and Elsberry (1994).

In a related study, Kimball and Evans (2002) modeled the interaction of a TC and an assortment of upper level lows (troughs). They used a high-resolution model with 2 one-way nested domains and 24 vertical levels along with values taken from Hurricane Dennis' (1999) analyzed fields. Their findings indicated a TC could advect and deform a TUTT cell's wind field and center based on their juxtaposition at specific levels. Their results support the idea that binary interaction between a TC and a TUTT cell is possible.

Lander and Holland's (1993) (furthermore LH93) observational study focused on TC-TC interactions and between multiple "TC scale vortices." LH93 sites but does not explicitly use "mesoscale cyclones *associated* with TUTT cells" as an example in their study. LH93 focused on the independent tracks and movement of each circulation relative to an unweighted centroid (i.e., average coordinates on a Mercator projection)

and described their motion characteristics. LH93 did not, however, speculate on what caused the motion of the two vortices. Their methods provide a good reference frame from which to draw conclusions about binary interaction characteristics.

1.4 Operational Justification for Research

Based on my operational experience at the JTWC from 1998 to 2000, numerical forecast models are notorious for inaccurately projecting the location, structure and intensity of TUTT cells. Consequently, forecast model output may be affected by their biases and inadequate incorporation of an entire TUTT cell wind field into a TC's environment, some of which have been well documented. Fitzpatrick et al. (1995) wrote specifically about the Aviation Model's systematic bias in the Atlantic and the implications to TC genesis, track and intensity forecasts. The cause of the numerical model errors and various limitations are usually blamed on low horizontal and vertical resolution, imperfect data and parameterization (convective, radiative) schemes. In some cases, Atlantic TC forecasters were even advised to use climatology over the model output! Carr and Elsberry (2000a, b) discussed similar problems with the U.S Navy's Geophysical Fluid Dynamics Laboratory model (GFDN) and the Navy Operational Global Atmospheric Prediction System (NOGAPS) in the northwest Pacific.

The JTWC has repeatedly identified problems with numerical model TC track guidance in their ATCR (JTWC 1994, 1996, 1998, 1999). According to the JTWC Technical Advisor, TC forecast models simply "do not handle (TC) forecast tracks very well when a TUTT cell is involved" (Ed Fukada, personal communication, October 12, 2005). Based on enormous forecast track errors (>2000 km) resulting from a lack of

TC/TUTT cell interaction understanding and training, JTWC has identified the need for an improved understanding of these interactions as a significant area of required research.

1.5 Goals and Dissertation Organization

The following work is an observational study. The goals of the research include:

    a. Search for evidence of a TUTT cell's capability to influence TC motion.

    b. Identify similarities between binary TC and TC/TUTT cell interactions.

    c. Provide operational forecast guidance in the form of a conceptual model.

    d. Compare observations to related model studies.

This research intends to also answer the following questions:

    a. How does a TUTT cell directly influence a TC's motion?

    b. Does a TC influence a TUTT cell's motion?

    c. What environmental steering guidance "best fit" an interaction?

    d. At what separation distance do TC-TUTT cell interactions take place?

    e. What role does the TC or TUTT cell intensity have on an interaction?

    f. Are other TUTT cell circulation characteristics important?

    g. What are the key indicators an interaction will occur or is occurring?

    h. How long do interactions last?

Chapter 2 provides an overview of the data and methodology. Chapter 3 provides a detailed discussion of sample cases, a summary of all 10 cases, conclusions based on this summary and a comparison with an Atlantic Ocean case. Chapter 4 provides a discussion of my results and provides an observational comparison to related model studies and Chapter 5 provides an overview of my basic conceptual model and conclusions.

CHAPTER 2

DATA AND METHODOLOGY

2.1 Introduction

Reanalysis data provides the best estimated hindsight view of the global state of the atmosphere. Though not perfect, reanalysis projects base there depiction on a collection of all available observational data sources (rawinsondes, surface observations, satellites) and short-term computer forecast models that apply the most current theories in atmospheric dynamics and physics. The data set is ideal for my research especially since it deals with such a remote part of the globe.

2.2 Data

2.2.1 ERA-40 Reanalysis

This study utilizes the latest 45 year (1957-2002) European Center for Medium Range Weather Forecasts (ECMWF) ReAnalysis (ERA-40) 6-hourly dataset at near model resolution (~1.125° of latitude). According to Uppala et al. (2005), ERA-40 was intended to be the best possible reanalysis data set considering the evolving observation system and available computer resources. ERA-40 also benefits from the previous reanalysis' (ERA-15) lessons-learned, provides greater horizontal and vertical resolution and incorporates more observations of all types (Table 2.1).

ERA-40 data assimilation employed short-term (6-hour) forecasts, known as background information, based on the previous time step analysis. The new background information and current observations were then combined using statistically-based estimates of their individual errors to make a full analysis of the new time step.

Observations were included from 3 hours on either side of each 6 hourly valid time (00Z, 06Z, 12Z and 18Z). This provided a good estimate of the atmospheric state at any given time and included data that may not have previously been available to forecasters or numerical models at the actual valid time.

It is important to note the variability of observations across the northwest Pacific Ocean basin. Close to the Asian continent and over the Philippine Sea, observational data sources for the ERA-40 assimilation were (and are) relatively dense. Toward the international dateline, however, in situ sources are sparse and reliance on satellite-derived observations becomes greater. This observational data source "gradient" from eastern Asia to the central Pacific may have impacted numerical model TC forecast performance across the region and is addressed later in the paper.

Satellite-derived observations, such as geostationary cloud drift and water vapor wind measurements, provided the ERA-40 with increased wind speed and direction data over otherwise data spare regions. The data especially improves the reanalysis' depiction of features in the upper half of the troposphere, such as TUTT cells and TC outflow (~100-400 hPa) (Velden 1997). Cloud drift winds can also help to identify lower level winds near the trade wind inversion (~850 hPa) over fields of tropical cumulus clouds (Dunion and Velden 2002).

The specific ERA-40 version used was recreated by the National Center for Atmospheric Research (NCAR) and was transformed to a 256x128 regular Gaussian grid at T85 spectral truncation (from $\approx 1.125°$ to $1.406°$ (~156 km) horizontal resolution) with 23 pressure levels (UCAR Data Support Section 2006). In a side-by-side comparison, both the full model resolution (1.125°) and the NCAR re-creation (1.406°) appeared to

- 16 -

match previously documented *large-scale* structures of the two circulations reasonably well. Both resolutions failed, however, to capture the core structure of any TC analyzed. In particular, the TC's tangential wind speed and warm cores was very poorly depicted. For example, the maximum tangential winds resolved reached only ~26 m s^{-1} (51 kts) for a 67 m s^{-1} (130 kts) TC. Both datasets also revealed a large and highly unlikely radius of maximum winds of 200-250 km, obviously not correct eye wall structure. Similarly, warm temperature anomalies expected to be found within a TC's core were underestimated. Anomalous values reached only ~ +2-3 K versus what has been found in observational composites (+15°K at 300 hPa by Frank 1977a). Considering an average TC's eye and eye wall could "fit" between two ERA-40 data points as well as the lack of observational data from within the TC core, these results are not surprising.

Atmospheric fields utilized included zonal and meridional wind components, geopotential, temperature, PV and relative vorticity (ζ_r) fields. Most of these fields have been used in previous large scale studies of both phenomena and are reasonably well depicted within the ERA-40 data. Some fields, such as ζ_r and PV, are also directly related to the horizontal wind field components and are dependent on their accuracy. Increased data density provided by satellites over the data sparse ocean was expected to improve the continuity and realism of the wind and related fields in this study compared to previous studies using all or mostly rawinsonde data (Frank 1977a, b, Chan and Gray 1982, Kelly and Mock 1982).

2.2.2 Tropical Cyclone and TUTT Cell Database

To ensure homogeneity of the ERA-40 database and access to geostationary

satellite imagery, TC case studies are constrained to 1994-2001 (Fig. 2.1). Cases are further temporally constrained within each year from June through October based on North Pacific TUTT climatology. The JTWC ATCR and best track data files are used as a reference for developing case studies and for 6-hourly TC location and intensity. best track positions are determined by a Typhoon Duty Officer or other skilled JTWC staff member who reanalyzes the record of hourly TC position fixes after the TC has completely dissipated. They use all available TC center fix reports from worldwide reconnaissance network sites and observations (satellite imagery, surface reports) to develop a final or "best" TC track to within .1° for historical reference. Weaker and/or less organized TC centers of circulation are often the most difficult to pinpoint and can result in the greatest location variability between reconnaissance reports (sometimes 100+ km). During the review, old and new data sources are considered and fix positions may change slightly from the original valid time to the final best track position and intensity published in the ATCR. This variability is important especially when dealing with slower moving TCs since it can significantly change the results of steering flow statistical analysis. For example, if a TC moving 285° at 2.1 m s^{-1} was repositioned only 28 km (~.25°) further west for a 6-hourly fix due to poorly defined circulation center, direction would change nearly 10° (to ~276°) and speed would increase by over 50% (to 3.3 m s^{-1}).

The center of a TUTT cell is not as well-defined or easy to locate as a typical strong TC nor are there any best track datasets available for these circulations. As a result, I use the Grid Analysis and Display System (GrADS) to streamline the ERA-40 wind data at 200 hPa. I determine each circulation's center at every time step to create an independent TUTT cell "best track" dataset to .1° in order to match the JTWC TC dataset. This

approach is similar to the hand streamline analysis performed by Kelley and Mock (1982) and Chen and Chou (1994) used to determine the centers of circulation during their TUTT cell composite studies. TUTT cell intensity is determined by identifying the cell's maximum 200 hPa relative and potential vorticity values.

Infrared and water vapor imagery from the Japanese Geostationary Meteorological Satellite (GMS) is also used to provide basin-wide coverage of TCs, TUTT cells and surrounding features. This imagery helps check ERA-40 realism and allows for anomalous convection and other features in the basin to be monitored and estimated. Convective asymmetries are "eyeball estimated" based on my experience at the JTWC. Figure 2.2 provides examples of convective asymmetry estimates.

2.3 Methodology

2.3.1 Case Study Identification and the Definition of "Interaction"

Criteria required to identify a case study are set, *all* of which must be for a TC to be selected. The intent is to have the most uncorrupted interactions possible in order to isolate the TUTT cell's influence on TC motion and demonstrate their *potential* influence for application during "normal" conditions. The criteria included:

a) *A non-standard TC track based on the JTWC ATCR.* Examples include "stair step" track patterns, sudden and/or unexplained track deviations in speed and/or direction ("kinks") and rare southward motion. ATCR commentary, often reflecting the thoughts of the Typhoon Duty Officer at the time, is also considered. Some inaccurate JTWC forecasts for non-standard tracks are explicitly blamed on a TC's "interaction" with a nearby TUTT cell (JTWC 1998).

b) *A TUTT cell exists within 2000 km (~ 18° latitude) of the TC at the time of the track deviation.* The criteria are confirmed by both the ERA-40 data and GMS imagery. The 2000 km limit is based on the greatest published separation distance for binary TC interaction to occur (~1400 km) by Brand (1970) plus an arbitrary 600 km buffer to account for the different scale/size between an average TUTT cell and TC.

c) *Other transient mesoscale or larger atmospheric features* known to influence TC motion *are not present within approximately 2000 km of the TC and its path.* This criterion is confirmed by both ERA-40 data and GMS imagery analysis. Examples of transient features include mid-latitude troughs, transient anticyclones and other TCs.

d) The *TC is at tropical storm strength or greater* (> 17 m s^{-1}). A weaker TC core circulation (tropical depression) may not extend up to a level in which an average TUTT cell extends down toward the surface and, therefore, would make an interaction between the two circulations less likely. This criterion is intended to increase the chance of an interaction using a common TC category division.

These criteria greatly limit the number of available cases where an influence by a TUTT cell on TC motion is believed to have taken place. As anyone who has studied or lived in the northwest Pacific basin may know, "there always appears to be something (convectively) going on somewhere in the basin during its chaotic typhoon season" (Dr. Greg Holland, September 2006, personal communication). Examples include multiple TCs, shear lines, westerly wind bursts, monsoon trough convection and mesoscale convective systems. In all, ten cases are identified. As in LH93 for two TCs, unweighted centroid-relative motion of the two circulations in each case is analyzed to determine the

periods of the binary TC/TUTT cell interactions. This method is used to identify change-points in motion between the two circulations and does *not* assume a *mutual* interaction.

The general shapes of LH93's 10 TC pairs are individually compared to my 10 case's unweighted centroid-relative motion tracks. Though obviously not the same scale or structure as two TCs nor with the fidelity of two TC best tracks, interaction *similarities* between TCs and TUTT cells are expected since they are both essentially, and very simplistically, large tropospheric vortices. The interaction start point is identified and defined by a notable change (e.g., a "kink") in the 2-point (6-hour) running average centroid-relative track around the start of each TC's non-standard track. The sharp directional change typically results in a counterclockwise turn of the centroid relative motion by ~25° to ~45°. The kinks are usually preceded by a straight 2-point running mean line but sometimes show additional though lesser kinks probably due to inaccurate TUTT cell best track analysis of the coarse ERA-40 200 hPa wind fields. The period between the two time steps that comprised either side of the kink become the start point of the interaction period. The interaction end point is defined by the time steps which comprise the next significant kink in the centroid relative motion track and approximately correspond with the end of the non-standard track and/or the dissipation of the TUTT cell. The time between the start and end points then defines the interaction period.

2.3.1.1 Minor Exceptions to Case Study Criteria

Three of the ten cases' environmental characteristics slightly violate the case study criteria yet are selected anyway since they do not appear to affect TC motion or the TUTT cell interaction. These exceptions increase the initial number of cases by ~50%

and include Bart, Polly and Rex2. All three involve minor violations of the "2000 km limit" criteria from Section 2.3.1.c.

Bart's environment reveals the leading edge of a weak upper level (above 300 hPa) mid-latitude trough ~800 km to its northwest moving very slowly eastward. The trough's gentle northeast-southwest slope, nearly stationary status and general structural discontinuity allows the TUTT cell to remain in proximity on the opposite side of the TC before the TUTT cell dissipates and the TC accelerates northeastward.

Polly's environment has another TC, Oscar, ~1600 km to its north-northeast moving rapidly away at over 21 m s^{-1} as Polly slows prior to its TUTT cell interaction period. The increasing separation distance between the two TCs and decreasing separation distance between Polly and the TUTT cell prevents an influence by Oscar.

Rex2's environment also reveals the leading edge of a nearly stationary mid-latitude trough located ~800 km to its northwest. As Rex2 moves slowly (< 2 m s^{-1}) toward the north, it begins to turn toward the east and in the direction of one of the study's more intense TUTT cells. Since the trough appears stationary and the TC does not seem influenced by its flow, the case is included.

2.3.2 Forecast Model Comparison

The error magnitudes for three separate forecast sources at 6-hourly intervals through 48-72 hours are determined for each case based on the limited JTWC records. The three forecasts include the JTWC, NOGAPS and a CLImatology and PERsistence model (CLIPER). These three products span the spectrum of complicated numerical model-based (dynamic) to simpler climatology-based (statistical) forecast models. Each

methodology's skill is quantitatively rated and discussed with respect to how environmental conditions along with the availability of observations could impact forecast performance. The intention is to focus on the time when the models show larger errors and how the TUTT cell and geography may contribute to forecast degradation.

The JTWC forecast represents the human factor in TC forecast development. Forecasters interpret the available guidance and create subjective forecasts based on a number of considerations, including a TC model's previous performance, applicable TC motion theory, proximity to major population centers or ports (socio-political), forecaster workload and experience. Ideally, the JTWC forecast should have the least error when these issues are not a factor. This is not always the case, especially when a TUTT cell is nearby. The JTWC also applies the Systematic Approach to TC Forecasting by Carr and Elsberry (1994) to their forecasts process. Their use of pattern-recognition involves various scenarios of large-scale features interacting with TCs but lacks a scenario with TUTT cells or upper-level lows in the northwest Pacific. Boothe, Elsberry and Carr (2000), however, do provide general steering flow recognition (polar or equator-ward) guidance for upper level lows near Atlantic TCs.

NOGAPS (version 3.4) is a fully dynamic global spectral model in the horizontal and an energy conserving finite difference in the vertical (Hogan et al. 2002). It consists of a T159 spectral truncation (~80 km in mid-latitudes) with 18 vertical levels for the earlier period but expands to 24 vertical levels in 1998. There are no changes in horizontal resolution from 1994 to 2001. Virtually every source of data available to the ERA-40 reanalysis is also incorporated into NOGAPS model runs, including polar orbiter atmospheric temperature soundings, GMS cloud-drift and water vapor winds.

The NOGAPS TC Vortex Tracker model is the output actually used to determine the NOGAPS forecast error and is derived from the NOGAPS 6-hourly forecast fields. A TC vortex is tracked by converting the 1000 hPa zonal and meridional wind component fields into isogons, or lines of constant wind direction. It is initialized with information from the most recent JTWC warning and based on the last TC position, speed and direction of motion. The program searches for the next cyclonic center representing the TC at each forecast time step. Confidence factors are then created and may be modified by a quality control program prior to forecaster use (JTWC 1998).

On the other end of the model-complexity spectrum is CLIPER, a 5-day statistical model. CLIPER applies persistence from 12 hours of previous TC track to the first 12 hours of forecast track. The model then considers the current TC location, intensity, motion vector and Julian date to create a statistical forecast based on climatological TC paths with similar characteristics. CLIPER does not change during the years of this study except for the possible addition of previous year's "historical" TC tracks to its database. CLIPER forecasts are considered a "no-skill" output and are used as a baseline to show a level of value-added by other forecasts (Franklin 2006).

2.3.3 Environmental Steering Layer Identification

There are literally thousands of horizontal (radial bands) and vertical (layer) combinations possible for determining a TC's most accurate environmental steering. This study generically refers to all of these as environmental steering layers, or ESLs. As a first guess, radial band and layers statistically demonstrated in many previous studies to provide the best general guidance in the northwest Pacific for TC translation are selected.

Additional horizontal and vertical combinations are also analyzed after which the group of ESLs is narrowed down. Mean wind components for each ESL at each 6-hourly time-step are ascertained and compared to the track taken by the TC from a time-step then forward 6 hours, similar to what a forecaster might utilize (vs. after-the-fact).

2.3.3.1 Environmental Steering Layer Background

Sanders and Burpee (1968), Pike (1985), Dong and Neumann (1986) and Neumann (1979 and 1992) applied the use of mass-weighting the 10 standard level winds from 100 to 1000 hPa (Table 2.2). Their results indicated that this deep layer mean (DLM) provides the best representative height field and corresponding wind field for *short-term* (≤ 24 hour) forecasts. Since my study focuses on short 6-hourly increments, use of the weighted DLM application is justified. Chan and Gray (1982) utilized mass-weighted layer-averages with various radial bands around TC centers in the northwest Pacific and statistically determined the 5°-7° (556–778 km) radial band of the DLM flow correlates best to TC motion. Their study used only sparse rawinsonde data without the advantage of a large scale wind fields provided by satellite and reanalysis. The 5°-7° radial band is, therefore, analyzed along with all environmental winds within 7° of the TC center. Mass-weighted *and* non-weighted (e.g. arithmetic mean) ESLs are also computed.

Elsberry (1995) indicated that the best ESL agreement with composite TC motion *should be* the 1°-3° radial band from 300-850 hPa. This layer avoids most TC convergence and divergence and is not too far removed from the core. Studies utilizing solely rawinsondes would rarely have acquired data from directly within this radial band. The same holds true for the ERA-40 data to some extent, but the ERA-40 is expected to

provide a comparatively *more* accurate representation of the atmosphere. A weighted and non-weighted 1°- 3° radial band ESL for this layer is also used along with the 3°- 5° radial band to fill in the gap between the 1°-3° and 5°-7° radial bands.

2.3.3.2 Initial Environmental Steering Overview

Additional ESLs are defined based on the each circulation's average structure. This is intended to determine case-specific TUTT cell influences on the various TC ESLs, akin to a "best fit" method. In all, this study starts with 32 ESLs which included weighted and non-weighted mean values for 1°-3°, 3°-5° and 5°-7° radial bands (degrees of latitude) for the following layers (together with 0-7° for the DLM):

- 100-500 hPa (upper layer, 7 ERA-40 levels used) (6 ESLs)

- 500-1000 hPa (lower layer, 4 ERA-40 levels used) (6 ESLs)

- 400-700 hPa (middle-shallow layer, 3 ERA-40 levels used) (6 ESLs)

- 300-850 hPa (middle-deep layer, 5 ERA-40 levels used) (6 ESLs)

- 100-1000 hPa (DLM, 10 ERA-40 levels used) (8 ESLs)

It is important to note that there is no single "correct" ESL, level or layer for all TCs at any given time. Franklin (1990) demonstrated the high variability and uncertainty of radial band averaging in Hurricane Josephine. Most previous studies provide the best statistical correlation for a large number of TCs at various intensities and latitudes. These studies are used as guidelines. The intention here is to dissect the different layers of the troposphere and determine their contribution to a TC's environmental steering flow. The 32 original ESLs are now narrowed down based on the initial case study analysis.

2.3.3.3 Selection of the Best Environmental Steering Layers

All ESLs are individually compared both statistically and analytically for each case. The statistical analysis included determining the Pearson correlation (most at 90% level of significance) between each ESL's vector direction and magnitude independently against the same TC motion vector components. This method separates the two attributes of TC motion important to a forecaster instead of correlating U and V components which incorporate part of both attributes simultaneously. Correlations are performed separately during the defined interaction period and during the entire utilized dataset (typically +/-24 hours on either side of the interaction period). Analysis includes graphically depicting each ESLs deviation from both TC direction and speed at every independent 6-hourly time step and visually comparing the results.

Use of the Spearman Rank Correlation was considered. Most cases, however, involve TC and ESL vectors that changes together (speed/direction) during the same short interaction periods (typically 4-8 time steps). Without a reordering the rank of each series due to greater motion characteristics variability, correlation values are frequently perfect ($r = 1$). This statistical method was, therefore, excluded.

Larger surface areas, of course, contain more ERA-40 analysis points. For example, the 1°-3°, 3°-5° and 5°-7° radial bands typically contain approximately 15, 30 and 45 analysis points (respectively) at any time step and/or location. More analysis points allow for more smoothing of the associated mean values whereas radial bands with fewer analysis points are subject to more skewing by one or two outliers.

Initial analysis indicates that the 5°-7° radial band of the layers is closest to TC motion for most of the ten cases using the case's entire data period. The 3°-5° then inner

7° radial bands are usually the next closest to TC motion. Some cases, however, require consideration of the TC's proximity to the associated TUTT cell. For example, Typhoon Amber (1997) involves a small TUTT cell with its center ~740 km from the TC's surface center during the interaction period. Since this is within 7° of the TC (Fig. 2.3), the 5°-7° radial band envelopes some of the return flow from the far side of the TUTT cell's circulation. The return flow is southward which is evident in the DLM's 5°-7° radial band mean wind during the interaction period. The TC, however, deviates northward during this period and more in line with the flow associated with the leading half of the TUTT cell's circulation (southerly flow). The 3°-5° and 1°-3° radial bands indicate this northward component which incorporates the TUTT cell's southerly flow and are closer to TC motion. In most cases, however, the flow around the TUTT cell rarely moves to within ~3° of a TC's center at 200 hPa.

The upper (100-500 hPa) and lower (500-1000 hPa) layers are retained as the layers expected to either include the influence of a TUTT cell's circulation or be mostly void of it, respectively. The DLM (100-1000 hPa) is also retained since it incorporates both of the aforementioned layers. The two "middle" layers (300-850 hPa and 400-700 hPa) are nearly identical in most cases. The 300-850 hPa layer, however, typically yields direction and speed slightly closer to TC motion, so the 400-700 hPa layer is discarded.

Significant differences between mass-weighted and non-mass-weighted (arithmetic mean) ESLs exists *only* in the DLM and the upper layer ESLs (less-frequently). On average, the mass-weighted ESLs of these two layers are closer to TC motion. Non-mass-weighted ESLs is, therefore, discarded.

Table 2.3 lists the final ESLs (13 from the original 32). The 5°-7° annulus is typically the closest radial band to TC motion followed by the 3°-5°, 1°-3° and inner 7° (DLM only). Any combination of these radial bands is used on a case by case basis.

2.3.3.4 Quadrant Analysis: TUTT Cell Contributions to Tropical Cyclone Motion

A TUTT cell is expected to contribute only *partially* to the overall steering environment incorporated into TC motion. TC position relative to the TUTT cell is understandably critical for an analysis. To focus on the fractional contribution of a TUTT cell using a geographically fixed reference system, the upper layer is subdivided into quadrants around the TC, including northeast (NE), northwest (NW), southwest (SW) and southeast (SE). Observing variations of each quadrant's mean wind value in a time series shows how the TC's upper layer and, therefore, TC motion responds to its environment. This fixed coordinate system also allows for an inter-comparison of the quadrants (i.e. TUTT cell influenced versus non-influenced) and provides consistency for discussion of a TC's surrounding features. Anticipated changes due to the incorporation of a TUTT cell's circulation within a fixed quadrant(s) can then be deduced. Two observations should help identify evidence of a TUTT cell's influence on TC motion:

a. An identifiable change in the mean wind flow of a fixed quadrant(s) containing the greatest amount of TUTT cell flow which coincides with TC motion changes. This is based on contributions by the flow to the upper layer and DLM.

b. A relative steady-state or TUTT cell related deviation of the other quadrant(s).

Another process is then applied to remove a large potion of the TUTT cell's influence from the mass-weighted DLMs at various radial bands. A comparison between

a TC's DLM with and without much of the TUTT cell's influence removed is meant to give an idea of where the TC might have tracked without the TUTT cell's presence. Since a TUTT cell is primarily confined to the upper layer of the troposphere (100 to 500 hPa), the TC's upper layer quadrant closest to the TUTT cell (i.e. quadrant adjust with time) is removed to eliminate much of the TUTT cells wind field and, therefore, influence on TC motion. The new upper layer is then comprised of the remaining three quadrants while the lower layer (500 to 1000 hPa) remains unchanged (Figs. 2.4a, b). Both layers are then combined to make up the TC's new mass weighted DLM. This new DLM is compared to the original DLM vectors helps to provide evidence of a TUTT cell's influence on TC motion and is discussed further in Section 3.1.

2.3.4   Residual Vector Analysis

The difference between the TC motion and an ESL vector is referred to as the residual vector. This vector incorporates all components of the TC propagation vector as encompassed in the ERA-40 dataset. Characteristics of the theorized beta effect, or generally a north through westward direction with a magnitude of $\sim$1-3 m s^{-1} (Carr and Elsberry, 1994), are expected to dominate the residual vector *in the absence of strong VSHW or asymmetric convection.*

The distance from which the anomalous beta gyre circulation extends from the TC's center is important since the beta gyres anomalous flow should already be incorporated into the ERA-40's wind field. Regarding the 5°-7° radial band for an average TC, "...the (beta) effect should be somewhat muted, but not lost" (Dr. Greg Holland, personal communication, 15 January 2008). Research is unclear as to the

precision to which this can be determined. With this in mind, the DLM of the 5°-7° radial band in this study is treated as a mostly "beta drift free" environment. The residual vector is then expected to have the anticipated beta drift characteristics. The 3°-5° radial band is also analyzed since it should typically incorporate more of the TC's beta drift in its environmental flow and have a reduced beta drift signature.

2.3.5   Vertical Shear of the Horizontal Wind Analysis

TC motion has been modeled to the left of the mean (background) VSHW vector (Wu and Emanuel 1993, Flatau et al. 1994, Wang and Holland 1996). These studies generally involved homogeneous easterly or westerly shear at varying magnitudes across the TC's environment. The result was a tilted coupled vortex (cyclone/anticyclone) which deflected each other and translated together to the left of the mean wind shear vector. My intent is to observationally test these numerically modeled results.

Fields of VSHW, defined as the vector difference between 200 hPa and 850 hPa U and V wind components, or:

$$\text{VSHW} = [(U_{200} - U_{850})^2 + (V_{200} - V_{850})^2]^{.5} \qquad (2.1)$$

are developed for each 6-hourly time step. Given that there is no set definition of a TC's "environment", this study uses the 5°-7° radial band since it already fits nicely as a TC steering environment. The inner 7° and 10° radii are also used to incorporate the TC and even *more* of their surrounding environment. Chen et al. (2006) used a similar method with the same VSHW definition as above but at a distance of 200-800 km (~2° to ~7° latitude) from their TC center. Variations in mean VSHW component values indicate changes in the TC's environment while standard deviations reveal the variability.

2.3.6   Conceptual Model Development

My desire for operational application is to create a quantified conceptual model as guidance for the JTWC. The guidance is intended to emulate the Carr et al. (1997) pattern-recognition conceptual model for track-altering binary TC scenarios (Fig. 2.5). Their conceptual model displays different orientations/scenarios of TCs and various large-scale environmental steering sources with only separation distances quantified. The following, at a minimum, is projected to be incorporated into my conceptual model:

    a.   A maximum separation distance for an interaction to occur

    b.   Orientation (relative positioning) of the two circulations

    c.   TUTT cell and TC intensity criteria

    d.   TUTT cell characteristic thresholds to determine the likelihood of an interaction

    e.   Forecast deviations to a TC's motion (a track bias)

    f.   A graphical depiction of interaction types for pattern recognition

In Chapter 3, we will look at three Pacific cases and one Atlantic case in-depth to show how qualitative and quantitative criteria are attained and utilized from all eleven total cases.

CHAPTER 3

CASE STUDIES

3.1 Introduction

Satellite imagery is typically the first and primary tool used by forecasters to locate a TC and its surrounding features. The imagery provides only cursory information compared to the addition of numerical simulations and satellite-measured tropospheric observations. With this in mind, the ten selected TC/TUTT cell cases are each initially viewed using solely GMS infrared and water vapor imagery along side the TC best track. The "appearance" of the TUTT cell in the satellite imagery and the influence it is believed to have exerted on the TC's track (change in TC direction or track speed) based on the orientation of the two circulations is noted. Each TUTT cell is subjectively labeled as having an "intense", "moderate" or "weak" appearance *without* consideration of their ERA-40 wind field analysis (Fig. 3.1a). An initial conceptual model is created that fits the anticipated result of adding TUTT cell winds into a TC's environmental steering (Fig. 3.1b). For example, TUTT cell flow that appears to move across a TC's track would be expected to cause a change in radial direction. TUTT cell flow moving directly into (e.g., "headwind") or from behind a TC (e.g., "tailwind") would be expected to decelerate or accelerate the TC's forward speed, respectively. The TC motion biases (to left/right, faster/slower) are determined by comparing JTWC and NOGAPS forecasts just prior to and at the interaction start point with the actual TC best track.

Each of the ten cases are then analyzed using the methods described in Chapter 2 to determine if there is an identifiable influence of the TUTT cell's wind field on TC motion. All cases are expected to show some evidence of an influence by the TUTT cell

- 33 -

on the TC's motion based on the initial conceptual model. Using my analysis, cases can either reveal or not reveal the anticipated evidence. Evidence is primarily based on the vector difference between the TC's mass-weighted DLM and a new computed DLM with the upper layer quadrant closest to the TUTT cell removed (Section 2.3.3.4). If the DLM vector difference does not match the addition of the TUTT cell's flow into the TC's environment, the case is considered to have provided *no* evidence. Explanations of why a case does or does not provide evidence are qualitatively and quantitatively discussed. Tables 3.1a.-f summarize the metrics taken for this analysis and are discussed at greater length in the case summary (Section 3.4) and referenced in the forthcoming discussions.

Section 3.2 provides two examples of cases where evidence of the TUTT cell's influence on TC motion is found. The first case provides an in-depth discussion of the analysis method. The second case uses the same analysis methodology in a more succinct manner. Section 3.3 provides one example of a case where evidence is not found. A summary of all ten cases and a comparison with an Atlantic TC (Erin) follows. TC intensity labels *are not included* to avoid confusion about TC intensity and structure during the periods used in this study versus what their official intensity label (super typhoon, typhoon, tropical storm) might otherwise suggest.

3.2 Sample Cases With Evidence of a TUTT Cell's Influence on TC Motion

3.2.1 Rex-2 (06W) 1998

According to the 1998 JTWC ATCR, "the influence of three distinct TUTT cells caused Rex to deviate from its forecast northeastward track three separate times" and was considered the "paramount forecasting challenge" of the year in the northwest Pacific.

The first and second of these interactions are two of the ten distinct Pacific cases included in this study. Rex's third TUTT cell interaction, deemed the weakest of the three by the ATCR, did not meet case study criteria since another TC (07W) developed in the wake of Rex within 2000 km (and closing) after the second TUTT cell interaction (Rex2).

Rex was a long-lived TC with an initial JTWC warning on 24 August and a final on 7 September. The TC tracked generally east-northeastward from the Philippine Sea into the north central Pacific Ocean (Figs. 3.2a, b) and reached a maximum intensity of 59 m s^{-1}. The TC maintained typhoon intensity during both of the first two interactions.

Forecasting difficulties were apparent from the start. The first two "stair steps" in the TC's track were both preceded by northward motion and JTWC forecasts that the TC would threaten Tokyo. The second stair step began around 00Z 31 August with numerical model forecasts that continually exhibited a strong northward bias even as the TC tracked due east to southeastward. JTWC forecasters, however, were urged to be as certain as possible the TC was no longer a threat to Tokyo before adjusting their long range forecast away from the city and returning to a more "meteorologically sound" forecast. This is an example of a "sociopolitical influence" toward conservative persistence and not a fully scientific product. Constant adjustments to longer-range forecasts (48 to 72+ hours) based on short-term TC track deviations or fluctuating model guidance may lead to forecast vacillations over time and a loss in decision-grade forecast products and client confidence. Continuity between forecasts is, therefore, essential and the preponderance of evidence should point to a new forecast philosophy before a significant change is made (Col. Wendell Stapler USAF (Ret), JTWC Director 1998-2000, personal communication, 9 July 2007). Based on my personal experience, some of

the JTWC's rare but extreme forecast error events (2000+ km at 72 hours) are a direct result of these considerations.

3.2.1.1 Background and Identification of the Interaction Period

Rex2 was a strong TC (46-57 m s^{-1}) just prior to this case's interaction period as it tracked north at ~2 m s^{-1} before a northeastward turn. The apex of its northward motion approximately coincides with the identified interaction "start point" between the TC and a very broad and "intense" TUTT cell to the east-northeast. An infrared satellite loop shows the TC and TUTT cell initially approaching each other followed by the TC rotating around the SW periphery of the TUTT cell during the interaction period as the TUTT cell drifts slowly north (Figs. 3.3a, b). The imagery is reminiscent of Fujiwhara turning. The rotation ends with the two circulations oriented more north-south, ebbing of the TUTT cell and a resumption of the TC's northeastward track. The orientation of the two circulations begins with the TUTT cell directly ahead of the TC's path but changes to ahead and left of the TC's path. This is expected to accelerate the TC's forward speed and cause a right (southward) cross-track bias ("Right Fast" in Figure 3.1).

The separation distance between the two circulation centers at the start point is ~1340 km and just within Brand's (1972) 1390 km maximum distance for the onset of mutual cyclonic rotation between two TCs (Figs. 3.4a, b, for all cases). Based on Tables 3.1a, b, and f, the TUTT cell's maximum associated 200 hPa PV (6 PVUs) and relative vorticity (1.5 x 10^{-4} s^{-1}) (Fig. 3.5 for all ten cases) along with a deep (< 500 hPa) and moderately broad diameter (~1000 km) 200 hPa closed circulation at the interaction start point categorizes it as "intense" compared to the other cases. Figure 3.6 provides a

vertical cross-section of relative vorticity (100-850 hPa), approximately through the centers of circulation. The images offer an outstanding visualization of the circulation's intensity and depth for comparison. The interaction start point is identified by an abrupt change in the 2-point running average centroid-relative motion of the two circulations between 00Z and 06Z 31 August and a change from an initial direct approach to an apparent counter-clockwise rotation (Fig. 3.7a). The centroid-relative motion pattern is similar to LH93's Polly and Rose (1974) but appears more convex (Fig. 3.7b). After the start point, the TC turns toward the east then accelerates (~5 m s^{-1}) southeastward. This rare motion continues for ~42 hours before the TC curves back toward the east then northeastward. The "end point" of the interaction is marked by the dissolving of the *closed* 200 hPa TUTT cell circulation in the ERA-40 wind field between 18Z 1 September - 00Z 2 September and coincides with the end of the TC's southward motion.

3.2.1.2 Forecast Analysis

All three forecasts used in this comparison do very poorly (Fig. 3.8). Surprisingly, CLIPER performs the best overall with mean forecast errors (12Z 29 August – 12Z 1 September) at 24, 36, 48 and 72 hours of 178, 298, 563 and 895 km, respectively. NOGAPS performs best for the first 12 hours due to the model's initially slower forecast speeds compared to JTWC and CLIPER.

The center of the 200 hPa TUTT cell circulation remains between 156°E to 162°E and 30°N to 35°N, an area void of in situ upper air observations (rawinsonde, aircraft) and heavily reliant upon available satellite observations for model analysis (Fig. 3.9). Considering the limited in situ data available to NOGAPS at the time and the continual

sharp northward forecasts after only 12 hours (Fig. 3.10), it is reasonable to expect that NOGAPS did not accurately forecast the TUTT cell as intense or deeply structured as depicted by the ERA-40 reanalysis. The actual NOGAPS analysis was, unfortunately, not available for a direct comparison with the ERA-40 data. Improperly forecast TUTT cell structure and/or location by NOGAPS would lead to an inaccurate forecast influence by TUTT cell and poor forecast guidance. CLIPER's fundamental reliance on persistence, conversely, allows for a continuation of ~5 m s^{-1} southeastward motion with a more subtle climatological turn back toward the northeast. This significantly reduces the model's long-term errors by allowing the TC to catch up to older forecast positions.

The JTWC needed to address sociopolitical concerns before following a more meteorologically-driven forecast. This distinct change in forecast philosophy begins with their 12Z 31 August forecast after which the JTWC forecast error drops significantly. No forecasts indicate *any* southward motion until it is already well underway after 06Z 31 August. This strongly suggests an underestimation of the TUTT cell's influence on TC motion. Even after the TC is moving southeastward, all except the JTWC forecast continue to show a quick return to eastward then northward motion after only 12 hours when, in fact, the TC tracked southeastward for ~2 days.

3.2.1.3 Environmental Analysis

U and V wind components at each TC best track position are used to create mean ESL wind vectors. The final group of 13 ESLs (Section 2.3.3.3) is then statistically analyzed and visually compared to the average motion taken by the TC over the *next* six hours (i.e. ESLs represent the initial conditions). Pearson correlation coefficients

between the components of ESL and TC motion for both the entire selected period and the interaction period are determined separately. Some groups of data, however, provide only a few samples due to their short interaction period and coarse 6-hour temporal resolution (24 hours = 4 or 5 data points). Fewer samples reduce the confidence of the correlation values compared to larger data sets. Analytical depictions, though, provide graphical time series for a direct comparison.

Tables 3.2a, b list correlation values between ESLs and Rex2's direction and speed of motion. During the interaction period, TC direction correlates very well with the DLM 5°-7° (r=.96), inner 7° (r=.95) and the middle layer's 5°-7° (r=.97) along with the upper and lower layer's 5°-7° (r=.93, r=.91) radial bands. For TC speed, however, only the upper layer's 5°-7° (r=.77) and 3°-5° (r=.75) radial bands correlate well. All other ESLs have lower and/or negative speed correlations during this period. The entire data period yields generally lower correlation values. For direction, the DLM 5°-7° and inner 7° radial bands decreased to r = .77 and .82, respectively. The two inner radial bands indicate a slightly greater correlation while the 5°-7° middle layer radial band drops to r = .80. The upper and lower 5°-7° radial bands drop significantly (r = .28 and .76, respectively) while other ESLs retain correlation values of .82 or less. Speed correlations are highest within all radial bands of the upper layer and the 3°-5° DLM radial band.

Based on these results, the TC's motion is dominated by its translation during the interaction period, mostly due to strong upper layer flow. This is evident in the TC's steady 5 m s^{-1} motion and ~115° heading during much of the interaction period. Slower TC speed (~2 m s^{-1}), higher variability in TC direction and lower correlations outside the interaction period reflect the weaker and more erratic environmental steering conditions.

Figure 3.11 shows a time series of the differences between various ESL trajectory and TC motion. The four DLM radial bands (5°-7°, 3°-5°, 1°-3° and inner 7°) fluctuate slightly between time steps but remain within ~15° of the TC's direction of motion with the 1°-3° radial band furthest away. Similarly, ESL speeds remain within +/- 2 m s^{-1} of the TC's speed during most of the period. Compared to typical TC speed, this is a large but understandable variation due to the coarseness of the ERA-40 wind data. Figure 3.12 shows the same as in Figure 3.11 but only for the upper layer which begins far (~90°) from the TC's direction. The upper layer, however, line up better during the interaction period which is reflected in the higher correlation values. The most significant difference between TC motion and the mean upper layer wind vectors occurs near the beginning and end of the interaction period. This is reflected in lower correlations values. These time series, though helpful to the author, do not provide the reader a clear picture of the situation. Another method is now utilized which readily displays how ESLs change with the TC's track and helps to determine how each layer contributes to the TC's motion.

Figure 3.13 shows a time series of the mass-weighted mean wind vector for each of the four selected layers [100-500 hPa (upper) in blue, 500-1000 hPa (lower) in green, 300-850 hPa (middle) in red, and 100-1000 hPa (DLM) in purple] of the 5°-7° and 3°-5° radial bands. Based on this analysis, it is clear that the lower layer do not contribute to the TC's southward motion during the interaction period. Only the TUTT cell-influenced upper layer yields an increased southward component (especially the 5°-7° radial band) followed by the middle and DLM layers 12-18 hours into the interaction period. The speed of the TC is also greater than all layers *except* the upper layer during this period. Outside the interaction period, the upper layer's mean flow is more zonal and with a

significantly reduced magnitude. It is obvious the upper layer contributes to, and even dominates, both the direction and speed of the TC during the interaction period. But what caused the upper layer to yield such strong southward flow during this period?

Figure 3.14 shows the TC's upper layer subdivided into four geographically fixed quadrants and a mean wind vector for each quadrant at each time step. The two southern quadrants (green and red) remain relatively unchanged with only a slight increase in magnitude toward the middle of the interaction period. The two northern quadrants, NE (blue) and NW (pink), both indicate a significant change from weak/northward and strong/northward, respectively, to both strong/southward. The NE quadrant leads the NW quadrant during the first 24 hours of the interaction period. Figure 3.15 shows this is consistent with the time it takes the TUTT cell's wind field to move from the NE into the NW quadrant merged with flow from an upper level anticyclone ~14° to the west of the TC. More importantly during this first 24 hours, the TC has already begun to move southeastward while *only* the NE quadrant has a strong southward component. *This evidence implies the TUTT cell significantly influenced the southeastward motion of the TC during this period.*

Further evidence is provided by removing the TC's upper layer quadrant closest to the TUTT cell at each time step (Section 2.3.3.4) and creating a new DLM. This process removes a large portion of the TUTT cell's influence on the TC's steering environment and gives us an idea how the TC may have tracked had the TUTT cell not been present. Figure 3.16 shows the original mass-weighted DLM vector (pink) and this new DLM (blue). Notice the 5°-7° radial band of the new DLM has ~50% less magnitude than the original DLM and no southward component during the interaction period. This

- 41 -

reinforces the argument that the TUTT cell influenced TC motion. Without the TUTT cell, the TC would have taken a more east to east-northeastward track and been closer to JTWC and numerical model predictions. Prior to the interaction start point, the new DLM vector is of similar magnitude and less than ~25° to the left of the original DLM.

Observations that slightly detract from the assertion of a strong TUTT cell influence on TC motion is that the environmental winds of the two northern quadrants remain relatively strong and southward for another 6 to 12 hours *after* the interaction end point as the TC turned more east-northeastward. One should note that the end of the interaction period is marked (by definition) with the dissipation of the TUTT cell's closed 200 hPa circulation. A very sharp *trough* meshed with flow from an anticyclone to the west of the TC, however, remains for another 6 to 12 hours (Fig. 3.17). This provides modest but weakening southward flow in the upper layer. Results are also initially unclear as to why the TC turns eastward at all if the southward upper layer flow, though weakening, continues after the interaction end point? Analysis of the four layers (Fig. 3.13) indicates the lower layer (500-1000 hPa) nearly doubles in magnitude around this time toward the northeast. A transition occurs from a weakening upper layer to a strengthening lower layer dominated environmental flow which results in a DLM change and a corresponding turn in the TC's track.

Figure 3.18 shows the 5°-7° and 3°-5° radial band DLM residual vectors. Both radial bands have the anticipated north through west at ~1-3 m s^{-1} characteristics for less than half of the time steps. The results do not clearly support the anticipated beta effect theory, especially 5°-7° from the TC's center where the environment was believed to be mostly free of beta drift incorporation into observations. Prior to the interaction period,

the vectors average a westward direction at 1-2 m s^{-1}. During the interaction period, however, they gradually reverse and increase slightly in magnitude. Afterwards, the residual vector returns to a variable north-northwestward direction.

The residual vectors do show some interesting consistency/continuity. In most cases, neither their direction nor magnitude is random in time. Rather, they *gradually* and smoothly reorient from west-northwestward to eastward as the TC motion changes from northward to eastward after the interaction start point. Other potential contributing factors, such as convective asymmetries, are only minor to short-lived moderate, and located mostly to the east and southeast of the TC's center in the direction of TC motion.

Figure 3.19 shows fields of VSHW vectors and contoured magnitudes for set time steps. The fields reflect an environment far from homogeneously relative to the TC's center. A distinct shear maximum is present near the centroid of the two circulations for each time step until the TUTT cell dissipates. Elsewhere, the vertical shear looks somewhat weak and uniform except for a large and persistent maximum over the Sea of Japan, which is due to the presence of the stationary polar front jet.

Table 3.3 lists the mean VSHW direction and magnitude values prior to and during the interaction period for the three defined environments. Standard deviation values for magnitude (not displayed) over the three defined environments range from 6 to 11 m s^{-1}. This suggests a non-homogenous environment compared to the horizontally uniform environments typically used in computer modeling studies. Rex2's motion biases are found *to the left of the mean VSHW vector*. This leftward bias support results from aforementioned studies (Sections 1.2.3 and 2.3.5) which modeled TC motion in a vertically sheared environment. As a well-developed TC, Rex2 fits the proposed concept

of mutual steering between the cyclone/anticyclone couple of the TC's structure as modeled by Wu and Emanuel (1993), Flatau et al. (1994) and Wang and Holland (1996).

3.2.1.4 Rex2 Overview

Evidence shows that Rex2 was steered from a slow northward track to the east then rapidly southeast for nearly two days under strong and deep upper layer flow associated with an intense TUTT cell initially to its east-northeast. TC motion most closely matches the mass-weighted DLM 5°-7° radial band which, in turn, is dominated by this upper layer flow. Quadrant analysis of the upper layer indicates changes in the mean flow of the NE quadrant matched changes in the mean upper layer flow and TC motion. Winds around the TUTT cell predominantly flowed through the NE quadrant which links its influence on TC motion during this period. As the TUTT cell fills, southeastward upper layer flow weakens while northeastward flow within the lower layer increases. In response, the DLM adjusts and the TC turns back toward the east and then northeast.

3.2.1.5 An Alternative Viewpoint to Rex2

Chan et al. (2002) applied the concept of convective asymmetries (diabatic heating/PV distribution) and its associated effect on TC motion to Rex2 at about the same start point as the TUTT cell interaction (00Z – 06Z 31 August). Their research stated the TC *should have* tracked north to northeastward since it was embedded in a 500 hPa large-scale trough. Instead, they claimed TC motion responded to a convective maximum east to east-southeast of the TC's center. Numerical modeling of asymmetric diabatic heating's influence on TC motion indicated propagation speeds of ~1 m s^{-1}.

- 44 -

My research indicates that very different mechanisms caused the east then southeastward turn of Rex2. Analysis of the various layers and radial bands clearly shows the dramatic change in the upper layer as a whole and, more specifically, the TC's DLM and upper layer winds over mostly its NE quadrant due to the presence of a deep and intense TUTT cell (Figs. 3.13 and 3.14). The TUTT cell's wind field simply dominated the TC's environmental steering at the interaction start point. As a result, the mean wind vector of the upper layer turns southeastward on 06Z 30 August and nearly doubles in magnitude over 24 hours. This change in direction and magnitude of the upper layer controlled the TC's DLM and turned it from northeast to east then southeastward and accelerated from 2 to 5 m s^{-1} during this period.

3.2.2 Babs (20W) 1998

Babs began as a tropical depression over the southern Philippine Sea and developed into a super typhoon (Fig. 3.20). According to the ATCR, the TC interacted with a TUTT cell while moving west as a tropical storm. This interaction caused the TC to slow, weaken and turn toward the south for ~36-hours. Figures 3.21a, b, provides a water vapor and infrared satellite image of the two circulations near the interaction start and end points. Though not quite as obvious as the Rex2 example, the immense size of the associated TUTT cell is evident. As the TUTT cell moved away and filled, the TC rapidly intensified and moved northwestward across the Philippines as a super typhoon.

3.2.2.1 Background and Identification of the Interaction Period

Babs was a weak to moderate tropical storm (20-28 m s^{-1}) just prior to and during

most of the TUTT cell interaction period. Based on Tables 3.1a, b, and f, the TUTT cell's maximum associated 200 hPa PV (4.5 PVUs) and relative vorticity (1.4×10^{-4} s^{-1}) (Fig. 3.5) along with a deep (< 500 hPa) and very broad (1700 to 2200 km) 200 hPa closed circulation at the interaction start point categorizes it as "intense" compared to the other cases. Figure 3.22 shows vertical cross sections of relative vorticity where the lopsided scale and magnitude of the TUTT cell over the TC, especially early on, is apparent. The interaction start point (12Z – 18Z 17 October) is identified by a ~90° right turn and the onset of a counterclockwise orbit after an initial direct approach of the circulation's unweighted centroid-relative motion (Fig. 3.23a). This is followed by another sharp right turn 48 hours later which marks the end point (12Z – 18Z 19 October). The pattern is similar to LH93's Mac and Nancy (1979) but again slightly more convex during the orbit period (Fig. 3.23b). The separation distance between the two circulation centers at the start point is ~1500 km (~810 nm), greater than Brand's (1972) 1390 km (750 nm) maximum distance for two TCs (Figs. 3.4a, b), and remain less than this distance throughout the interaction period. The two circulations begin oriented with the TUTT cell to the rear and right of the TC. This orientation is expected to add a strong left (southward) cross-track bias and a deceleration of its westward motion ("Left Slow" in Figure 3.1).

3.2.2.2 Forecast Analysis

All three forecasts perform fairly well (Fig. 3.24). The JTWC forecast performs best out to 12, 24, 36, 48 and 72 hours with errors of 94, 152, 211, 260 and 333 km, respectively. Compared to Rex2, this TC's slow motion (1-2 m s^{-1} versus 5-6 m s^{-1}) and

accompanying forecasts (similar speed, though typically wrong heading) played a key role in keeping forecast errors small since none of the forecasts reflect the TC's southward motion during the first half the interaction period (Fig. 3.25). Only JTWC and CLIPER indicate southward motion after this point and for only the first 12 hours.

NOGAPS forecasts north through northwestward motion during the interaction period with nonlinear tracks 24 hours either side of the start point. A comparison with some of LH93's binary TC cases suggests that the model may have forecast a binary interaction between the TC and the TUTT cell. Due to the TUTT cell's large size (Fig. 3.26), depth and similar appearance of the two circulations from just below 400 hPa down to 700 hPa (Figs. 3.27 a-d), this would not surprising. Additionally, the TUTT cell's comparatively data-rich location near the Marianas Islands should have provided rawinsonde, surface and aircraft observations which support this hypothesis (Fig. 3.9).

3.2.2.3 Environmental Analysis

Tables 3.2a, b shows correlation values between the ESLs and Babs' direction and speed of motion, many of which are rather low especially with respect to direction during the interaction period. Low correlation values may be due to the TC's slow speed and poorly defined center during the period (18Z 15 October through 12Z 20 October).

During the interaction period, the highest speed correlation for the 5°-7° radial band is with the middle layer ($r = .77$). The 3°-5° and 1°-3° radial bands yield speed correlation coefficients between .51 and .48 for the DLM and .68 and .70 for the upper layer, respectively. Regarding TC direction during the interaction period, the 5°-7° radial band for the middle layer correlates best ($r = .71$). For the entire period, ESL direction

correlation is much higher overall. The 5°-7° middle layer and DLM are highest, increasing to r = .85 and .82, respectively. Speed correlation values, conversely, decrease with the 3°-5° middle layer yielding the highest correlation (r = .51).

Based on Figures 3.28a, b, c, the DLM and middle layer for all radial bands are close to the TC's trajectory up to the start point. Afterwards, all DLM steering vectors turn south in response to the influence of the upper layer in all three radial bands. The TC (21 m s^{-1} intensity) responds with slow southward motion. The 5°-7° and 3°-5° DLM radial bands are closest to TC motion during the interaction period while the 1°-3° radial band continues to turn further left. It is evident in this analysis that the upper layer provides all southward flow to the DLM since the lower layer remains northward and at half the magnitude as the upper layer. After the interaction end point, the upper layer in all three radial bands, followed by the DLM, lower and middle layers, turns more westward and decrease in magnitude as the TC tracks toward the northwest.

It is noted that the initial similarity of the DLM's 3°-5° and 5°-7° radial bands changes as the TC intensifies (Fig. 3.28d). Prior to and throughout the first half of the interaction period, Babs is a weak to moderate tropical storm. Both radial bands are similarly close to TC motion with 3°-5° radial band actually closer to TC motion. As the TC reaches super typhoon strength, however, the DLM's 5°-7° radial band becomes consistently closer to TC motion. Compared to Rex2, Babs has a much weaker and less organized wind field at the start of its interaction period (Fig. 3.29). DeMaria and Kaplan (1994) suggested a simple statistical correlation between TC intensity and the size of its associated wind field for "typical" TCs in the Atlantic. A "weak" TC and, thus, smaller horizontal wind field with height implies the best radial band for TC steering should be

closer to its center compared to a TC of typhoon intensity. This is the case for Babs. As the TC intensifies, the radial band closest to actual TC motion extends further out from the TC's center and results in a more accurate 5°-7° radial band of the DLM.

Figures 3.30a, b. show the geographically fixed quadrant analysis of the upper layer. Notice the SW quadrant (green) radial bands remains relatively unchanged while significant changes in the NE quadrant (blue), the quadrant closest to the TUTT cell, coincide with those of the upper layer as a whole and TC motion (Fig. 3.28). The NW quadrant's vector changes in a similar manner as the NE quadrant but with a ~24 hour lag, about the same time it takes for the TUTT cell's northerly flow to move into the NW quadrant (Figs. 3.31 a, b). The SE quadrant is similar to the NE quadrant (only at 5°-7°) but with considerably less magnitude due to its greater distance from the more intense TUTT cell flow. The TC responds to these upper layer flow variations and links the TUTT cell's influence to the TC's southward motion.

Figures 3.32a, b show the original mass-weighted DLM vector (pink) and a new DLM vector (blue) with the quadrant closest to the TUTT cell removed. Both the 5°-7° and 3°-5° radial bands of the *new* DLM indicate magnitudes ~50% less than the original DLM before the interaction period and with much more eastward flow compared to the original DLM's southward flow. This reinforces the evidence that the TUTT cell influenced the TC's motion.

Figure 3.33 displays Babs' residual vectors. Prior to the interaction period when the TC is a very weak tropical storm, the residual vectors are northeastward with moderate (2-3 m s^{-1}) magnitudes. During and after the interaction period as the TC reaches moderate to strong tropical storm then typhoon and super typhoon status, both

radial bands gradually turn northwestward (~1 to ~2.5 m s^{-1}), similar to beta drift characteristics. The 5°-7° radial band provides a slightly better representation of beta drift characteristics as it remains northwestward longer than the 3°-5° radial band and retains a greater magnitude. Similar to Rex2, there is regularity and consistency with the vectors. Regarding other contributing TC propagation factors, initial moderate to strong vertical shear displaces convection asymmetrically toward the south, though this decreases significantly towards the end of the interaction period.

Similar to Rex2, fields of VSHW for Babs (not shown) yield a maximum near the centroid of the two circulations during the interaction period. A substantial extension of high VSHW values (15 - 20 m s^{-1}) extends over the TC's center prior to and during most of the interaction period which resulted in the TC's weak intensity. As shear values decrease after the interaction, the TC rapidly intensifies.

Table 3.4 provides the mean VSHW direction and magnitude values prior to and during the interaction period for the three defined environments. Every time step and environment indicates a direction of TC motion to the *right* of the mean shear direction. This is contrary to Rex2 results and does not support the left-of-mean-shear-vector bias. Based on the theorized mechanism for the bias, this weaker and less developed TC does *not* have a mature, vertically coupled cyclone-anticyclone structure during the period of study as did the more intense and well-developed Rex2. To support this reasoning, we compare Rex2 and Bab's 100 hPa winds (Fig. 3.34). Notice Babs' upper levels are dominated by easterly to northeasterly flow and the approaching TUTT cell. Rex2, however, reveals a developed anticyclone, though displaced slightly to the west, with the TUTT cell to the east-northeast below ~150 hPa.

- 50 -

3.2.2.4 Babs Overview

Babs begins as a slow westward moving weak to moderate tropical storm within a highly sheared environment. Evidence indicates the TC's motion changed from westward to southward due to the modification of its surrounding upper layer by a large TUTT cell to its northeast. The upper layer modification causes the TC to turn toward the south for ~36 hours. TC speed during this period, however, remains rather slow due to the TC's weak intensity and poorly developed structure. As the TUTT cell moves away and the TC intensifies, the TC slowly accelerated back toward the west then northwestward in a reduced shear environment. This case also reveals evidence that the radial band closest to TC motion can vary from the 3°-5° to the 5°-7° during a TC's intensification based on an expanding wind field with increasing intensity.

3.2.2.5 Comparison of the Rex2 and Babs Response

Rex2 and Babs are cases with similar separation distances and TUTT cell characteristics but with very different TC intensities. Rex2 is a strong typhoon (~50 m s$^-$^{1}) and Babs is a moderate tropical storm (~25 m s^{-1}) during their interaction periods. Rex2 responds promptly to the radical change in upper layer flow (turns and accelerates to ~5 m s^{-1}) while Babs' response is much less impressive (gradual ~1-2 m s^{-1} turn). Had Babs been more well-developed under the same conditions, a greater response might have been expected based on the deeper layer of environmental steering associated with more intense TCs and incorporate more of the upper layer flow (Dong and Neumann 1986, Velden and Leslie 1991).

A TC's intensity also affects its resistance to shearing (radial motion) in a vertically sheared environment. Holland (1983a, 1984) suggested that inertial stability, or the rotational stiffness of the TCs inner few hundred kilometers, provides resistance to various flow distortions based on the governing equations of motion. He referred to Eliassen's (1952) inertial stability parameter for an axisymmetric vortex, essentially the absolute vorticity multiplied by the absolute angular moment, defined as:

$$(\zeta_r + f)(f + 2v_s/r) \tag{3.1}$$

where v_s is the symmetric wind speed higher and r is the radius of flow. According to Holland, a horizontal perturbation across a positive radial gradient of absolute angular momentum will produce a gradient wind imbalance and resistance to further radial motion. Stronger inertial stability means a greater resistance. Inertial stability is greatest at a TC's lower layer and decreases with height due to a shrinking radius of cyclonic winds (i.e. the "effective radius") and reduced wind speed. The TUTT cell's wind field predominantly influences the upper half of the TC's circulation. Figure 3.35 shows meridional cross sections of each circulation's relative vorticity field (5×10^{-5} s^{-1} highlighted) near the case's respective interaction start points. In this comparison, Rex2 is the more intense and well-developed of the two TCs and has greater resistance to horizontal shearing. Babs, on the other hand, is a weak and less developed TC with less resistance to shearing. The lower half of its circulation responds slowly to the southward shear in the upper half and lags behind compared to Rex2 which moves as a whole. A comparison of the two TC's 850 hPa and 500 hPa circulation centers in the ERA-40 data (not shown) reveals Babs with nearly twice the average separation distance of the two level's circulation centers compared to Rex2 (~315 versus ~162 km, respectively) during

their respective interaction periods. This amount of tilt is highly unlikely within an actual TC and is certainly not evident in the TC's satellite imagery. It does, however, emphasize the structural difference between the two TCs of differing intensity.

3.3 Sample Case Without Evidence of a TUTT Cell's Influence on TC Motion

3.3.1 Bart (24W) 1999

Bart formed in the central Philippine Sea east of Taiwan and eventually accelerated northeastward over western Japan (Fig. 3.36). It was during this final northward advance that a TUTT cell moved to the TC's east then in tandem to the north. The TUTT cell appears large and intense on water vapor imagery (Fig. 3.37), but investigation into the TUTT cell's structure reveals a perfect example of misleading satellite imagery.

3.3.1.1 Background and Identification of the Interaction Period

Bart was an intense typhoon (> 50 m s^{-1}) during the entire period. Based on Tables 3.1a, b, and f, the TUTT cell's maximum associated 200 hPa PV (2.5 PVUs) and relative vorticity (9 x 10^{-5} s^{-1}) (Fig. 3.5) along with a shallow (250 to 300 hPa) and moderately narrow (550 to 950 km) closed 200hPa circulation at the interaction start point categorizes it as "weak" compared to the other cases. Figure 3.38 shows relative vorticity vertical cross-sections and a 300 hPa (lowest level with a closed circulation at anytime during the interaction period) streamline analysis of the two circulations at various times around the case's interaction period. The shallowness of the TUTT cell compared to Bart is obvious. The interaction start point (18Z 21 September - 00Z 22 September) is identified by a ~45° right turn after an initial direct approach (Fig. 3.39a), similar to

LH93's Polly and Rose (1974) (Fig. 3.39b). The separation distance at the start point is ~1065 km (575 nm) (Figs 3.4a, b) and remains within this distance until the TUTT cell dissipates. The orientation of the two circulations begins with the TUTT cell to the right of the TC's track. This is expected to mostly decelerate the TC's forward speed and add a slight right (eastward) cross track component of motion ("Right Slow" in Figure 3.1).

3.3.1.2 Forecast Analysis

NOGAPS forecasts perform the best followed by JTWC and CLIPER (Fig. 3.40). Similar to Babs, the TUTT cell and TC are located within a data rich region. The initial slow motion of the TC and uncertainty over the timing of its acceleration toward the northeast caused much of the low forecast error. With the TUTT cell nearly due east of the TC, northerly return flow on the TUTT cell's western half is expected to impinge on the TC's environment by adding a southward component to the upper layer winds. This meridional contribution is expected to turn the TC southward or simply slow its northward progression. It is doubtful that any of the forecasts (models or JTWC) anticipated a direct interaction with this TUTT cell based on their rather linear forecast tracks and relatively accurate speed assessments (Fig. 3.41).

3.3.1.3 Environmental Analysis

TC and ESL speed correlations are rather high (Tables 3.2a, b). During the interaction period, the 5°-7° and inner 7° (DLM) radial band correlate well for all layers (r > .89) except the lower layer. Correlations for the same ESLs decrease during the entire period with the upper layer retaining the highest values at 5°-7° (r = .93). The inner radial

bands all correlate less. Regarding TC direction, overall ESL correlations are lower. During the interaction period, the DLM inner 7° radial band has the highest correlation (r = .62). Other ESLs retain much lower correlation values (r < .44 or negative). During the entire period, however, both the DLM inner 7° and upper layer 5°-7° radial bands indicate high correlation (r = .96) with TC motion.

Figure 3.42 shows the mean 5°-7° ESL vector time series for all layers and shows an upper layer influence consistently to the right of and with similar magnitude (+/- 1 m s^{-1}) as the TC's trajectory. The other layers are more aligned with TC motion. There is no clear evidence of a more southward (reduced northward) influence on the upper layer by the TUTT cell. A small eastward bias might also be expected as winds flows around the southern periphery of the TUTT cell toward the east, but none is found.

Analysis of Bart's 200 hPa wind fields indicate the flow associated with the TUTT cell barely extend to within 5° of the TC's center even though its separation distance is closer than many other cases (Fig. 3.43a). The TUTT cell's shallow circulation simply could not produce an identifiable influence on the upper layer as a whole (Fig. 3.43b).

Based on the orientation of the two circulations, the TC's two eastern quadrants are expected to reveal the influence of the TUTT cell on the upper layer. Only the SE quadrant, however, suggest a possible influence of the TUTT cell by basically not providing any northward component of motion to the upper layer while other quadrants do (Fig. 3.44). The SE quadrant remains weak and eastward as the TUTT cell's flow is countered by southerly flow within the same layer/quadrant that is not associated with TUTT cell's circulation (i.e. from 300 to 500 hPa). The TC's upper layer is instead dominated by the NE and NW quadrants.

Figure 3.45 shows the original mass-weighted DLM vector (pink) and the new DLM vectors (blue) with the TC's upper layer quadrant closest to the TUTT cell removed. Before the start point, both the original and new DLMs are similar in both magnitude and direction. During the interaction, however, the new DLM has a reduced magnitude (~10-40%) and suggests the TC would have tracked even *slower* toward the north *without* the closest quadrant's contributions. Since the TUTT cell provides flow that counters the TC's northward motion, it appears that this TUTT cell did not influence the TC's upper layer and motion even though there are shared characteristics with cases with an identifiable TC response. The new DLM's direction, meanwhile, remains close (< 20° to the left) of the original DLM.

Figure 3.46 shows Bart's residual vectors with a steady west to southwestward vectors from .5 to 3 m s^{-1}. This provides little support for the anticipated beta effect characteristics. There is, however, persistence towards the same direction and continuity of the vectors over time. Between the two vectors, the 5°-7° radial band retains greater magnitude, reflecting the lack of an included beta drift in its environmental observations.

A distinct VSHW maximum (20 to 25 m s^{-1}) is located near the centroid of the two circulations during the interaction period (not shown). Elsewhere within 7° of the TC's center, values are comparatively low (< 15 m s^{-1}) except for an extensive area to the north through west of the TC related to the stationary polar front jet. Table 3.5 provides the mean VSHW direction and magnitude values (VSHW only) prior to and during the interaction period. TC direction is to the left of the mean VSHW direction in all of the periods and environments which is consistent with Rex2 and results from the aforementioned studies.

3.3.1.4 Bart Overview

Bart was a well-developed and intense TC during its interaction period. A TUTT cell approached from the east and turned north in tandem with the TC. At the interaction start point, conditions met all of the criteria as in the previous cases but did not have an identifiable influence TC motion. The greatest distinction between this case and the two previous cases was the shallow depth and weak intensity of the TUTT cell. This was surprising since it initially had an impressive but misleading appearance on satellite imagery. The western half of the TUTT cell's wind field only penetrated into the TC's 5°-7° radial band at 200 hPa which prevented an anticipated alteration of TC motion in either the entire upper layer or any of its quadrants during the interaction period.

3.4 Summary of All Ten Pacific Cases

Tables 3.1a-f list the ten cases and provides quantified and qualified summaries of each TC's and TUTT cell's characteristics and analysis results. A line is now drawn between cases that show evidence of a TC's response to an associated TUTT cell wind field and those that do not based on the methods applied in this study. Most TUTT cell characteristics fit nicely into these two groups except for one outlier from each group, Amber and Fred (Fig. 3.47), which will be discussed further in Section 3.4.1.

Comparing the two groups against my initial satellite-only assessment reveals four of the ten initial estimates are incorrect. One case appears to have a weak TUTT cell yet provides evidence of its influence on the TC's motion (Amber). Three other cases (Bart, Fred and Saomai), conversely, had moderate or intense "looking" TUTT cells expected to provide identifiable evidence of their influence on TC motion using my methods, but did

not. These results emphasize the need for forecasters to look at TUTT cell structure in addition to satellite imagery.

Interaction periods range from ~24 to ~48 hours with an average of ~30 to ~36 hours (Table 3.1c). Separation distances at the interaction start point vary from ~680 to ~1900 km with an average of ~1370 km and a standard deviation of ~410 km. The average for all cases is essentially the same as Brand's (1972) 1390 km maximum distance for the onset of mutual cyclonic rotation between two TCs. Three of the cases (Babs, Rex1, Bolaven) with evidence of a TUTT cell's influence on TC motion, however, have separation distances of ~110 to ~310 km (~1° to 3°) greater than this average. Forecasters should be aware that interactions between TC's and TUTT cells can occur at distances beyond Brand's 1390 km distance (up to ~1700 km) due to the larger scale of the TUTT cell's wind field.

Similar characteristics exist between the onset of TC – TUTT cell interactions and the onset of binary TC interactions, as found by LH93. First, interactions begin rather quickly (< 12 hours) based on the analysis of unweighted centroid relative motion. LH93 stated that this approach did not always reveal the true center of rotation for two TCs but was necessary since they could not objectively compute the net circulation of each TC due to data limitations and the lack of a unique separation between the TC and its environment. Likewise, a weighted approach is not applied in my study for these reasons but also due to the dissimilarity and a lack of a mutual "standard" between the two circulations (e.g., intensity and size). Second, most (80%) TC – TUTT cell cases, versus only half of LH93's cases, reveal approach rates that are fastest prior to their interaction start point with a gradual slowing during and afterwards their interaction periods (if two

cyclones are still present). This may have more to do with each circulation's environmental steering prior to the interaction period than an attraction between the two vortices. Finally, as with LH93's binary TC study, 30% of the TC – TUTT cell cases suggest an *anticylonic* unweighted centroid-relative orbit prior to their interaction periods.

Most cases involve TUTT cells north of the TC's latitude and typically to the east of the TC's longitude. This orientation may simply be a factor of each circulation's genesis region and motion characteristics. In half of the cases, the TUTT cell is "ahead" of the TC's track and affects its leading quadrant(s). Other orientations include moving in tandem with the TC (e.g., Bart) and approaching the TC from behind (e.g., Babs).

Comparison of the TUTT cell's closed circulation down toward the surface from 200 hPa find that the deeper the TUTT cell circulation, the more likely there is evidence of the TC's response to the TUTT cell's wind field (Table 3.1a). Closed circulations down to 400 hPa or lower usually lead to an unidentifiable influence on TC motion (except for Bart). Deeper circulations result in a greater influence on the upper layer and, therefore, the TC's DLM. Above 200 hPa, the closed circulation typically disappears between 150 hPa and 100 hPa due to the presence of a warm core near the tropopause.

The broadness of the TUTT cell's 200 hPa wind field alone (estimated with the outermost closed 10 m isoheight) is less of a factor than depth. Since the broadness and separation distance between the circulations are interdependent, the TUTT cell must obviously flow to within the TC's steering environment (~7°) to influence its motion. TUTT cell associated winds on the order of ~15 m s^{-1} at each TC interaction start point are also necessary based on the cases that provide evidence of the TUTT cell's influence.

TUTT cell intensity, or the maximum 200 hPa relative vorticity and PV near the interaction start point, is also a factor. Cases where evidence is found typically yield maximum 200 hPa PV values of greater than 2.5 PVUs and ζ_r values greater than 1.1 x 10^{-4} s^{-1}. Fred is the only exception to this finding.

TC intensity is a factor with respect to how the TC responds to the TUTT cell's wind field. TCs Rex2 and Babs (Section 3.2.2.5) provide an example of the range of responses in TC motion between two TC under similar conditions but with significantly different intensity (25 and 50 m s^{-1}). The intensity difference leads to variations in the TC's optimal steering layer and its inertial stability with height.

Most cases indicate the 5°-7° radial band of the DLM and middle layer statistically correlate and graphically match best with TC trajectories during their identified interaction periods. These results generally support findings provided by previous observational TC motion studies. In situations where TC – TUTT cell separation distances are under ~700 km (Ewiniar, Amber), the 5°-7° radial bands incorporate the far side of the TUTT cell circulations and the inner two radial bands (3°-5° and 1°-3°) often appear closer to actual TC motion. The 5°-7° radial band, meanwhile, usually provide unrepresentative guidance during the interaction period.

The residual vector was expected to have the characteristics discussed in Section 2.3.4 (north through west, ~1-3 m s^{-1}) within the DLM 5°-7° radial band. Figure 3.48a shows polar charts of the residual vectors for all ten Pacific cases. Only one of the ten cases retained the expected characteristics for all of their utilized time steps (Amber, Fig. 3.48b), three of the remaining nine for 50-99% of the time and the rest below 50%. Wang and Li (1992) had suggested a latitudinal dependence on beta drift magnitudes

(~45% decrease from 10°N to 30°N), but variations in residual vector magnitude with latitude is not obvious within my results.

The residual vectors do have some interesting characteristics, though. First, six of the cases (Amber, Bolaven, Babs, Rex1, Fred and Bart) have reasonably tight groupings, though only Amber and Babs are toward the northwest. Second, most cases reveal a smooth directional transition of the vectors with time (Rex2 and Babs in Figures 3.18 and 3.33, respectively). This suggests order to the modulation of the TC's propagation components. Perhaps the presence of a TUTT cell, which typically increases a TC's environmental VSHW, is involved since the greatest change in the residual vector's direction is often centered on the defined interaction's start and end points.

Beta gyre modulation is another possible mechanism for residual vectors other than toward the northwest at ~1-3 m s^{-1}. Fiorino and Elsberry (1989) described the rotation of the beta gyres by the TC's own cyclonic (inner) circulation in a quiescent barotropic environment. Wang and Li (1992) modeled an adiabatic upper level anticyclone (550 – 100 hPa) and lower level cyclone (1000 – 550 hPa) in their baroclinic model. The two circulations lack of vertical coupling resulted in a separate southwest drift of the anticyclone and a northwest drift of the cyclone. Including diabatic processes (convective heating), however, Wang and Li suggested an integral circulation could be held together by the vertical coupling. They further suggested the two components of beta drift would essentially cancel each other out. Li and Wang (1993) suggested TC intensity changes and development over time may lead to significant rotation/modulation of the beta gyres. Their results yielded northeastward orientation of the beta drift and even TC looping in a quiescent environment. Wang and Holland (1996) modeled both

adiabatic and diabatic (vertically coupled) baroclinic vortices in a similar manner. They noted an anticyclonic rotation of lower-level beta gyres due to the cyclone's coupling with its upper level anticyclone. Similarly, one could speculate the onset of strong upper layer TUTT cell winds over a large portion of the TC may contributed to an adjustment of the beta drift by a modulation of the beta gyres.

Subjective "eyeball" estimates (minor, moderate or significant) of TC convective asymmetries using time lapse infrared satellite analysis and based on the author's experience reveals seven of ten cases have minor, two have moderate and one has significant convective asymmetries during periods used in each study (Table 3.1e). Five of the six cases with tight residual vector groupings have minor asymmetries while the sixth (Babs) has moderate. The cases with moderate or significant convective asymmetries tend to be asymmetric in the direction of TC motion and downwind vertical shear. It is unclear, however, if this resulted in an influence on TC motion or if the vertical shearing of the TC's environmental winds are simply steering the TC.

VSHW analysis indicates 8 of the 10 cases support a "left-of-VSHW" mean vector bias. Two of the eight TC cases sustain this leftward bias only outside of their interaction periods. A strong relationship between weaker TCs and a lack of support for this leftward bias is also found. This relationship is speculated to be due to the less-intense TC's weaker upper-level outflow and the lack of an anticyclone/cyclone couplet compared to the stronger, more developed TCs.

3.4.1 Outlier Cases

Amber provides evidence of an influence on TC motion though it the characteristics

of its TUTT cell fit into the group of cases that do not provide evidence (Fig. 3.47). The TUTT cell's closed circulation depth is shallow (down to ~300 hPa) and it has a weak circulation maximum 200 hPa PV (~2 PVUs) and ζ_r (~1 x 10^{-4} s^{-1}) compared to other cases with discernable evidence of a TUTT cell's influence on the TC's motion (Tables 3.1a, b and f). These characteristics are likely overshadowed by the TC's genesis which coincided with the TUTT cell's proximity (< ~700 km). The TC's intensification and increasing vertical-structure just prior to and during the interaction period allows the two circulations to "feel" one another. The TUTT cell wind field, though shallow, is able to reach close to the TC's inner core circulation (versus outer 5°-7° envelop) and add a northward component of motion.

Contrary to Amber, Fred has a very deep and intense TUTT cell but at a relatively large separation distance (1600 km). The TUTT cell has an expansive wind field at 200 hPa (Table 3.1f) but narrows quickly with descending height. During most time steps, only the 200 hPa wind field reaches to within 7° of the TC's center. The TUTT cell does not seem to influence enough of the upper layer to yield an identifiable response from the TC. Rather, synoptic analysis of the basin suggests a large stationary anticyclone to Fred's north, at times meshed with the TUTT cell's flow on its eastern periphery, is responsible for Fred's westward motion and an ~18 hour southward (left cross-track bias) dip originally credited to the influence of the trailing TUTT cell.

3.4.2. Application of a TUTT Cell Induced Bias

A track "bias" is considered a deviation to TC motion based on the contribution of the TUTT cell's wind field meshed with the TC's environmental steering and with all

other surrounding environmental features taken into account. An unforecast but transpiring bias is identified by a TC best track position consistently to one side (or ahead/behind) of an ensemble forecast that fits an anticipated contribution by the TUTT cell's wind field to the TC's environmental steering.

The TC motion contribution is based on an overlap of the TUTT cell's wind and TC's environment (inner 7°). An example might be if a TC is moving north toward a stationary TUTT cell. An initial eastward track bias would be expected due to the contribution of predominantly eastward flow around the southern periphery of the TUTT cell into the TC's steering environment. Deep, broad and intense TUTT cells would produce a greater eastward deflection in the TC's track than their weaker counterparts as would more intense versus weaker TCs. As the orientation of the TC and TUTT cell change, so would the forecast TC track bias as long as the TUTT cell is a factor.

If it could be established that a numerical model is failing to incorporate a TUTT cell's wind field into its products, guidance provided by this study could help reduce forecast errors by providing decision-grade criteria and scenario-based TC track biases (i.e. a nudge) to their future ensemble forecast. If a bias is suspected to have already begun, a future forecast could be adjusted to match the bias by applying greater persistence (e.g., for 12 to 24 hours instead of the "normal" 6 to 12 hours) or even by increasing the bias if warranted. This guidance is based on the better performance of CLIPER over NOGAPS in cases where NOGAPS fails at representing the TUTT cell's influence even after non-standard TC motion is well under way (e.g., Rex2). The application of persistence is more important if the TC is moving quickly due to the amplifying effect on forecast error with time. NOGAPS and, to a lesser extent, the

JTWC (due to their higher reliance on numerical over statistical models) do not incorporated persistence. Conversely, in cases with a low likelihood of an influence by the TUTT cell's wind field on TC motion, NOGAPS performed better than CLIPER. A bias in TC motion would not be expected and forecasters would give greater weight to numerical models in forecast development.

3.5 An Atlantic TC Comparison

An Atlantic TC is selected to run an initial test of the developing conceptual model and the quantifiable values for determining the likelihood of a TUTT cell interaction as ascertained through analysis of the ten Pacific cases. Erin (1995) is believed to have interacted with "an upper level low" (Rappaport 1995). The ERA-40 analysis indicated the low's structure was very similar to previous TUTT cells with a source (24°N, 45°W) near the north Atlantic TUTT. Tables 3.6a-f list the quantitative and qualitative characteristics for Erin and its associated TUTT cell.

Erin developed over the Bahamas and tracked west-northwestward from 31 July to 3 August (Fig. 3.49). Around 00Z 1 August (the interaction start point), the TC deviated northwestward for 12 to 18 hours which defines the interaction period The TUTT cell, meanwhile, was generally tracking southwestward, ahead of the TC which had just reached category 1 status ($\sim$33 m s^{-1}).

Infrared satellite imagery indicates a somewhat erratic pattern to the TUTT cell's motion. Compared to the ten Pacific cases (Tables 3.1a-f), the TUTT cell is of "moderate" intensity with a maximum 200 hPa PV of $\sim$3.7 PVUs, a maximum relative vorticity of $\sim$1.2x10^{-4} s^{-1} (Fig. 3.5) and a moderately deep ($\sim$400 hPa) and broad ($\sim$650

km) closed circulation at the interaction start point. Figure 3.50 shows relative vorticity cross-sections which clearly demonstrate the similarity in scale of the two circulations. The separation distance during the period closes quickly from ~650 km to ~370 km due to the developing TC's proximity to the approaching TUTT cell, similar to Ewiniar and Amber. Erin, as with Ewiniar in the Pacific, has a moderately deep TUTT cell circulation which leads to convergence of the ERA-40 wind fields at some levels and occasional difficulty with isolating the TUTT cell's separate 200 hPa center. Regardless, the orientation of the two circulations is expected to add a cross track (to the right or northward) component to the TC's motion with some acceleration late in the interaction.

NHC forecasts are linear toward the west-northwest through 48 hours for every 6-hourly issuance from 00Z 31 July to 00Z 2 August (Fig. 3.51). No change in forecast philosophy (e.g., a track deviation) occurs prior to or during the period in which the TUTT cell's "steering currents" are described to have biased the TC's track to the right (north). Consequently, TC motion biases remain to the right of the NHC forecasts prior to and during the interaction period. Two dynamic forecast models, the NCEP Global Forecast System (AVN) and Geophysical Fluid Dynamics Laboratory (GFDL), share similar forecast tracks. The GFDL, however, accurately forecasts a subtle northward deviation with its forecasts 6 to 18 hours before the actual northwestward TC track bias. CLIPER, meanwhile, indicates a gradual recurve scenario toward the north.

Figures 3.52a-c shows the mean contribution by each ESL. The figure clearly illustrates a northward deviation of the upper layer within the 1°-3° and 3°-5° radial bands throughout and for 6-12 hours on either side of the interaction period. The lower layer does not contribute to the northward bias whatsoever. At 5°-7°, the upper layer displays

weak and/or southward steering as it incorporates some of the TUTT cell's southward return flow while the lower layer maintains a vector close to TC motion. Results indicate that the upper layer (within 5°) is a significant factor in the TC's unexpected northward deviation.

The NW quadrant of the TC's upper layer was expected to show the greatest contribution by the TUTT cell based on their orientation. Both the NW (1°-3° radial band) *and* NE (1°-3° and 3°-5° radial bands) quadrants, however, are the principle contributors to the mean upper layer winds (Figs. 3.53a-c). They are both dominated by TUTT cell associated flow due to the circulation's proximity. The NE quadrant's flow is also a mesh between the TUTT cell's wind field and the TC's own outflow enhanced by the TUTT cell's presence (Fig. 3.54). The SE and SW quadrants in all radial bands, meanwhile, remain comparatively negligible.

Figures 3.55a-c shows the original mass-weighted DLM vector (pink) with the new DLM vectors (blue) with the upper layer quadrant closest to the TUTT cell removed. An indisputable influence by the TUTT cell is evident within the two inner radial bands of the new DLM. They both show reduced magnitudes (~10-20%) but, more significantly, reveal a direction consistently 30° to 55° to the left (westward) of the original DLM during the interaction period. The 5°-7° radial band of the new DLM, meanwhile, stays close to the original DLM in both direction and magnitude.

In summary, evidence found here of a TUTT cell influence on TC motion fits the developing conceptual model guidance. Furthermore, the results adds credence to the NHC's post-analysis claim that steering flow associated with an upper level low caused Erin to deviated more northwestward than forecast.

3.6 Frequency of Occurrence

TCs develop in the northwest Pacific Ocean basin throughout the year, but predominantly occur during the summertime along side the TUTT and associated TUTT cells. During the period of this study, the JTWC ATCR documented 169 TCs at tropical storm (17 m s^{-1}) or greater intensity. Each TC lasted ~5 days at tropical storm intensity or greater which yields ~845 total days. Initially, 25 (~15%) of these TCs had a TUTT cell within 2000 km at some point in its life as a tropical storm or stronger TC, though only nine were used due to the case study criteria. The average TC-TUTT cell interaction in this study lasted ~1.5 days. Add another ~1.5 days before and after the interaction period for the time forecasters would monitor the TUTT cell yields a total of ~4.5 days per event. This leads to ~112 days total for the initial 25 TCs, or ~13% of the time a TC was active. Even if we count only the six of the original ten cases used in this study with evidence of the TC's response to a TUTT cell's wind field we get ~8% of the time (~1.5-2/year). This is rather frequent considering this TC basin is the most active in the world and that there is no known operational guidance for such occurrences.

CHAPTER 4

DISCUSSION AND AN OBSERVATIONAL COMPARISON

4.1 Discussion

This section provides succinct answers to the questions raised in Section 1.5 and are based on the analysis of the eleven cases in Chapter 3.

How does a TUTT cell directly influence a TC's motion? A TUTT cell affects a TC's environmental steering flow and, therefore, its motion. Cases in this study demonstrate this connection based on analysis of the TC's environmental flow within specific layers, at set distances (radial bands) and inside particular quadrants around a its center. The wind field of a TUTT cell, typically only in the upper half of the troposphere, can alter TC's DLM steering flow. Dependent on which ESL (layer and radial band) is most responsible for TC steering at the time, a change in the ESL due to the impingement of large scale TUTT cell winds can lead to a downwind bias in the TC's motion. The direction of this bias is most associated with the quadrant(s) of the TC closest to the TUTT cell's encroaching wind field based on the two vortices' orientation.

Does a TC influence a TUTT cell's motion? Yes, TCs appear to influence TUTT cell motion. Figure 4.1 shows all of the eleven cases' actual tracks and unweighted centroid-relative motion for the TCs (blue) and their associated TUTT cells (red). Based on the tracks of two independent *cyclones*, most cases could arguably look as if there is a mutual influence on motion between the two circulations. Even the centroid-relative motion looks similar to LH93's binary TC findings. My method, however, is used solely for identifying change-points between the two tracks in order to define an interaction

period and does not assume a mutual interaction. Section 4.2, however, provides a baroclinic perspective on TC-induced TUTT cell motion.

Satellite loops reveal varied outcomes depending on the circumstances. Broader and more intense TUTT cells at greater distances from an associated TC (i.e. Rex2) do not appear to respond to the TC's wind field. Cases with smaller TUTT cells and in proximity, however, typically appear to reveal an interaction reminiscent of binary TC interactions (e.g., Fujiwhara). These cases included Ewiniar, Amber and Erin.

We must consider the structural differences of the two circulations if we are to look at TC-induced TUTT cell motion as a whole. Compared to LH93, my cases do not have similarly structured cyclones. Rather, the two circulations have an inverted structure. At the most intense level of TUTT cell (200 hPa), the TC is typically dominated by its anticyclonic outflow and has a much broader scale than its cyclonic inflow (Fig. 1.2). It would seem the *anticyclone* should be the primary part of a TC that reaches high enough and with sufficient horizontal extent to exert an influence on TUTT cell motion. Looking at Figure 4.1 and visualizing an anticyclone in place of the TC makes it much more difficult to imagine a binary interaction has taken place in most cases.

There have been no known observational studies to determine what steers a TUTT cell as there has been for TCs. Sadler suggested that TUTT cells are advected in part by summertime easterlies in the lower stratosphere (Whitefield and Lyon's 1993). Similar to other atmospheric vortices, it is safe to assume the TUTT cell's environment, including TC-related flow, is involved. TUTT cells in this study, though, did not clearly move with TC-associated (anticyclone) surrounding flow between 100 hPa and 300 hPa. About half of the TCs have anticyclonic flow aloft during their periods of study while the remaining

cases produced a divergent area at 200 hPa or indicated straight line flow over the TC's center (weak TCs). Time lapse satellite imagery and ERA-40 200 hPa flow analysis (48-72 hours) for each TUTT cell reveals that adjacent synoptic-scale upper level anticyclones *not* associated with a TC have more of an influence on TUTT cell steering, but not in every case. Some cases even indicate southward flow to the east and west of the TUTT cell (beyond an induced ridge to the TUTT cell's east) from 100 hPa down to 300 hPa, yet the circulation propagates in a generally northward direction against the flow (Fig. 4.2). In cases where the TC and TUTT cell were close (< 750 km), the TC's cyclonic circulation may have been a factor. No definitive conclusions can be drawn, however, since the wind field data within the ERA-40 analysis often converges the two circulations and make them appear as one oblong circulation.

Which ESL "best fit" a TC-TUTT cell interaction? The mass-weighted DLM (followed by the middle layer) 5°-7° radial band generally provides the best estimate (first-guess) for TC environmental steering during an interaction. This fits previous TC motion studies results from Section 1.3.1. The ESL, however, is not closest to TC motion in *every* case and TC intensity. Results generally support those of Franklin (1990) for Hurricane Josephine. Namely, that the ESL is neither universal nor a conservative property. A layer or radial band may work well in the short term but predicting the optimal ESL beforehand is deterministically impossible.

Three other findings related to determining the "best" ESL for TC steering surfaced in my research. First, more intense TCs yield a DLM radial band most in-line with actual TC motion at distances further away from their centers compared to weaker TCs (i.e., 3°-5° vs. 5°-7°). Rex2 and Babs provide an example of this in Section 3.2.2.3. Second,

intense TCs with presumably better vertical development respond greater to the onset of strong upper layer winds from TUTT cells into their environmental steering than do weaker TCs. This is also discussed in the Rex2 comparison with Babs in Section 3.2.2.5. Third, mass-weighted ESLs yield better correlation with TC motion than do their non-weighted (arithmetic mean) counterparts (Section 2.3.3.3).

At what separation distance do TC-TUTT cell interactions take place? Unlike The greatest distance in which there is evidence of a TC's response to a TUTT cell's wind field is ~1700 km (~920nm, ~15° latitude). This is ~300 km greater than Brand's (1970) distance for the onset of binary TC interactions and is not a surprise based on the greater horizontal extent of a TUTT cell compared to a TC.

What role does the TC or TUTT cell *intensity* have on an interaction? TUTT cells with a maximum 200 hPa PV intensity of > ~2.5 PVUs and/or relative vorticity > ~1.1×10^{-4} s^{-1} indicate a "moderate intensity" and have an increased likelihood of influencing TC motion if other criteria (vertical depth, separation distance) are also met. Application of this guidance requires attention to be given to numerical model *analysis* of a TUTT cell's structure, location and stage in its life cycle (intensifying or weakening) prior to an anticipated TC interaction.

TC intensity is a factor with respect to how a TC responds to the onset of TUTT cell-induced upper level flow changes. Intense TCs respond to strong TUTT cell upper layer flow more than weaker TCs. This response was evident with greater track speed and directional deviation around their respective interaction periods. This greater response by more intense TCs is based on their intensity-dependent dominant level/layer of environmental steering and greater inertial stability.

Are other TUTT cell circulation characteristics important? Yes. The deeper the closed TUTT cell circulation, the greater the likelihood it will have an influence on a TC's motion if other conditions are met. More specifically, a TUTT cell with an analyzed closed circulation at or below 400 hPa indicates a better chance of exerting an influence on a TC's motion. The greater depth allows for a more significant alteration of the mean upper layer winds relative to the TC and, therefore, the DLM environment. Figures 3.22 (Babs) and 3.37 (Bart) provide a good comparison of cases with either a deep or shallow TUTT cell, respectively. Babs' TUTT cell is clearly responsible for steering the TC toward the south due primarily to its deep vertical extent. Bart's TUTT cell, conversely, is unable to provide an identifiable influence on its TC's motion due primarily to its shallow structure.

TUTT cell size (horizontal extent as defined by its closed 200 hPa wind field) is important with respect to separation distances. If a deep and intense TUTT cell does not have a broad enough wind field through sufficient depth ($\sim$ 400 hPa) to influence a TC's environment ($<\sim7°$), it will not cause a response by the TC. If a weaker and more shallow TUTT cell is very close to a TC ($<\sim700$ km), there will likely be some response by the TC. Fred and Amber are two examples of this (Section 3.4.1).

What are the key indicators an interaction will occur or is occurring? Not all TCs in this study provide evidence of a track response to the presence of their associated TUTT cell. Six cases did provide evidence while four did not. Based on the distinctions between these two sets of cases and excluding the two exceptions (Fred and Amber), key indicators a TUTT cell will have an influence on TC motion (i.e. an interaction) include:

1. The 200 hPa TUTT cell center is within 1700 km ($\sim15°$) of the TC.

2. The TC and TUTT cell separation distance is decreasing.

3. The TUTT cell's 200 hPa winds field (>15 m s^{-1}) is within ~800 km of the TC's center.

4. The TUTT cell has maintained a maximum 200 hPa PV of 2.5 PVUs and/or relative vorticity of 1.1×10^{-4} s^{-1} or greater (during the past ~12+ hours).

5. The TUTT cell has consistently maintained a *closed* circulation at or below 400 hPa.

6. The TC is at tropical storm intensity or greater.

If these criteria are met, there is a high likelihood the TC will respond to the TUTT cell's wind field, but all other contributing environmental steering factors and their influence on TC motion must also be taken into account.

How long do interactions last? Based on the cases where evidence of a TUTT cell's influence on TC motion is found, the duration of an interaction is around one to two days [average of ~36 hours (Fig. 4.3)].

4.2 An Observational Comparison to Kimball and Evans (2002)

Kimball and Evan's (2002, hereafter KE02) research focused on the complex nature of the interaction between TCs and upper level lows (troughs) of varying intensity (2-6 PVUs) and under different vertically sheared environments (2.5 to 8.0 m s^{-1}). They used a three-dimensional, non-hydrostatic, fine-resolution model with explicitly resolved convective processes to follow the evolution of the two circulations. Their primary intent was to determine how TC intensity could be affected. KE02 used conditions similar to an actual event (Hurricane Dennis, 1999) to initialize their model and allowed the two circulations to approach each other at various speeds dependent on the VSHW profile and with an initial separation distance of ~1300 km (~12° latitude).

Besides the varying effects that upper level lows have on TC intensity and radius of maximum winds, KE02 also followed the motion of the trough's centers of circulation at three different levels (200 hPa, 300 hPa and 400 hPa) during an interaction. A level of the TC advected the trough's circulation center at that same level differently than other levels of the TC did their juxtaposed trough circulation center. The different advective characteristics of the TC were due to variability within a TC's vertical structure. Once the three trough centers were advected from their initial vertically stacked position, the trough's own three levels of circulation steered the other level's circulation centers. The advection of one level's circulation center by another level's flow is based on the notion that a cyclonic flow around that level's center extends through a depth proportional to its horizontal extent (Hoskins et al. 1985). KE02's results led to a distinct meridional elongation (deformation/tilt) of the troughs with height which was followed by a self-induced rotation into a more zonal orientation (Fig. 4.4). This model process is now observationally compared to one of my cases.

A few criteria must be met to make this comparison. Possible cases are those with similar initial conditions as the Hurricane Dennis scenario. A clear and identifiable cyclonic circulation center for both the TC and TUTT cell should be present at 200 hPa (anticyclone for the TC), 300 hPa and 400 hPa during an interaction period. This requires an intense TC and deep TUTT cell in order to follow their centers at each level using the ERA-40 reanalysis data.

Rex2 proved to be the best candidate. Figure 4.5 provides a visual comparison of KE02 (PV) and Rex2 (ζ_r) at the start of their interactions. Relative vorticity is used in lieu of PV for Rex2 due to low ERA-40 resolution. For KE02, aircraft observations and

dropsonde data provided a higher resolution depiction of Dennis' inner PV structure. Rex2's interaction period begins with nearly the same separation distance (~1340 km), has similar trough (6 PVUs) and TC (46 m s^{-1}) intensities and both are arranged in a geographically similar manner but in reverse order. KE02 modeled anticyclonic flow centered on their TC at 200 hPa. Rex2 also reveals very broad anticyclonic flow around the TC's environment, though sometimes displaced up to 6° (level dependent) from the TC's center in the ERA-40 data. The size of the Rex2 TUTT cell also appears larger than the KE02 trough at 200 hPa.

If observations are to support the KE02 model results, there are a few expectations based on the orientation of the two circulations. These include:

1. Development of a southward deformation (tilt) of the TUTT cell's uppermost circulation center (200 hPa) after an initial northward climatological tilt due to the flow associated with the TC's northeast upper level anticyclone quadrant.

2. After an initial meridional restructuring of the TUTT cell centers with height (northward to southward tilt), a self-induced counter-clockwise rotation into a zonal tilt with height should result. This concept by KE02 neglects any influence by the TC's inner (< 6°) cyclonic circulation on the TUTT cell's lower two centers (300 - 400 hPa).

3. Though not mentioned in KE02, a southward displacement of the TC's upper most closed (300 hPa) circulation center due to southward flow around the TUTT cell's southwest periphery at this higher level (200 - 300 hPa maximum) could occur.

Figure 4.6 shows the tracks of the circulation centers during the period. A climatological northward tilt of the TUTT cell circulation centers with height is evident at the start of the period, resembling Kelly and Mock's (1982) TUTT cell composite

structure. As the two circulations close (< 1100 km), the TC's anticyclone above 200 hPa impinges upon the TUTT cell causing its 200 hPa center to move slower towards the northwest than the two lower centers (300 and 400 hPa). Meanwhile, the less-inhibited lower two layers moved from south to west-northwest of the 200 hPa center under southeasterly flow. The final TUTT cell orientation yields a west to east tilt with height.

The TUTT cell's reversed (southward) tilt with height generally supports KE02's model results (#1 above). The zonal component of the cell's tilt with height (#2 above) generally supports KE02's deformation results, though the direction of the rotation is clockwise versus KE02 counter-clockwise results. Clockwise rotation is counterintuitive based on the expected flow around the three cyclonic TUTT cell and self-induced rotation in Figure 4.4. Rather, it appears the slower 200 hPa TUTT cell center allowed the two lower centers to drift further west and north due to their different environmental flow. If a tilt with height resulted in a self-induced rotation, all TUTT cells would be in a constant state of self-induced ambulation since they are initially in a climatological tilt toward the north with height. This debunks the second KE02 expectation.

Finally, there is evidence of a slight (.5° to .75° latitude) southeastward displacement of the TC's 300 hPa circulation center from the 400 hPa center (#3 above). This occurs about 12 hours into the interaction period, persists for nearly a day and is at the point where the upper layer and TUTT cell flow has the greatest southeastward component across the TC's environment (reference Figs. 3.10 and 3.11). The TUTT cell's structure would suggest stronger winds at higher levels (200 - 300 hPa vs. 400 hPa) produced the southeastward tilt with height between these two levels of the TC, but satellite imagery does not support this.

Evidence found supports KE02's numerical model results that suggest a TC can influence the motion/structure of a TUTT cell. The result is a vertically restructured TUTT cell (from meridionally to zonally orientation with height). It is unclear as to whether the TC actually advects all of the circulation centers independently or if the TC's anticyclone inhibits only one level (200 hPa) of the TUTT cell's circulation and allows the lower levels to continue moving under different (non-TC related) environmental flow.

CHAPTER 5

CONCEPTUAL MODEL AND CONCLUDING DISCUSSION

5.1 Conceptual Model

Figure 5.1 is a graphical representation of the final conceptual model guidance for the influence of a TUTT cell on TC motion designed for operational use at the JTWC. On the left side, five scenarios provide possible orientations for forecaster pattern recognition. This method is similar to the Carr and Elsberry Systematic Approach to TC Forecasting (1994) design. Based on JTWC inputs, the graphic is designed for forecasters as a "quick-check" to be applied during each forecast cycle, as needed. Six yes or no questions provide initial decision criteria to determine if an interaction between the two circulations is likely. Questions include:

1. Is the 200 hPa TUTT cell center within 1700 km (~15°) of the TC?

2. Is the TC and TUTT cell separation distance decreasing?

3. Is the TUTT cell's 200 hPa winds field (> 15 m s^{-1}) within 800 km (~7°) of
   the TC's center?

4. Has the TUTT cell maintained a maximum 200 hPa intensity of either:
   4a. potential vorticity $\geq$ 2.5 PVUs (3 x 10^{-6} m^2 K s^{-1} kg^{-1}) or
   4b. relative vorticity $\geq$ 11 x 10^{-5} s^{-1}

5. Has the TUTT cell maintained a *closed* circulation at or below 400 hPa?

6. Is the TC at tropical storm intensity or greater?

Six "yes" answers indicate a strong likelihood the TUTT cell will exert a predictable influence on TC motion. If *any* answers are "no", an interaction is unlikely at

the time. If an interaction is likely, the forecaster can then select a scenario that fits the current situation based on a typical envelope of forecast models. This envelope is referred to as the model ensemble field (e.g., a multi-model ensemble array). The envelope in each conceptual model scenario is color coded with areas of likely and unlikely (green (annotated 'G') and red (annotated 'R'), respectively) speed and directional biases in the TC's forecast track to be applied after ensemble forecast track development. The biases fit the addition of the TUTT cell's flow primarily through the quadrant of the TC's environment closest to the TUTT cell.

The preliminary scenarios for the conceptual model are derived from the orientation of the circulations within the case study. Some other scenarios, however, are much less likely to occur and are not included. For example, a TC rarely moves southward in this basin unless forced to by substantial environmental steering, such as from a TUTT cell, transient anticyclone or another TC. A TUTT cell located south of a westward moving TC is another unlikely scenario example. Westward moving TCs are typically south of the subtropical ridge, at low latitudes and south of the TUTT's climatological position.

Realistic scenarios that did not occur within my cases are inferred. For example, Rex1 involves a northeastward tracking TC with a large TUTT cell directly in the TC's path. Rex1 is steered more eastward (right of track bias) during the interaction period as a result of additional south and eastward TUTT cell flow into to the TC's steering environment. During this time, all forecasts are to the left (northeast) and slower than the actual track taken by the TC. The results of this case can be similarly applied to an unrepresented scenario of a north*west*ward moving TC and a TUTT cell directly in its path by rotating the Rex1 scenario 90° counterclockwise. The addition of the TUTT

cell's wind field results in a more northward (to the right) and faster motion bias in the track of this hypothetical TC. Forecast characteristics of both circulations (orientation, intensity, separation distance) must be taken into account for continued use of the conceptual model. If the orientation of the two circulations matches one scenario at first but is expected to change to another over time, so must the application of the track bias.

The suggested use of persistence is also provided. Once an interaction is recognized to have begun, persistence should be more heavily weighed (out 12 to 24 hours) during the first 24 hours of an identified interaction period. After 24 hours, persistence should remain heavily weighed but only for the first 6 to 12 hours since the environment is likely to change in the near future. A change would normally be due to the dissipation of the TUTT cell, an increase in separation distance between the two circulations and/or a change in their orientation. At this point, more forecast weight would return to the traditional model ensemble forecast.

5.2 Summary and Concluding Discussion

My research explored a previously ignored but often referenced topic: the influence of a TUTT cell on TC motion. My research provides evidence, by the use of numerous case studies, that TUTT cells do play a significant role in steering TCs. Slight to very distinct deviations in TC tracks occur as a direct consequence of a TUTT cell's large-scale wind field contribution to the deep layer environment surrounding a TC. Improved TUTT cell analysis and the inclusion of its wind field are critical to more accurate numerical model TC track forecasts. Until the capability improves, the application of my operational guidance will help to decrease TC forecast track errors during these events.

The role of the TUTT cell in the motion of the ten TC cases is determined by the analysis of various tropospheric layers (upper, lower, middle, DLM) and an upper layer quadrant analysis. Analysis shows the circulations' separation distance, geographical orientation, intensity, and the depth and breadth of the TUTT cell's closed circulation are related to the TC track deviations. Specific indicators for an interaction are identified for determining the likelihood of an identifiable TC/TUTT cell interaction.

Support for previously documented "best" ESLs is found along with key indicators for and characteristics of TC – TUTT cell interactions. This includes use of the $5°$-$7°$ mass-weighted DLM as a first-guess for TC environmental steering. The $5°$-$7°$ DLM ESL is typically referred to as the most accurate for determining "average" TC motion. For less intense TCs ($< \sim30$ m s^{-1}) with less vertical development, however, the $3°$-$5°$ mass-weighted DLM sometimes proves to be more accurate regardless of the TUTT cell's role. The inward shift of the "best" radial band is linked to the relationship between TC intensity and the size of its associated wind field, as statistically determined by DeMaria and Kaplan (1994).

The residual vector (DLM $5°$-$7°$ radial band) was expected to reveal a north through westward component at ~1-3 m s^{-1} based on the beta effect theory. Only one of the ten cases revealed the anticipated residual vector characteristics throughout *all* of the time steps and 6 of the 10 cases below 50% of their time steps. The residual vectors did, however, have some interesting characteristics. First, six of the cases had reasonably tight groupings, though only two were toward the northwest. Second, most cases reveal a smooth directional transition of the vectors over time with the greatest variability occurring around the defined interaction TC/TUTT cell start and end points. Residual

vectors revealed consistency in their behavior and were not random. Some of these findings are speculated to be a result of modulation of the TC's beta gyre, similar to findings by Fiorino and Elsberry (1989a), Wang and Li (1992) and Wang and Holland (1996) which discussed beta gyre modulation by the TC's own circulation.

Based on the defined TC environments, vertical shear of the horizontal wind (VSHW) analysis indicates that 8 of the 10 cases support a motion to the "left-of-VSHW" mean vector as determined by previous numerical model studies. Two of the eight cases sustain this leftward bias only outside of their TUTT cell interaction periods. TCs that did not support the "left-of-VSHW" bias suggested by computer model simulations are typically weaker and less developed during their period of study compared to those that did support the bias. This relationship is speculated to be due to the mutual steering of a TC's anticyclone/cyclone couplet in a well-developed TC.

Evidence suggests TCs, primarily intense TCs (typhoons), can have an influence on TUTT cell motion. The appearance of unweighted centroid relative motion between TCs and TUTT cells along with observational support for theorized baroclinic advection between TC and trough circulation centers in KE02 subjectively support this possibility. Satellite imagery and analysis of the 100 to 300 hPa wind field around the TUTT cells also suggests this *mutual* rotation can occur, especially in cases where the TC and TUTT cell are close together (< ~700 km) and of similar scale. Larger, more intense TUTT cells at greater separation distances suggest a one-way influence on the TC's motion.

Operational guidance is developed in the form of a conceptual model. By the writing of this document, the guidance had already been reviewed and partially applied at the JTWC. The guidance is also being coordinated at the NHC and the Central Pacific

Hurricane Center (CPHC). The broad nature of the guidance is necessary since only ten cases are initially used from the Pacific and one from the Atlantic. Scenarios *not* directly acquired from the ten cases are inferred. The conceptual model is created to ensure forecasters recognize the potential and often overlooked influence a TUTT cell can have on TC motion. The inclusion of the TUTT cell's contribution to a TC's steering environment can help decrease forecast error, lead to a better forecast product and contribute to the many implications therein.

If numerical model represented TUTT cell forecast structure, movement and evolution accurately, there would be no need for this operational guidance. Possible causality for extreme NOGAPS forecast errors during some of my cases are provided in the discussions. It is speculated that the lack of in-situ observations over the immense basin, especially within the middle troposphere (~400 to ~700 hPa), prevents numerical models from depicting accurate TUTT cell structures. Data gaps leads to incorrect forecasting of the TUTT cell's life-cycle and an under-forecast influence on TC motion. Poor vertical and horizontal resolution of and inadequate radiative parameterization (handling of the TUTT cell's cold core) within the forecast models is more likely the culprit for inaccurate representation of TUTT cell structure and, therefore, forecasting of the circulation's life cycle.

A brief comparative analysis of an Atlantic TC, Hurricane Erin (1995), with the ten Pacific case reveals evidence of a TUTT cell's influence on TC motion within another basin. Application of the conceptual model as a hindsight analysis fit nicely. The results add credence to the NHC's preliminary report that explained TC motion prior to landfall.

Lastly, observational evidence compared to a previous computer model simulation

is explored. KE02 discussed a trough's (TUTT cell's) vertical structure and horizontal deformation when in proximity to a TC. My results found that there is some evidence of an elongation with height (vertical tilt). This vertical tilt is speculated to be due to the influence of the TC's anticyclone on upper levels of the TUTT cell with respect to environmental flow around various levels' circulation centers. A self-induced rotation of the TUTT cell, however, did not seem likely.

Future work on this topic involves two areas of focus: operational application and prospective research steps. The focus of the operational application is at the JTWC. Use in the Atlantic TC basin at the NHC and CPHC, however, is currently being coordinated and is strongly recommended. Prospective research steps are designed to answer remaining scientific questions and to address operational concerns.

The first step toward the operational application process began with the introduction and use of the initial conceptual model at the JTWC. Typhoon forecasters and the JTWC Technical Advisor both reviewed and provided feedback on an *initial* quantified conceptual model version. Following versions incorporated this feedback in an attempt to fit the guidance within the JTWC's warning cycle process, available analysis and forecast fields (in their respective units) and a decision-grade checklist with applicable quantifiable values to guide the forecasters through the graphic. As a result, a composite image with current water vapor imagery, NOGAPS 200 hPa winds and relative vorticity was developed for the JTWC's Joint METOC Viewer (JMV) system. JMV imagery also allows the TDOs to measure distances which permits the conceptual model checklist to be completed using just one image or loop in less than a minute. Unfortunately, this coordination occurred late in the northwest Pacific's typhoon season (Nov 2007) and no

documented operational applications of the conceptual model were possible prior to the writing of this paper. Officially incorporating the final conceptual model into the JTWC's forecast process is the next logical step.

Future work should focus on the utilization of actual numerical model forecast fields at the valid time for each case. Use of this real-time data (e.g., NOGAPS) versus values from the ERA-40 reanalysis would help refine the conceptual model's quantitative values and possibly help to determine why the forecat models often fail to forecast these events. A relaxation of the case study criteria and/or using cases from outside this study's 8-year period could further refine the guidance. This will require the consideration of other large-scale features (other TCs, mid-latitude trough) that could provide additional piecemeal contributions to TC steering.

There are many prospective areas of research stemming from my study. Some of these could indirectly improve TC motion forecasts while others would lead to a better understanding of TC/TUTT cell interactions. Ideas include:

1. Determine why NOGAPS fails to accurately forecast the structure and life-cycle of TUTT cells.

2. Determine how TUTT cells are steered. As with TCs, a TUTT cell's environment must be responsible for a large portion of its motion. A study on TUTT cell's environmental steering would yield results that could be directly incorporated into their potential influence on TC steering.

3. Perform a comprehensive composite study on the life cycle of a TUTT cell (versus only the mature structure) using a reanalysis data set.

4. Create a baroclinic model of a TC and a TUTT cell interaction under uniform flow to compare with observational results.

The JTWC and other TC forecasting agencies are advised to pursue a better understanding of these types of interactions. Use of my guidance and results followed by research into the aforementioned areas would help to solve another piece of the puzzle involved in accurately forecasting TC motion.

TABLES

Table 2.1 Average daily counts of various observation types used by the ERA-40 data assimilation for five separate periods (Uppala 2005). Red shade indicates the period of choice for my research. Green shade indicated observation type _not_ at a historical maximum during the same period.

	1958-1966	1967-1972	1973-1978	1979-1990	1991-2001
SYNOP/SHIP	15313	26615	28187	33902	37049
Radiosondes	1821	2605	3341	2274	**1456**
Pilot balloons	679	164	1721	606	676
Aircraft	58	79	1544	4085	26341
Buoys	0	1	69	1462	3991
Satellite radiances	0	6	35069	131209	181214
Satellite winds	0	0	61	6598	45671
Scatterometer	0	0	0	0	7575
PAOBS	0	14	1031	297	277

Table 2.2 Assigned weights and heights used based on the mass-weighted 100 hPa to 1000 hPa deep layer mean. Similar tables were created for all the other mass-weighted layers utilized in this study.

Level (hPa)	Weight Ratio	Weight Fraction
100	25 / 900	0.028
150	50 / 900	0.056
200	50 / 900	0.056
250	50 / 900	0.056
300	75 / 900	0.083
400	100 / 900	0.111
500	150 / 900	0.167
700	175 / 900	0.194
850	150 / 900	0.167
1000	75 / 900	0.083
DLM	**900 / 900**	**1.000**

Table 2.3 The final ESLs (from the original 32) for each radial band utilized.

Radial Band (degrees latitude)	Mass-Weighted Layer
1°-3°	Upper, Middle, Lower, DLM
3°-5°	Upper, Middle, Lower, DLM
5°-7°	Upper, Middle, Lower, DLM
inner 7°	DLM

Table 3.1a Summary table of all 10 cases' quantitative and qualitative metrics. Initial (subjective satellite-based) and final (data evidence-based) grade that a TUTT cell influenced the TC's motion, the maximum depth of the TUTT cell's closed circulation down towards the surface and the interaction start/end separation distances are provided.   Outlier cases, discussed in Chapter 3, are highlighted in purple.

Name / Year	TC Response to TUTT Cell	TUTT Cell	Interaction Sep
	Init Sat-Based Est / Evidence?	Closed Circ Depth	Dist (km) Start/End
Rex2 / 1998	Intense / Yes	< 500 hPa	1340 / 1050
Babs / 1998	Intense / Yes	600-700 hPa	1500 / 1300
Rex1 / 1998	Intense / Yes	400-500 hPa	1700 / 1360
Ewiniar / 2000	Intense / Yes	400-500 hPa	740 / 790
Bolaven / 2000	Moderate / Yes	400-500 hPa	1500 / 1300
Amber / 1997	Weak / Yes	< 300 hPa	680 / 640
Fred / 1994	Intense / No	500 to 600 hPa	1600 / 1330
Saomai / 2000	Moderate / No	< 300 hPa	1900 / 1500
Bart / 1999	Intense / No	250 to 300 hPa	1065 / 765
Polly / 1995	Weak / No	< 300 hPa	1650 / 1200

Table 3.1b Summary table of all 10 cases' quantitative and qualitative metrics. The TUTT cell's intensity at the interaction start point listed in both maximum associated 200 hPa relative vorticity (ζ_r) and potential vorticity (PV), and the TC's intensity range during the same period. ζ_r is in terms of s^{-1} and a PVU = 1x10^{-6} m^2 K s^{-1} kg^{-1}. Outlier cases, discussed in Chapter 3, are highlighted in purple.

Name / Year	TUTT Cell Intensity Max Rel. Vort @ Start Pt	TUTT Cell Intensity Max PV @ Start	TC Interaction Intensity
Rex2 / 1998	1.50E-04	6 PVUs	46-51 m s^{-1}
Babs / 1998	1.40E-04	4.5 PVUs	21-39 m s^{-1}
Rex1 / 1998	1.20E-04	3 PVUs	28-46 m s^{-1}
Ewiniar / 2000	2.60E-04	6.5 PVUs	33-28 m s^{-1}
Bolaven / 2000	1.40E-04	3+ PVUs	21-26 m s^{-1}
Amber / 1997	1.00E-04	<2 PVUs	26-33 m s^{-1}
Fred / 1994	1.70E-04	4 PVUs	21-44 m s^{-1}
Saomai / 2000	1.00E-04	<2 PVUs	46-28 m s^{-1}
Bart / 1999	9.00E-05	2.5 PVUs	67-51 m s^{-1}
Polly / 1995	5.00E-05	<2 PVUs	23-41 m s^{-1}

Table 3.1c Summary table of all 10 cases' quantitative and qualitative metrics. The interaction start and end point date/time, the centroid-relative 2-point running mean angle change at the interaction start points and the TC to TUTT cell orientation are provided. A '*' indicates there were multiple "kinks" in the centroid-relative 2-point running mean line after the start point mostly due to poor TUTT cell best track analysis (wind field merging, location jumps) within the ERA-40 dataset. Outlier cases, discussed in Chapter 3, are highlighted in purple.

Name / Year	Interaction Start Point / End Point	C-Rel Angle Chng at Start Point	Interaction Period: Cell Orientation from TC
Rex2 / 1998	31 Aug 00-06Z / 1 Sep 18-00Z	35*	ENE to NE
Babs / 1998	17 Oct 12-18Z / 19 Oct 12-18Z	25*	ENE to NE
Rex1 / 1998	25 Aug 18-00Z / 27 Aug 06-12Z	30*	E to NE
Ewiniar / 2000	11 Aug 00-06Z / 12 Aug 00-06Z	25	NNW to WSW
Bolaven / 2000	26 Jul 06-12Z / 27 Jul 06-12Z	45	E
Amber / 1997	21 Aug 18-00Z / 23 Aug 06-12Z	25*	NE to WNW
Fred / 1994	15 Aug 18-00Z / 17 Aug 12-18Z	45*	ENE
Saomai / 2000	4 Sep 18-00Z / 6 Sep 00-06Z	90*	ENE to NE
Bart / 1999	21 Sep 18-00Z / 23 Sep 12-18Z	45	ESE to ENE
Polly / 1995	17 Sep 00-06Z / 18 Sep 06-12Z	35*	ESE to ENE

Table 3.1d Summary table of all 10 cases' quantitative and qualitative metrics. The radial band and layer for the ESL that best correlated to the TC's speed and direction during the interaction and entire period and the Y/N results as to whether the TC's motion was to the *left of the mean VWS vector* are provided. The speed and direction correlations are listed first by radial band then by layer (D = DLM, M = Middle, L = Lower, U = Upper) with the two time periods separated by a '/'. For example from Ty Rex1 for speed correlation, 5°-7° M, L / 3°-5° M means the 5°-7° radial band of the middle and lower layer correlated best during the *interaction* period but the 3°-5° of the middle layer correlated best during the *entire* period (interaction period +/- 24 hours) used in the study. More than one ESL may be listed if correlation values were very close. The word "both" is listed if results were the same for both time periods. Outlier cases, discussed in Chapter 3, are highlighted in purple.

Name / Year	Best ESL TC *Speed* Corr Interaction / Entire Period	Best ESL TC *Dir* Corr Interaction / Entire Period	TC Motion "to left" Mean VSHW Vector
Rex2 / 1998	5°-7°, in7° D,M / 3°-5° D,U(all)	5°-7°, 3°-5° U / 3°-5°,1°-3° D, M	Y
Babs / 1998	3°-5°,1°-3° D, U / 3°-5° M	5°-7° M / 5°-7° D, M	N
Rex1 / 1998	5°-7° M, L / 3°-5° M	5°-7° M, all 7° D **for both**	Y
Ewiniar / 2000	3°-5° L, M **for both**	1°-3° D, M, U / various > 3°	Y
Bolaven / 2000	5°-7°,1°-3° U / 5°-7° D, M, L	3°-5° D, M / 3°-5° D, M, all 7°D	Y, only prior
Amber / 1997	3°-5° U / 3°-5° L	1°-3° L / 5°-7° L	N
Fred / 1994	all neg or < .3 / 5°-7° U	3°-5° D,U all 7° D **for both**	Y
Saomai / 2000	3°-5° M, L / 5°-7° M, L	3°-5° all / 5°-7° M	Y, only prior
Bart / 1999	all 5°-7°, in7° except L **for both**	in 7° D / in7° D, 5°-7° U	Y
Polly / 1995	5°-7° D, M / 5°-7°, 3°-5° M	5°-7° D, U, 3°-5° all / 3°-5° D, M	Y

Table 3.1e Summary table of all 10 cases' quantitative and qualitative metrics. The forecast model performance (least and most error), an "eyeball estimate" convective asymmetry summary for each TC and the percentage of time stesp the 5°-7° DLM residual vector of the case met the envelope of expectation for the beta effect (northwestward at 1-3 m s^{-1}) are provided.

Name / Year	Forecast Model Least / Greatest Error	Convective TC Asymmetry	Freq Resid vector Support B-Theory?
Rex2 / 1998	CLIP / JTWC	Minor to SE	24%
Babs / 1998	JTWC / CLIP	Moderate to S (decr)	69%
Rex1 / 1998	CLIP / NOGAPS	Minor to E then S	8%
Ewiniar / 2000	JTWC / CLIP	Minor (dur) Significant (after) to W	0%
Bolaven / 2000	NOGAPS / CLIP	Minor to S	54%
Amber / 1997	CLIP & JTWC / NOGAPS	Minor to S	100%
Fred / 1994	CLIP / NOGAPS	Minor to S	50%
Saomai / 2000	NOGAPS / CLIP & JTWC	Minor to Moderate S	27%
Bart / 1999	NOGAPS / CLIP & JTWC	Minor to S	8%
Polly / 1995	NOGAPS / CLIP	Minor to S (early)	46%

Table 3.1f Summary table of all 10 cases' quantitative and qualitative metrics. The approximate north to south and east to west (through 200 hPa center) extent of the TUTT cell wind field during the entire interaction period and at the interaction start point based on the outermost 200 hPa height field at 10 m intervals.

Name / Year	E-W / N-S (km) TUTT Cell Wind Field *at* Int. Start Point	Avg E-W / N-S (km) TUTT Cell Wind Field Dur Interact. Period
Rex2 / 1998	920 / 950	650 / 730
Babs / 1998	1600 / 2180	1360 / 1880
Rex1 / 1998	1410 / 1510	1070 / 1350
Ewiniar / 2000	800 / 1350	940 / 1350
Bolaven / 2000	1330 / 1500	1190 / 1360
Amber / 1997	1020 / 630	1110 / 1160
Fred / 1994	1580 / 1330	1360 / 1190
Saomai / 2000	950 / 1020	1050 / 800
Bart / 1999	550 / 950	410 / 650
Polly / 1995	*840 / 600*	*850 / 760*

Table 3.2a Correlation coefficients (ESL versus TC *speed*) for the 3 sample cases in Chapter 3. The "interaction" and "entire" periods (6-hour intervals between time steps) are included for the various mass-weighted radial bands of the DLM, upper, lower and middle layers. Values highlighted in red are referenced in the text.   The "N" value below each column indicates the number of available samples involved. Correlations were tested at a 90% level of significance.

	Speed	Rex2 Interaction	Entire	Babs Interaction	Entire	Bart Interaction	Entire
DLM	57wt	-0.33	0.32	0.39	-0.21	0.94	0.88
	35wt	0.11	0.73	0.51	0.00	0.83	0.89
	13wt	0.09	0.13	0.48	-0.05	0.64	0.57
	all7wt	-0.12	0.62	0.54	-0.16	0.89	0.89
MIDDLE	57wt	-0.31	0.03	0.77	0.27	0.91	0.80
	35wt	-0.04	0.36	-0.51	0.51	0.80	0.88
	13wt	0.04	-0.10	-0.06	0.07	0.56	0.59
UPPER	57wt	0.77	0.77	0.22	-0.42	0.95	0.93
	35wt	0.75	0.85	0.68	-0.36	0.88	0.84
	13wt	0.54	0.80	0.70	-0.32	0.35	0.45
LOWER	57wt	-0.76	-0.46	-0.04	0.12	0.83	0.57
	35wt	-0.67	-0.37	-0.36	0.35	0.75	0.84
	13wt	0.06	-0.53	-0.26	0.02	0.51	0.47
df=N-2		N=7	N=21	N=8	N=19	N=7	N=14

Table 3.2b Correlation coefficients (ESL versus TC *direction*) for the 3 sample cases in Chapter 3. The "interaction" and "entire" periods (6-hour intervals between time steps) are included for the various mass-weighted radial bands of the DLM, upper, lower and middle layers. Values highlighted in red are referenced in the text. The "N" value below each column indicates the number of available samples involved. Correlations were tested at a 90% level of significance.

	Direction	Rex2		Babs		Bart	
		Interaction	Entire	Interaction	Entire	Interaction	Entire
	57wt	0.96	0.77	0.39	0.82	0.36	-0.44
DLM	35wt	0.88	0.83	-0.16	0.68	0.37	-0.27
	13wt	0.79	0.82	-0.08	0.36	-0.18	0.23
	all7wt	0.95	0.82	0.21	0.80	0.62	0.96
	57wt	0.97	0.80	0.71	0.85	0.43	-0.21
MIDDLE	35wt	0.85	0.83	-0.38	0.47	0.40	-0.09
	13wt	0.72	0.85	0.11	0.58	-0.14	0.58
	57wt	0.93	0.28	0.00	0.58	-0.06	0.96
UPPER	35wt	0.73	0.15	0.11	0.68	-0.09	0.45
	13wt	0.64	0.21	0.44	0.75	-0.41	0.13
	57wt	0.91	0.76	0.59	0.75	-0.62	-0.13
LOWER	35wt	0.76	-0.14	-0.05	0.57	-0.41	-0.09
	13wt	0.75	0.81	-0.83	0.12	0.42	0.34
df=N-2		N=7	N=21	N=8	N=19	N=7	N=14

Table 3.3 Mean vertical shear of the horizontal wind (200-850 hPa) heading (degrees) and magnitude (m s^{-1}) for Rex2 prior to, during and after the interaction period. Values were determined for the 5°-7° radial band and within 7° and 10° radius of the TC center.

Rex2		Mean VSHW Heading	Mean TC Heading	Mean VSHW Magnitude (m s^{-1})
	Prior to	146.6	23.4	17.6
5-7 Radial Band	During	154.6	100.0	19.1
	Prior to	156.2	23.4	16.4
7 Radius	During	161.3	100.0	16.4
	Prior to	142.0	23.4	19.5
10 Radius	During	150.0	100.0	19.0

Table 3.4 Mean vertical shear of the horizontal wind (200-850 hPa) heading (degrees) and magnitude (m s^{-1}) for Babs prior to, during and after the interaction period. Values were determined for the 5°-7° radial band and within 7° and 10° radius of the TC center.

Babs		Mean VSHW Heading	Mean TC Heading	Mean VSHW Magnitude (m s^{-1})
	Prior to	238.8	270.9	18.1
5°-7° Radial Band	During	191.9	226.0	14.5
	After	198.6	294.8	11.9
	Prior to	241.3	270.9	18.7
7° Radius	During	207.3	226.0	14.8
	After	212.5	294.8	11.7
	Prior to	238.4	270.9	17.0
10° Radius	During	192.8	226.0	14.6
	After	193.8	294.8	12.1

Table 3.5 Mean vertical shear of the horizontal wind (200-850 hPa) heading (degrees) and magnitude (m s⁻¹) for Bart prior to, during and after the interaction period. Values were determined for the 5°-7° radial band and within 7° and 10° radius of the TC center.

Bart		Mean VSHW Heading	Mean TC Heading	Mean VSHW Magnitude (m s^{-1})
	Prior to	209.3	36.0	17.6
5-7 Radial Band	During	86.4	18.4	18.7
	Prior to	196.0	36.0	15.9
7 Radius	During	124.4	18.4	17.3
	Prior to	178.5	36.0	17.8
10 Radius	During	67.4	18.4	18.7

Table 3.6a-f Same as Tables 3.1a-f, except for the Atlantic Ocean case, Hurricane Erin.

a.

Name / Year	TC Response to TUTT Cell Init Sat-Based Est / Evidence?	TUTT Cell Closed Circ Depth	Interaction Sep Dist (km) Start/End
Hurr Erin / 1995	Moderate / Yes	400 hPa	700 / 450

b.

Name / Year	TUTT Cell Intensity Max Rel. Vort @ Start Pt	TUTT Cell Intensity Max PV @ Start	TC Interaction Intensity
Hurr Erin / 1995	1.10E-04	4.3 PVUs	27-34 m s^{-1}

c.

Name / Year	Interaction Start Point / End Point	C-Rel Angle Chng at Start Point	Interaction Period: Cell Orientation from TC
Hurr Erin / 1995	31 Jul 18-1 Aug 00Z / 1 Aug 12-18Z	40°	NNW to WSW

d.

Name / Year	Best ESL TC Speed Corr Interaction / Entire Period	Best ESL TC Dir Corr Interaction / Entire Period	TC Motion "to left" Mean VSHW Vector
Hurr Erin / 1995	3°-5°,1°-3° D,L/ 3°-5°D,M,1°-3°U	3°-5°L,1°-3°D,L / 1°-3°D,L	Y, prior to / during

e.

Name / Year	Forecast Model Least / Greatest Error	Convective TC Asymmetry	Freq Resid vector Support B-Theory?
Hurr Erin / 1995	GFDL / CLIP & AVNI	Minor / Mod to NE	50 – 90%

f.

Name / Year	E-W / N-S (km) TUTT Cell Wind Field *at* Int. Start Point	Avg E-W / N-S (km) TUTT Cell Wind Field Dur Interact. Period
Hurr Erin / 1995	700 / 540	700 / 730
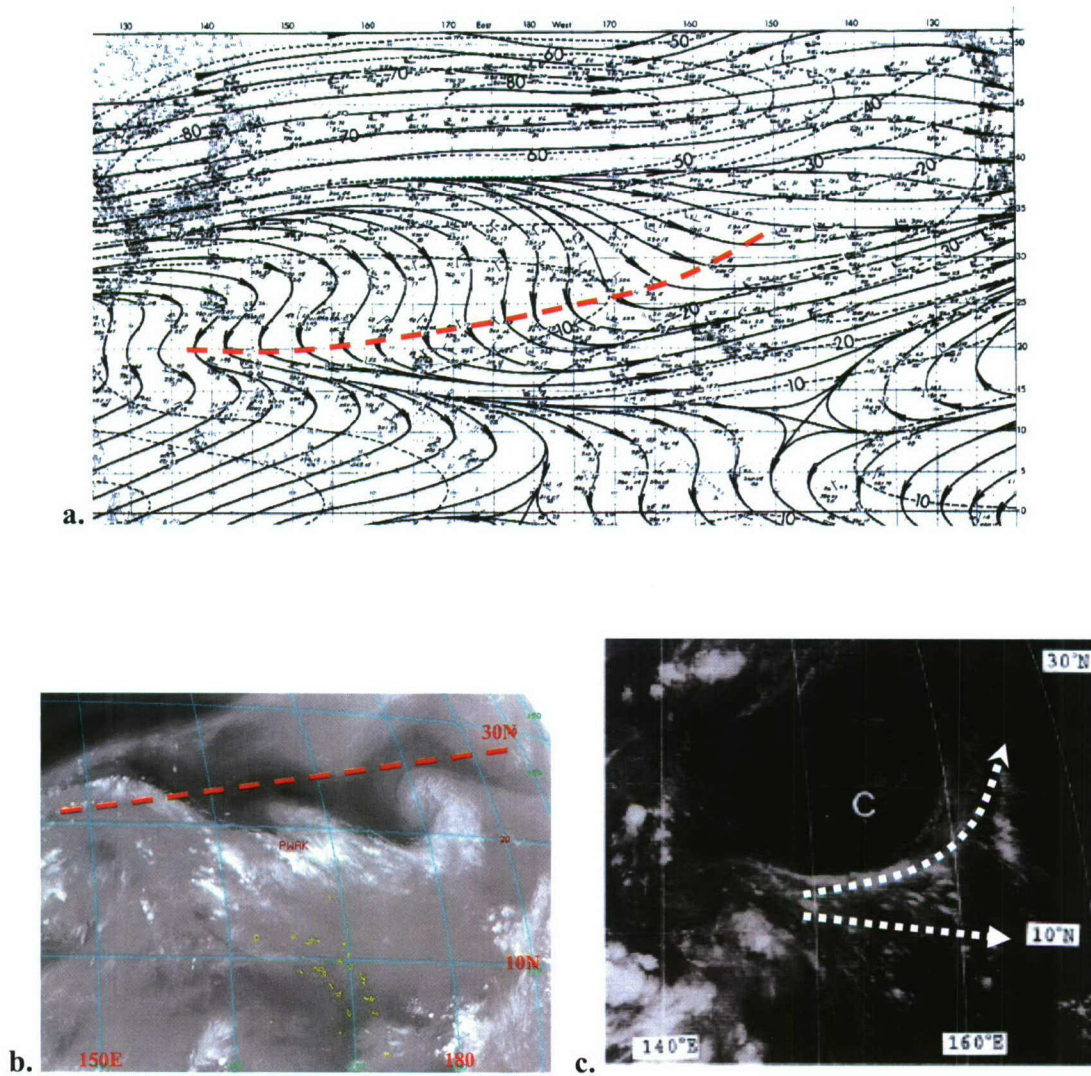
Figure 1.1 (a) The average monthly climatological 200 hPa wind streamline (solid line) and isotachs (dotted line) for September over the north Pacific Ocean (Sadler 1975). The dashed red line indicates the TUTT axis.   (b) An MTSAT-1R image of a classic (though late season) TUTT across the central Pacific Ocean on 29 October 2007. Wake Island is annotated "PWAK" near the center of the image. The dashed red line indicates the TUTT axis. (c) A GMS-3 infrared image from 12Z 16 June 1985. The center of the TUTT cell is annotated with a "C" (Chen and Chou 1994).   The divergent wind field is emphasized by the dotted lines/arrows.
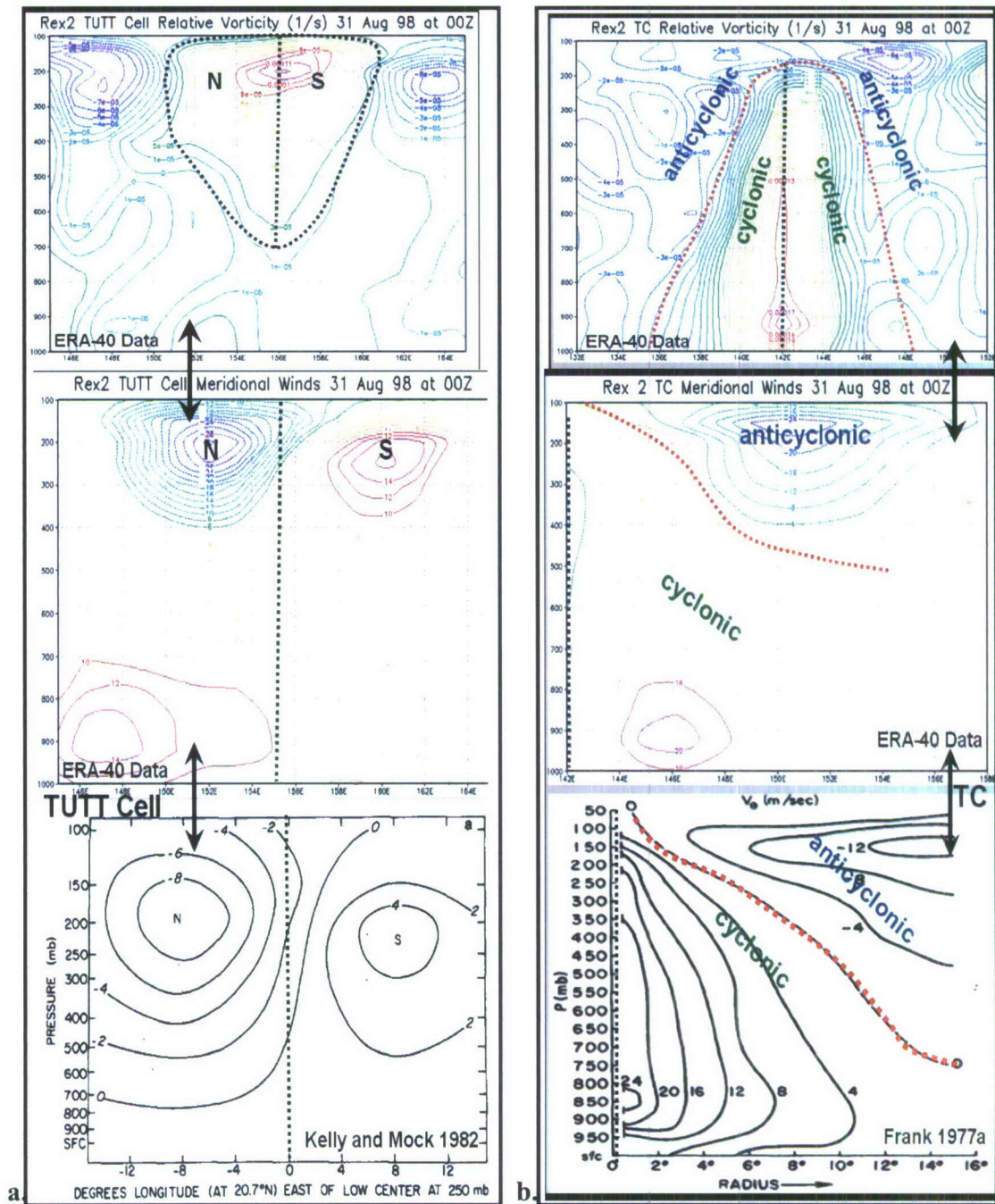
Figure 1.2 (a) Vertical profile of actual TUTT cell relative vorticity (s⁻¹) (top) and meridional wind field (middle) followed by a composite meridional wind field by Kelly and Mock (1982). (b) Same as in a., but for a TC with an azimuthal wind field composite (bottom) by Frank 1977a. Both circulations are from Rex2 at 00Z 31 August 1998. All wind speed is in m s⁻¹. Variability in either circulation's intensity can lead to variations in their vertical development. This, in turn, influences the likelihood and characteristics of an interaction between the two circulations.
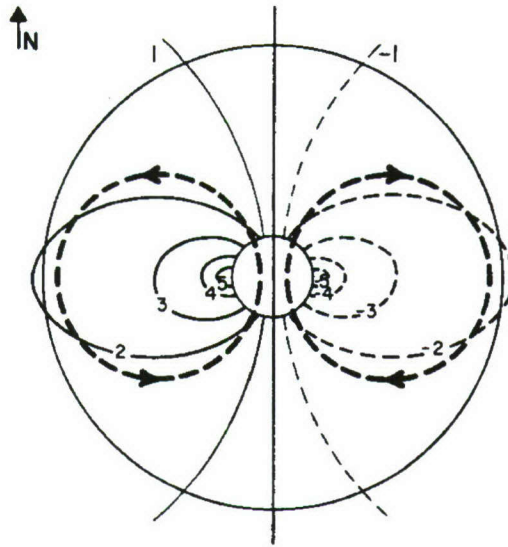
Figure 1.3 Field of $d\zeta_{\sigma r}/dt$, in arbitrary units, centered on a symmetric nondivergent Northern Hemisphere cyclone on a beta plane with no basic flow. Heavy dashed lines show the induced secondary circulation as a result of the vorticity changes (Holland 1983).
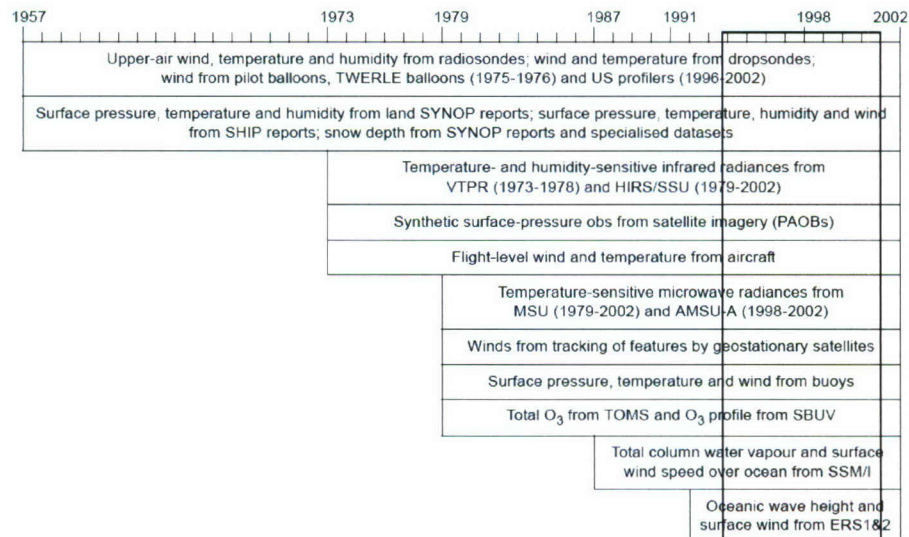
Figure 2.1 Chronology of the types of observations assimilated in ERA-40 (Uppala 2005). The red shaded area indicates the period of focus for this study.
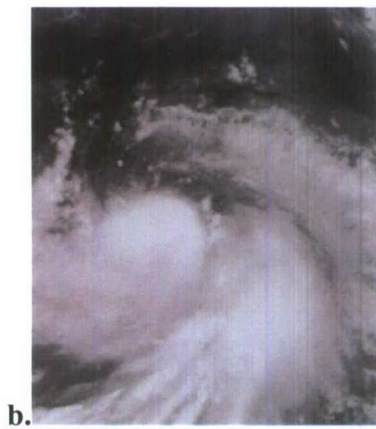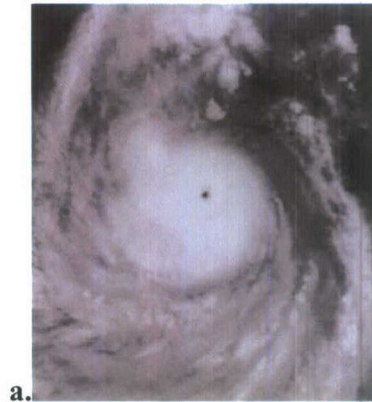
Figure 2.2 Examples of (a) minor (Bart, 12Z 21 September 1999) (b) moderate (Babs, 06Z 19 October 1998) and (c) significant (Ewiniar, 21Z 11 August 2000) convective asymmetries "eyeball estimates."
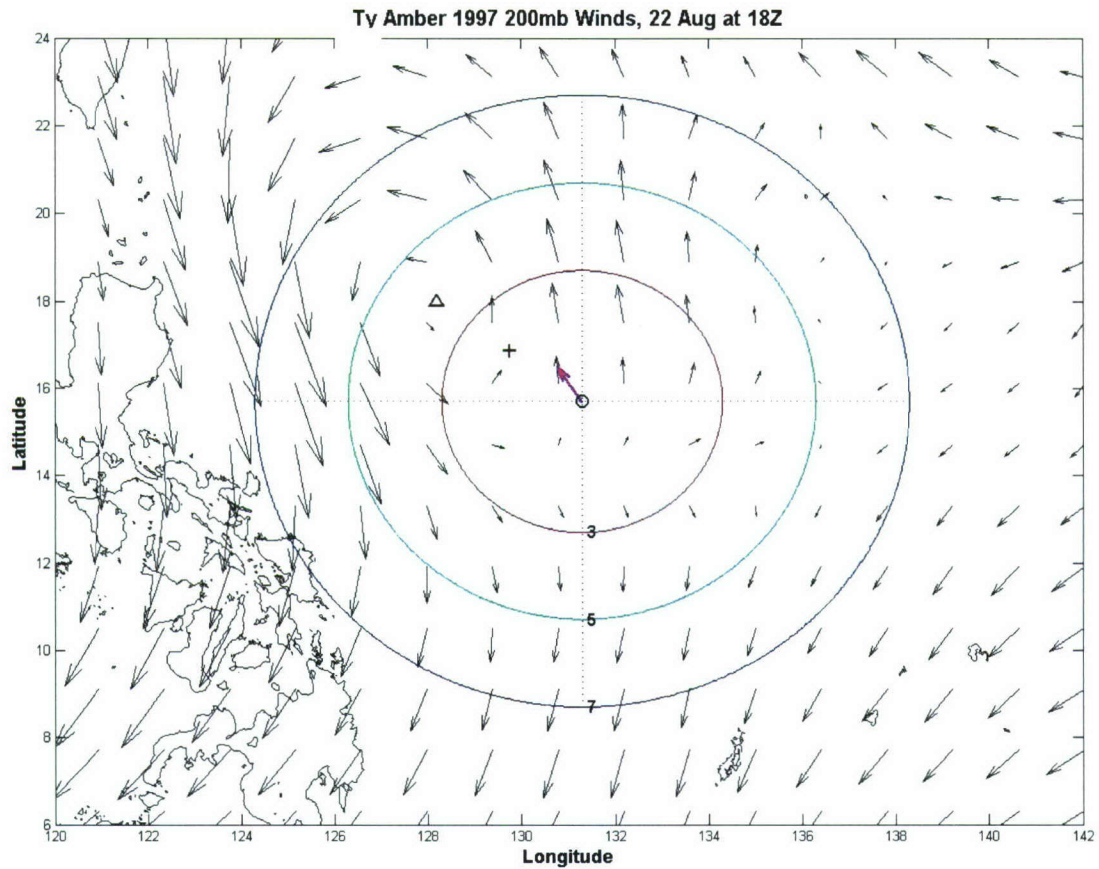
Figure 2.3 Amber (1997) 200 hPa wind field analysis at 18Z 22August 1997 in the *middle* of the case's interaction period. The "o" represents the Best Track low-level center of Amber. The "+" represents the centroid of the two circulations. The "Δ" represents the approximate 200 hPa TUTT cell circulation center. The red, green and blue circles represent the approximate 3°, 5° and 7° radii, respectively, and are divided into quadrants. The pink arrow represents the TC's trajectory. Notice the southward return flow of the TUTT cell meshed with anticyclonic flow to the west of the TUTT cell encompassed by the western half of the TC's 5°-7° radial band. This return flow leads to a mean southward direction of the outer radial band. The TC, meanwhile, moves towards the north-northwest.

- 101 -

Upper Half of Mass-Weighted Troposphere

TUTT Cell 200 hPa Center

+

Lower Half of Mass-Weighted Troposphere

=

New DLM

a.
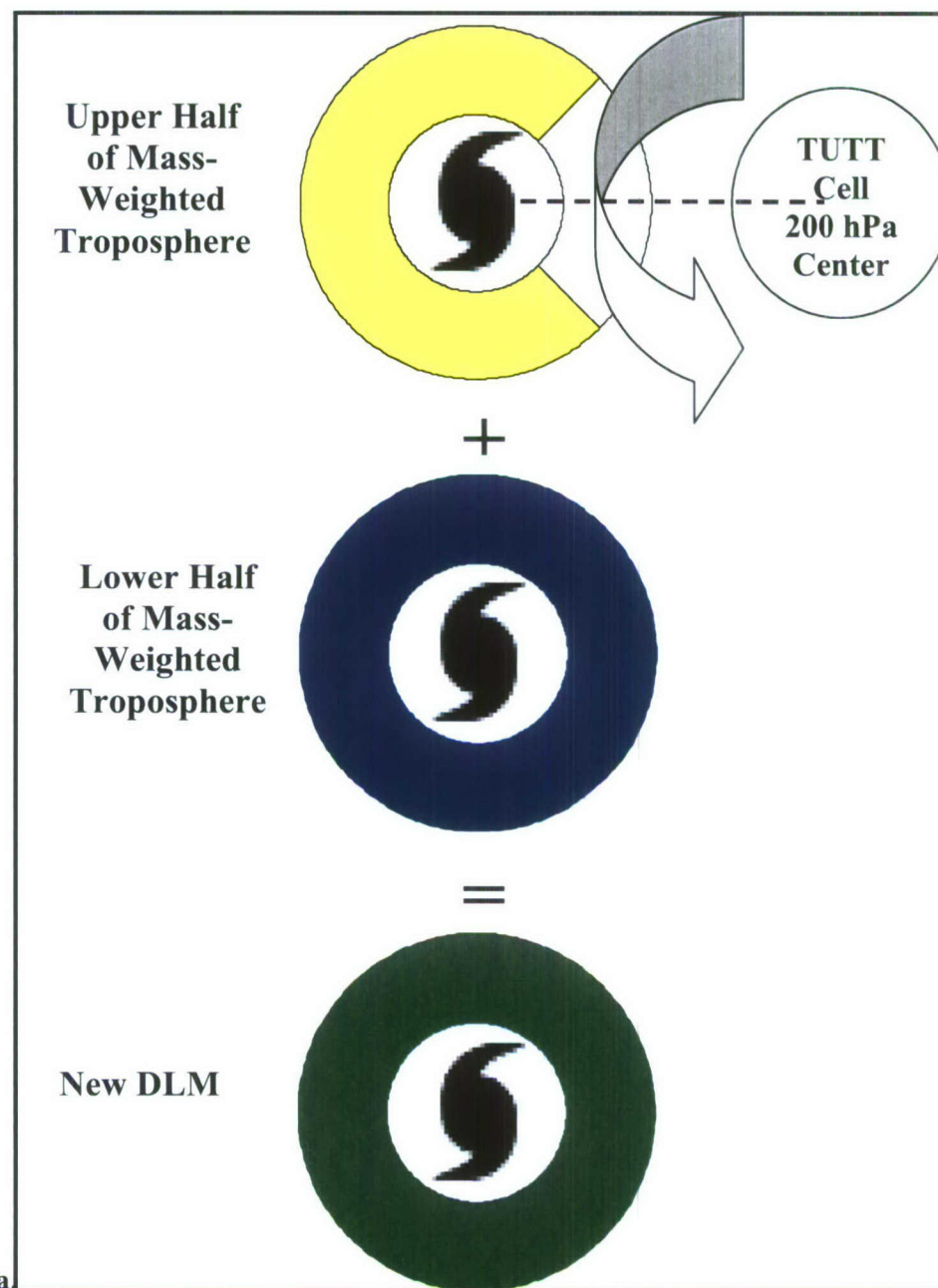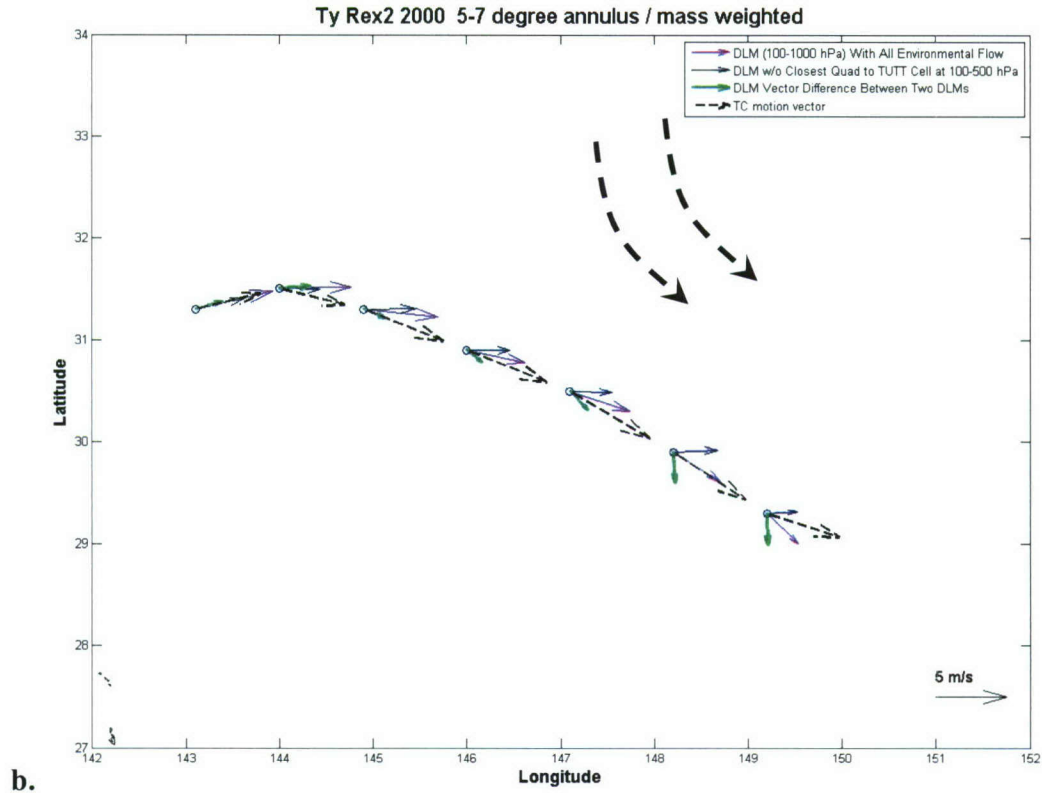
Figure 2.4 (a) Graphical depiction of the method used to remove a large portion of the TUTT cell's influence from the TC's upper layer environment in order to create a new mass-weighted DLM ESL without much of the TUTT cell's wind field and influence on TC motion. The ring around the TC symbol represents a particular radial band. The dashed line represents the radial connecting the TC (surface) and TUTT cell (200 hPa) centers of circulation. In this case, the radial is 90° or due east. The clear area within the radial band was excluded from the computation of the new DLM. (b) An example from Rex2 showing both the original DLM (pink), the new DLM with the upper layer quadrant closest to the TUTT cell at each time step removed (blue) and the difference between the two (green). The approximate large-scale TUTT cell flow based on their orientation at the time is superimposed with black dashed curving lines. My initial conceptual model for this case would expect a "tailwind" to accelerate the TC's forward speed and a southward component of motion to be added to the DLM.
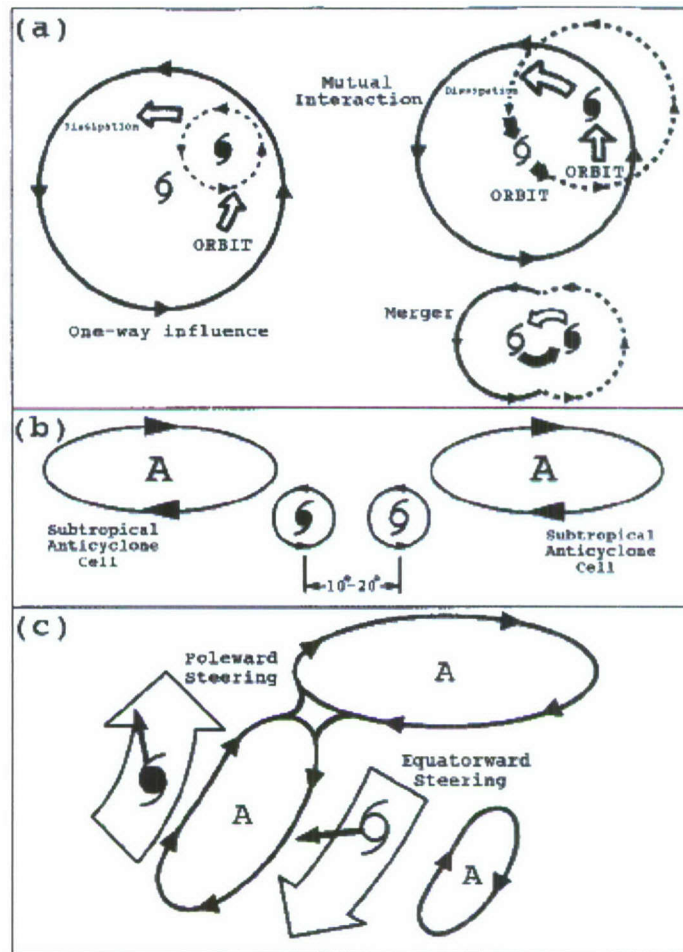
Figure 2.5 Conceptual models of binary TC interactions by Carr et al. (1997) and Carr and Elsberry (1998). (a) Three modes of direct interactions are the one-way influence, mutual interaction, and merger of the two TCs. (b) Semi-direct interactions involve another TC and an adjacent subtropical anticyclone. (c) Indirect interactions involve the anticyclone between the two TCs.

Weak Appearance

Amber 200 hPa Winds 22 Aug 97 at 00Z
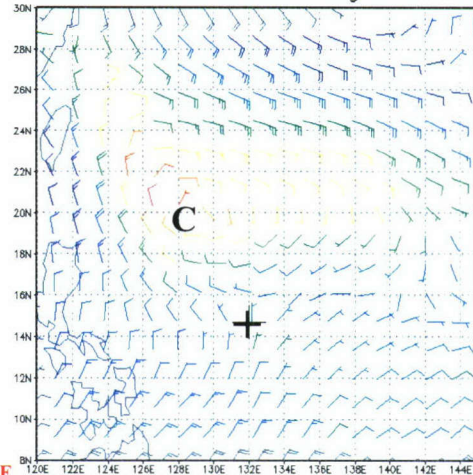
Moderate Appearance

Bolaven 200 hPa Winds 26 Jul 00 at 18Z
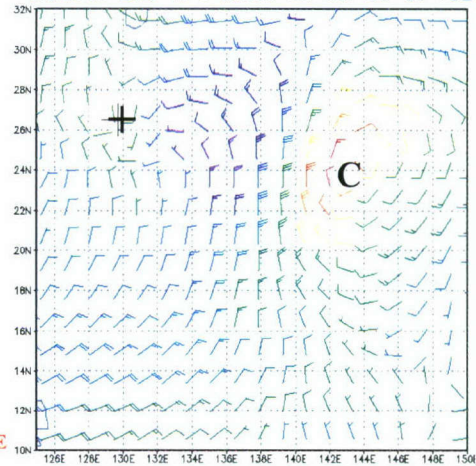
Intense Appearance

Rex2 200 hPa Winds 30 Aug 98 at 06Z

a.

TD 20W (RUMBIA) 4 OCT 2006 18Z OBJ AIDS

b.

Figure 3.1 (a) Examples of "weak" (Amber, 21Z 26 August 1997), "moderate" (Bolaven, 00Z 21 July 2000) and "intense" (Rex2, 03Z 30 August 1998) appearing TUTT cells in GMS water vapor imagery. The TUTT cell center is approximately marked with a 'C'. ERA-40 200 hPa wind fields from within +/- 3 hours are along side each image. (b) My initial conceptual model of a TUTT cell on a TC's track. The trapezoid is an estimated range of forecast TC motion and would encompass most of the forecast model track guidance. *A sample model ensemble and trapezoid field is provided to the right of the initial conceptual model.* Assuming an initial forecast down the center of the trapezoid box, track biases to the left or right, faster or slower than forecast without consideration of the TUTT cell's contributing flow would be annotated.

Figure 3.2 (a) Best Track and inset of track "stair steps" for Rex (06W) from the 1998 JTWC ATCR. Best Track intervals are 6 hours. Annotation is in the form DDHH S WW, where DD = day of the month, HH = GMT (Zulu) hour, S = TC's forward speed in knots and WW = TC's maximum 1 minute averaged sustained wind speed in knots (1 knot = 0.514 m s^{-1}). (b) A graphical depiction of both the TC (red) and TUTT cell (blue) tracks at 6-hourly intervals. The black arrow indicates general direction of TC motion. The red dotted lines indicate the start (00 – 06Z 31 August 1998) and end (18Z 1 September – 00Z 2 September 1998) points of the TUTT cell interaction period. The end point was due to the dissipation of a closed 200 hPa TUTT cell circulation. NOTE: The JTWC Best Track data and graphic in this case do not agree. The date-time-group for the northern most latitude of the TC prior to the second stair-step (green circle at 31.5°N at 12Z 31 August) does not match the annotated time on the graphic which (06Z 31 August). Times and positions from the actual Best Track data set were used in this study and not the values from the graphic.
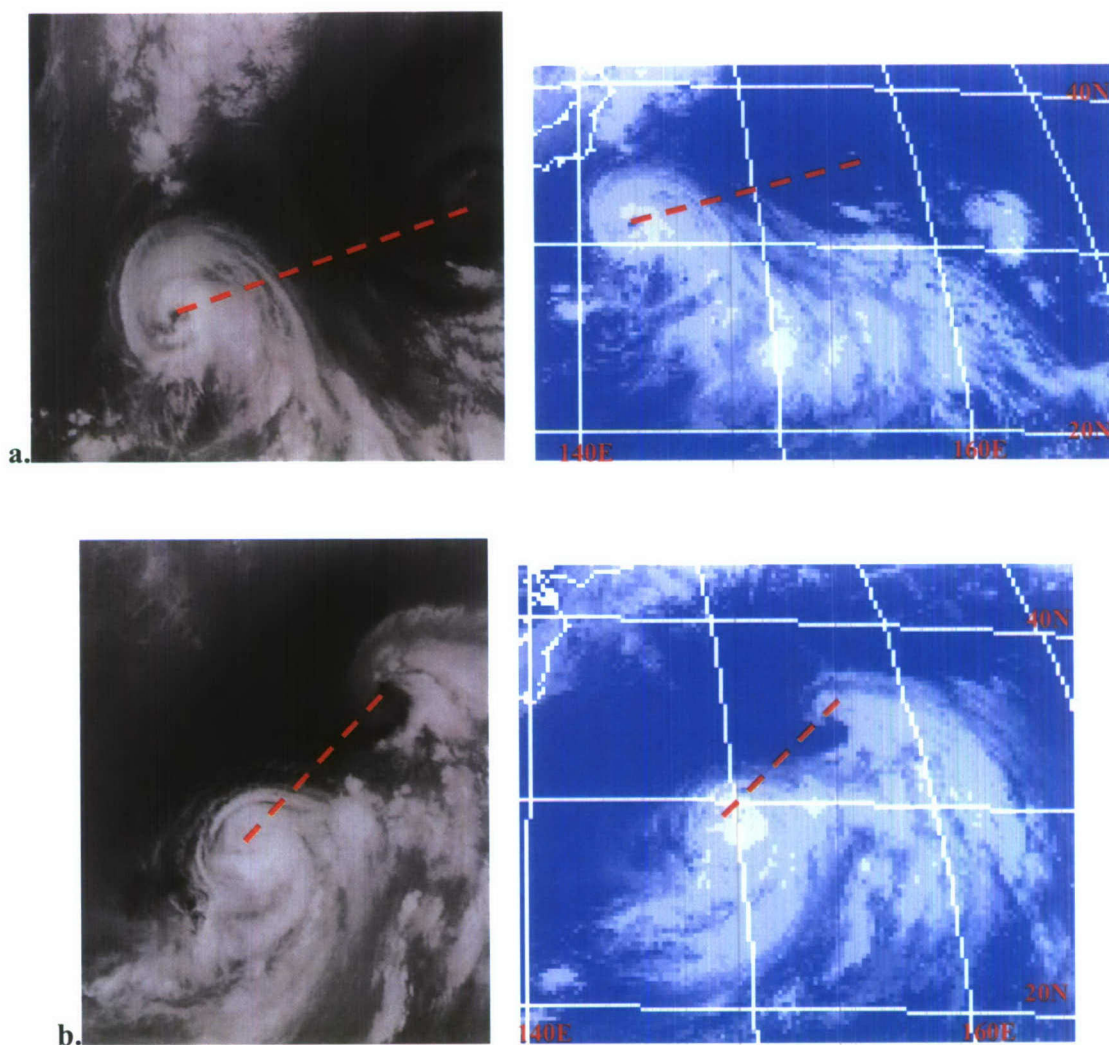
Figure 3.3 GMS-5 water vapor (left) and infrared (right) satellite imagery of Rex2 at (a) 00Z 31 August 1998, just prior to the start of the interaction period, and at (b) 18Z 1 September 1998 near the end of the interaction period and the dissipation of the TUTT cell's 200 hPa closed circulation in the ERA-40 data.   The dashed red line approximately connects the centers of the two circulations as defined by this study.
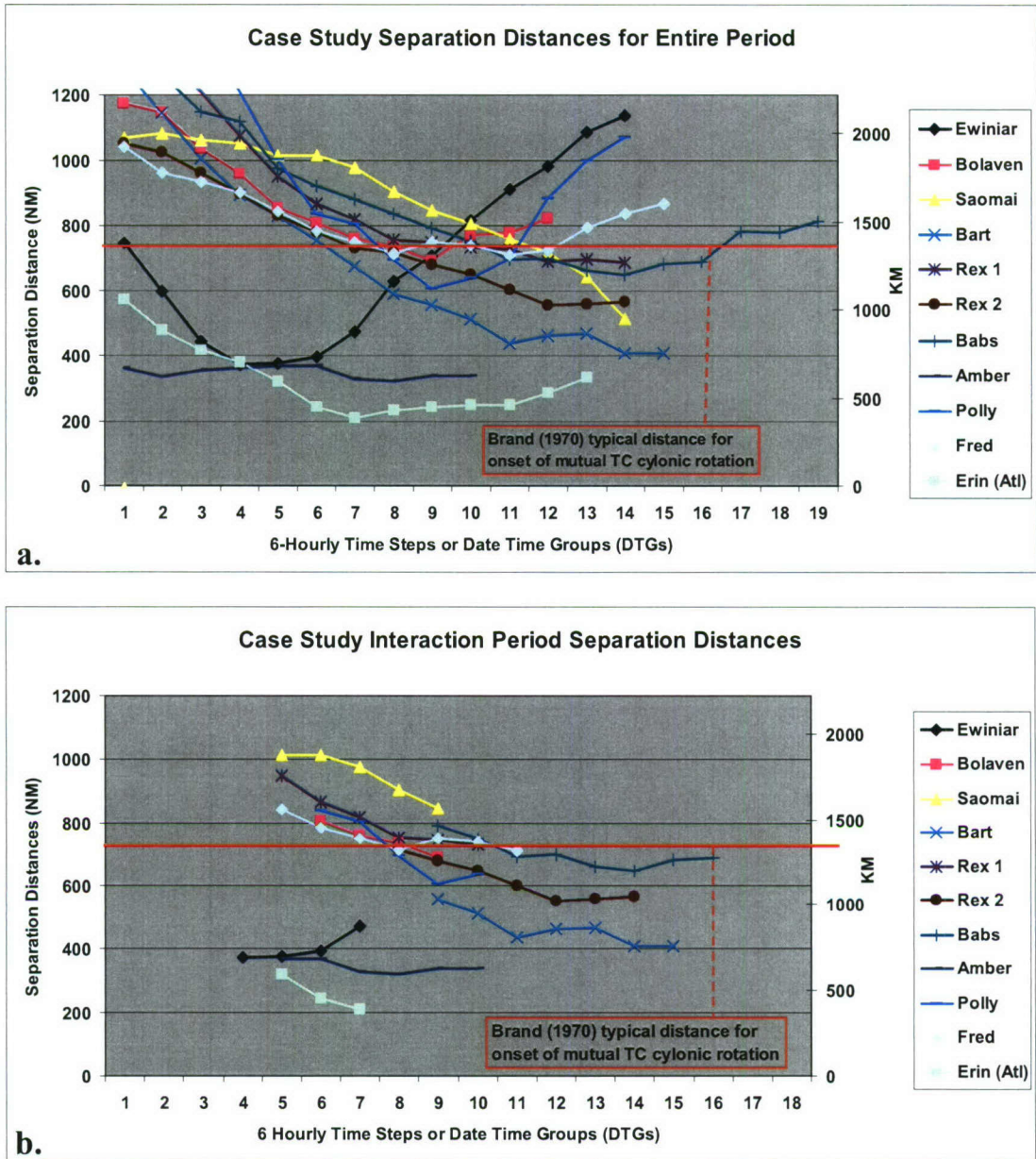
Figure 3.4 Case study summary of separation distances between the TC (sfc) and TUTT cell (200 hPa) circulation centers during (a) the entire period of time used in this study and (b) during only a case's defined interaction period. Brand's (1972) key maximum separation distance criteria for the binary interaction of two TCs is annotated.

a.

b.
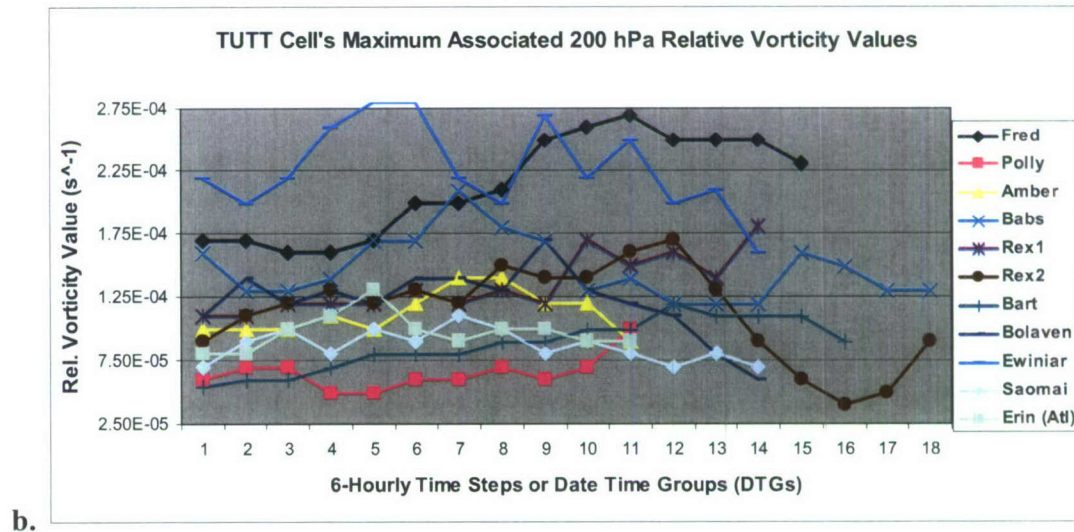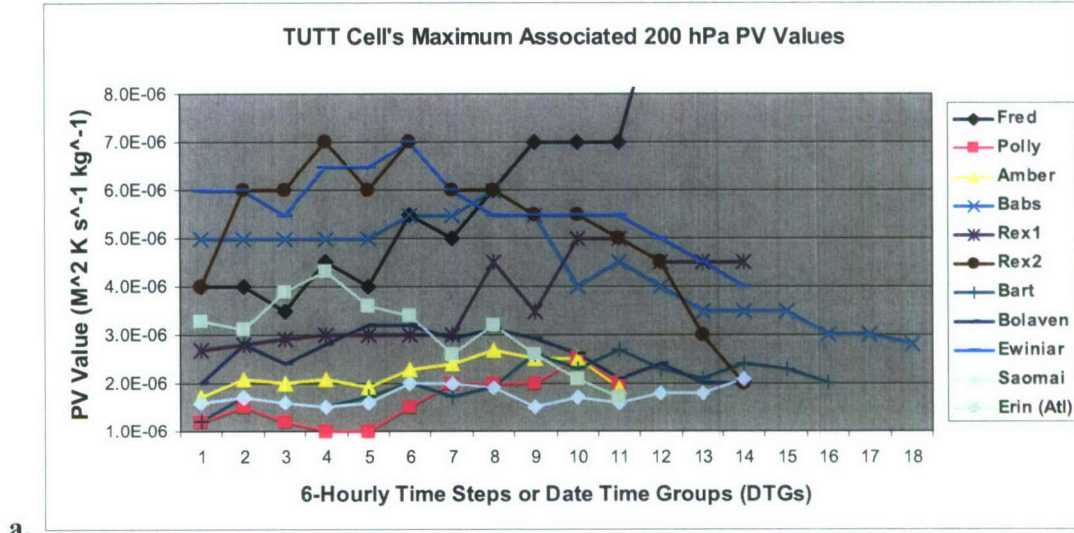
Figure 3.5 Time series (6 hourly time steps, or date time groups (DTGs), into a case study) of the maximum (a) potential vorticity and (b) relative vorticity associated with the TUTT cell for each case at 200 hPa.   This helps to provide a value for TUTT cell "intensity" in each case.
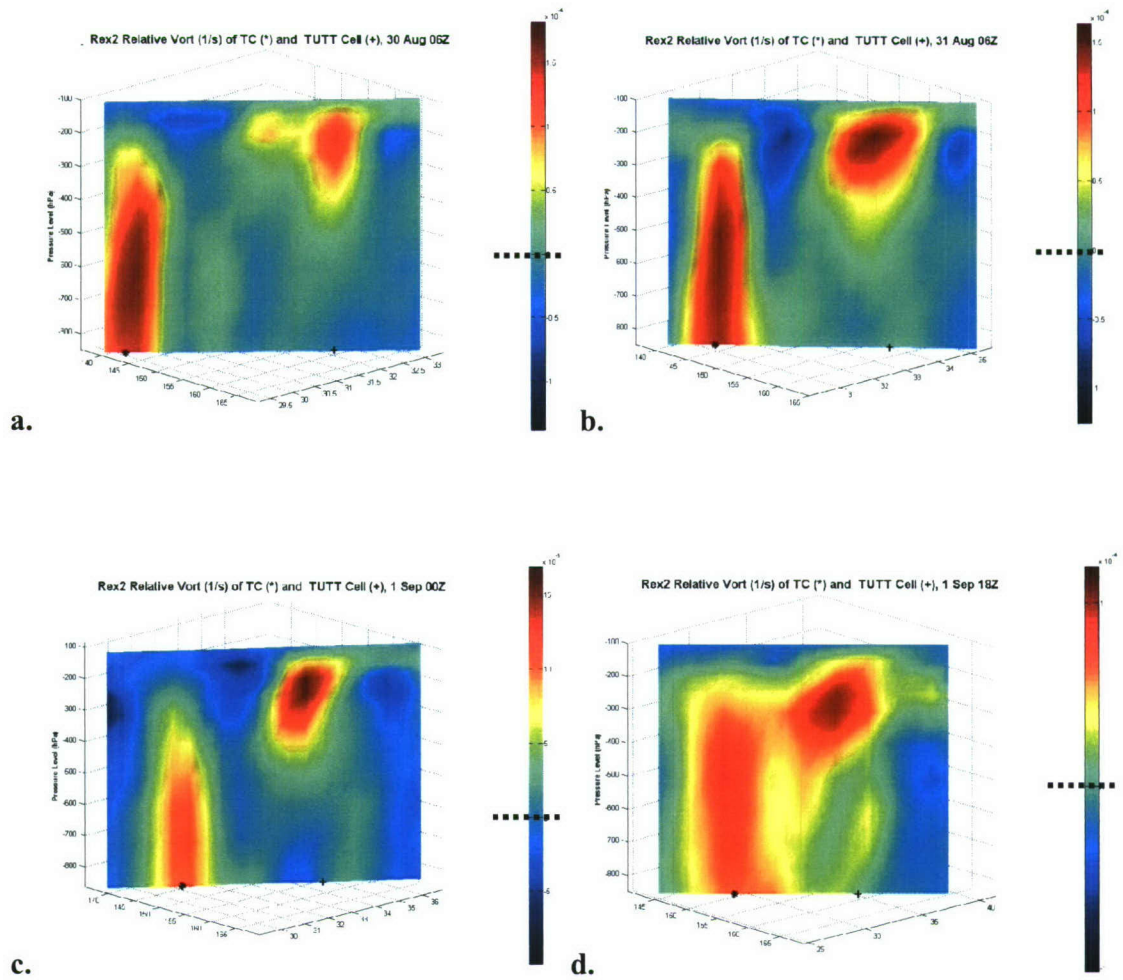
Figure 3.6 Relative vorticity (image dependent, 10^{-4} or 10^{-5} s^{-1}) cross-sections from 100 hPa down to 850 hPa for Rex2 at (a) 06Z 30 August (pre-interaction period), (b) 06Z 31 August (at interaction start point), (c) 00Z 1 September at (middle of interaction period) and (d) 18Z 1 September 1998 (near end of interaction period). Deeper yellow and red colors represent greater *positive* relative vorticity. The black dotted line represents $\zeta_r = 0$.
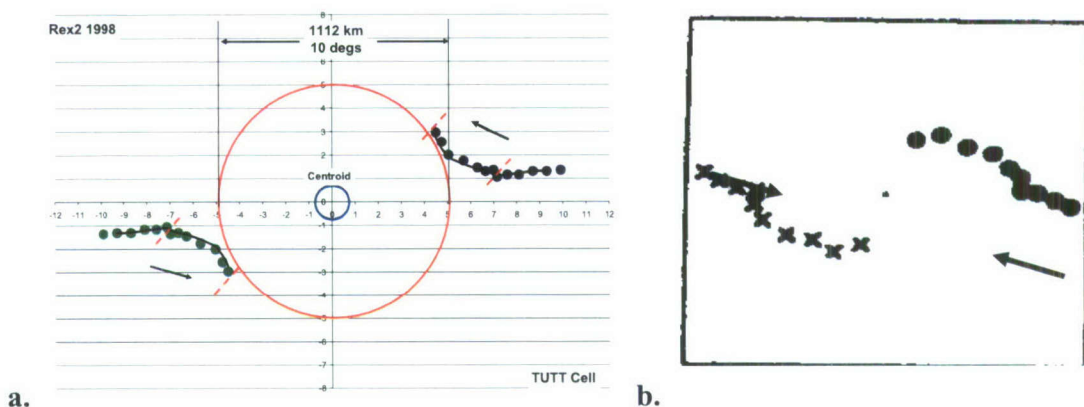
Figure 3.7 (a) Centroid relative motion using a 2-point running average (black line running through the green and dark blue dots) between Rex2 and the associated TUTT cell. The red dotted lines indicate the start (between 00Z-06Z 30 August 1998) and end (between 18Z 1 September – 00Z 2 September 1998) points of the TUTT cell interaction period. The black arrows indicate the general direction of motion. (b) LH93's Polly and Rose (1974) centroid relative motion.
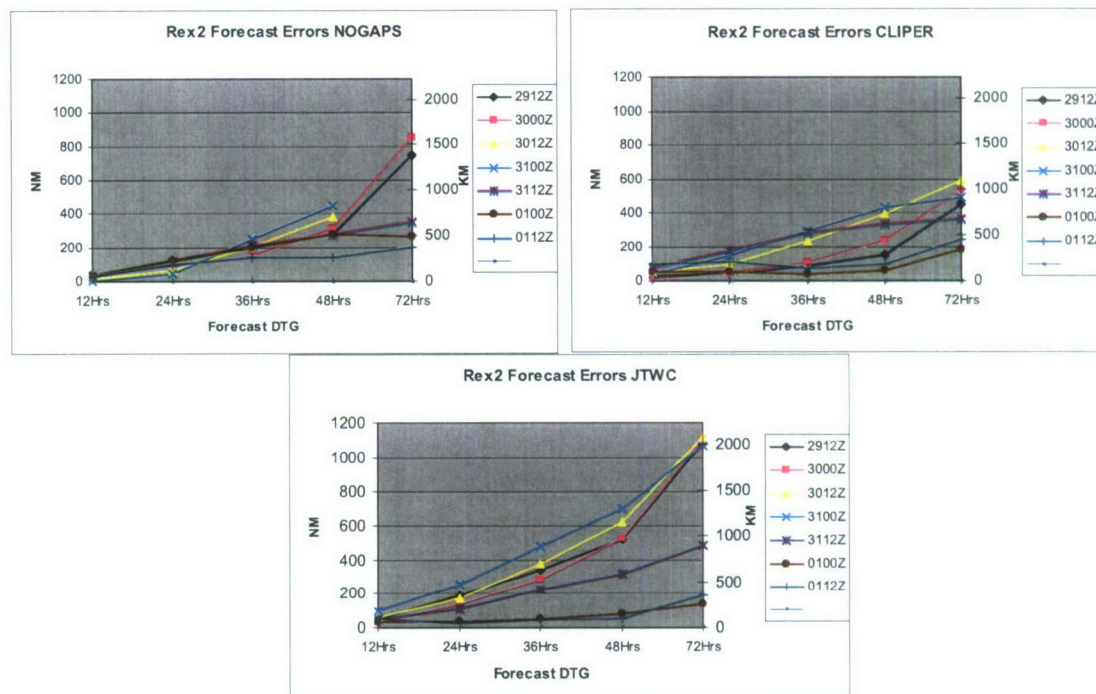
Figure 3.8 Rex2 12-72 hour forecast errors for NOGAPS* (top left), CLIPER (top right) and the JTWC (bottom). *Note: some 72 hour forecast data were missing from JTWC records.
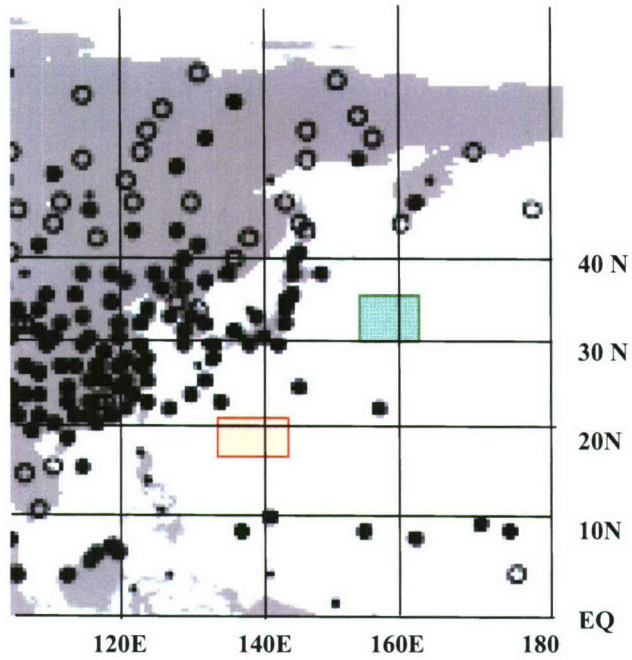
Figure 3.9 Frequency of radiosonde reports in 2001. Solid circles denote stations from which at least three reports are available every two days on average, open circles denote other stations reporting at least once every two days and small dots represent stations reporting at least once per week. (Uppala 2005). Green shaded area denotes the approximate location of the center of Rex2's TUTT cell. Red shaded area denotes the approximate location of the center of Bab's TUTT cell.
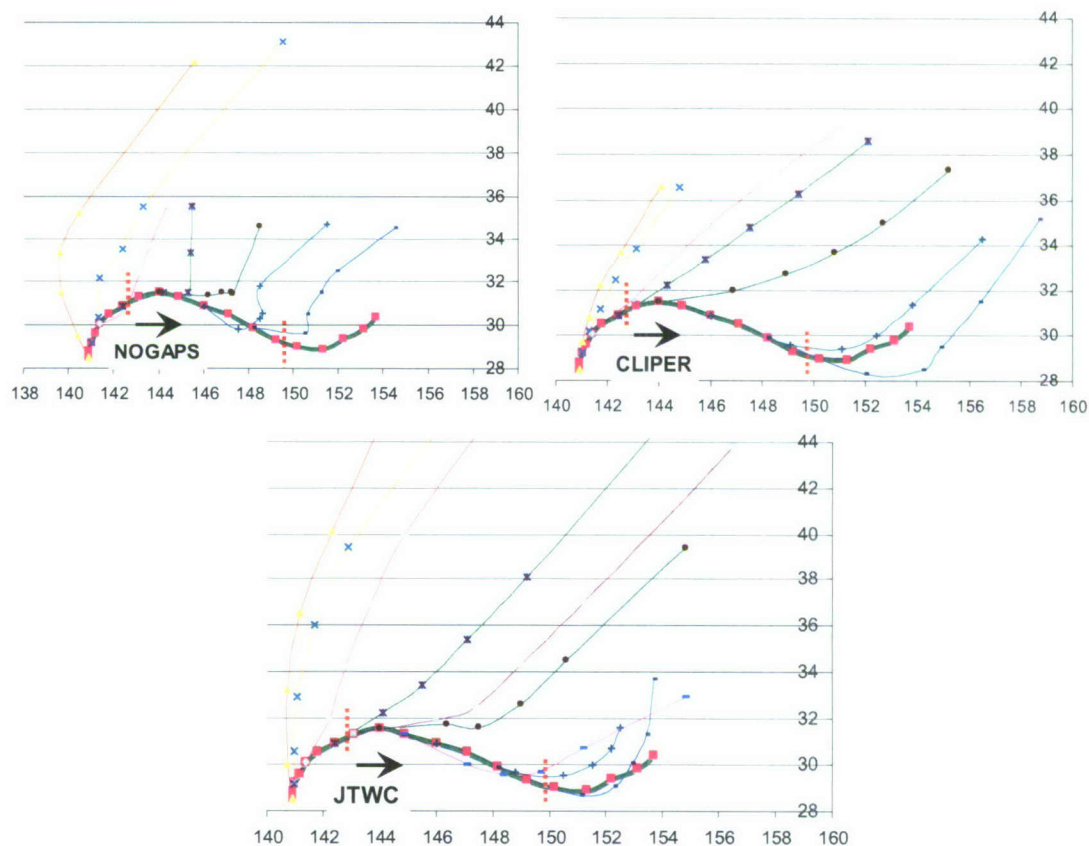
Figure 3.10 Rex2 forecast tracks at 6 and 12 hour intervals for NOGAPS (upper left), CLIPER (upper right) and the JTWC (bottom). The black arrow indicates general direction of TC motion. The red dotted lines indicate the start and end points of the TUTT cell interaction period. Red dotted lines mark interaction the start (00Z-06Z 31 August 1998) and end points (18Z 31 August– 0Z 1 September 1998).
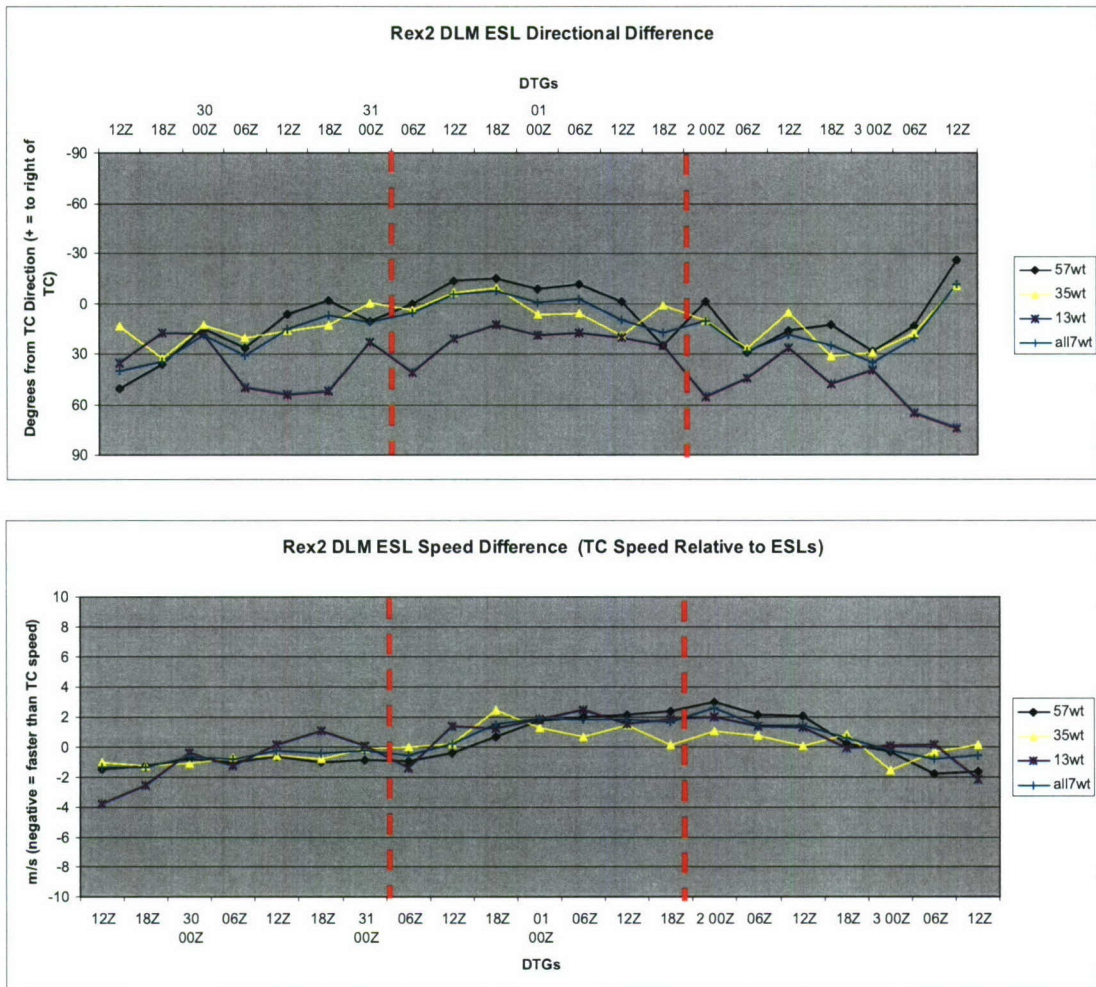
Figure 3.11 Example of the *initial* time series analysis tool used to observe variations in deep layer mean (DLM) ESL direction (top) and speed (bottom) relative to TC motion (Rex2). The red dashed lines indicate the approximate start and end points of the TUTT cell interaction period. The direction and/or speed are equal to the TC's if aligned with the bold dotted horizontal zero-line. For direction, positive (below dotted line) occurs when the ESL is to right of TC motion vector. For speed, positive (above the dotted line) occurs when the ESL is slower than TC's speed. ESLs are listed as radial band (13, 35, 57) and weighted (wt) or not weighted (noWT).
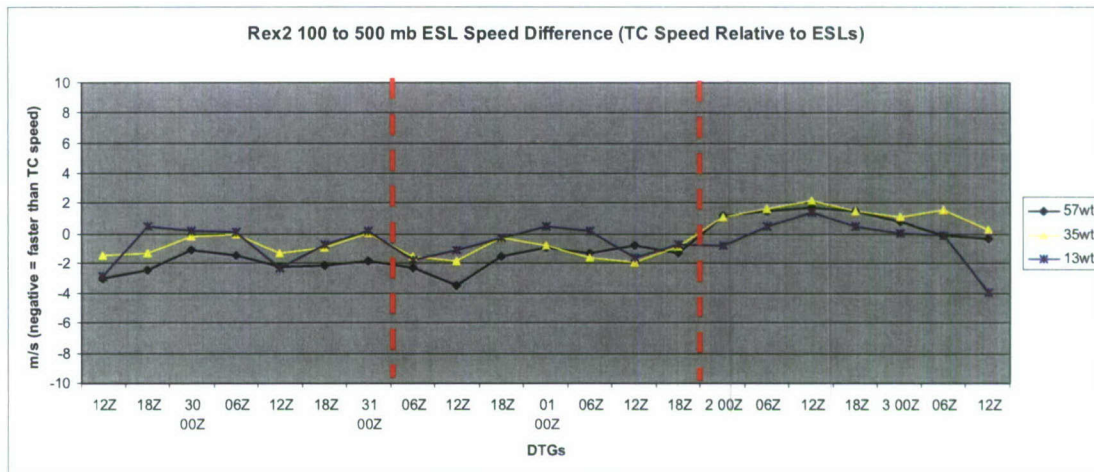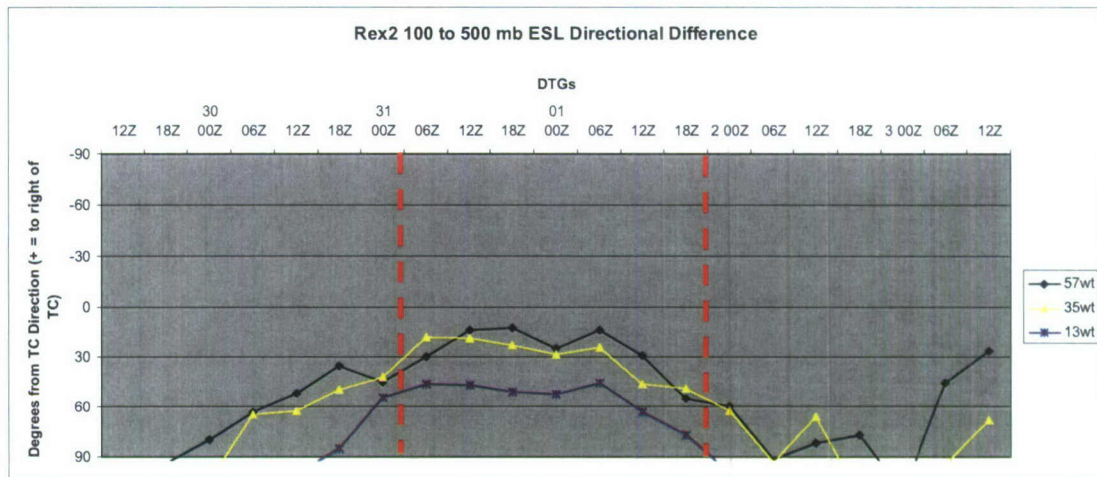
Figure 3.12 As in Figure 3.11 but for the 100 to 500 hPa (upper) layer.
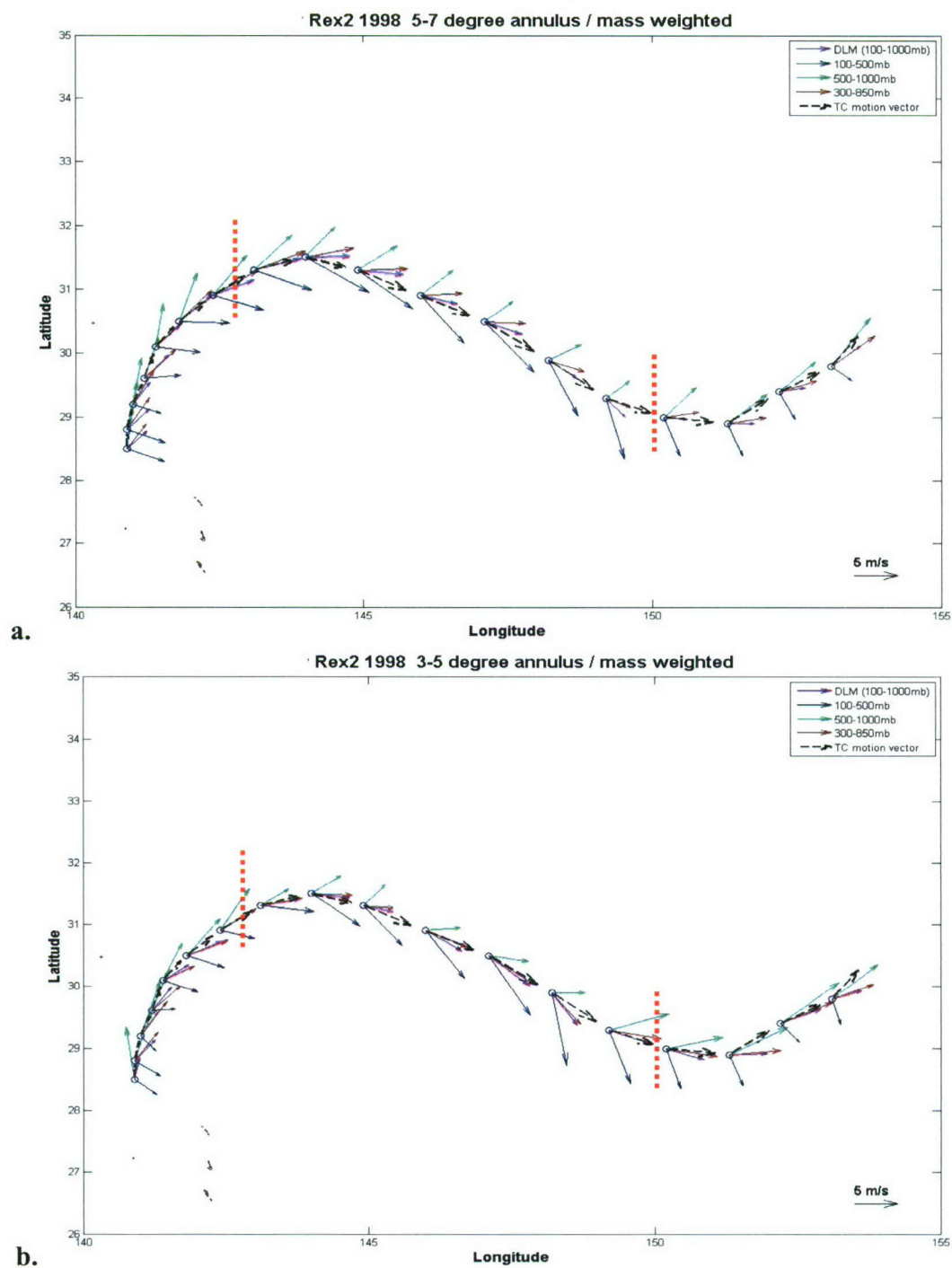
Figure 3.13 Four-layer mean wind field analysis for Rex2. Vectors are scaled to the average speed of the TC between each 6 hourly time step. Vectors point in the mean radial direction for (a) the 5°-7° and (b) the 3°-5° radial bands. Red dotted lines mark the interaction start (00Z–06Z 31 August) and end points (18Z 31 August– 00Z 1 September 1998).

- 117 -
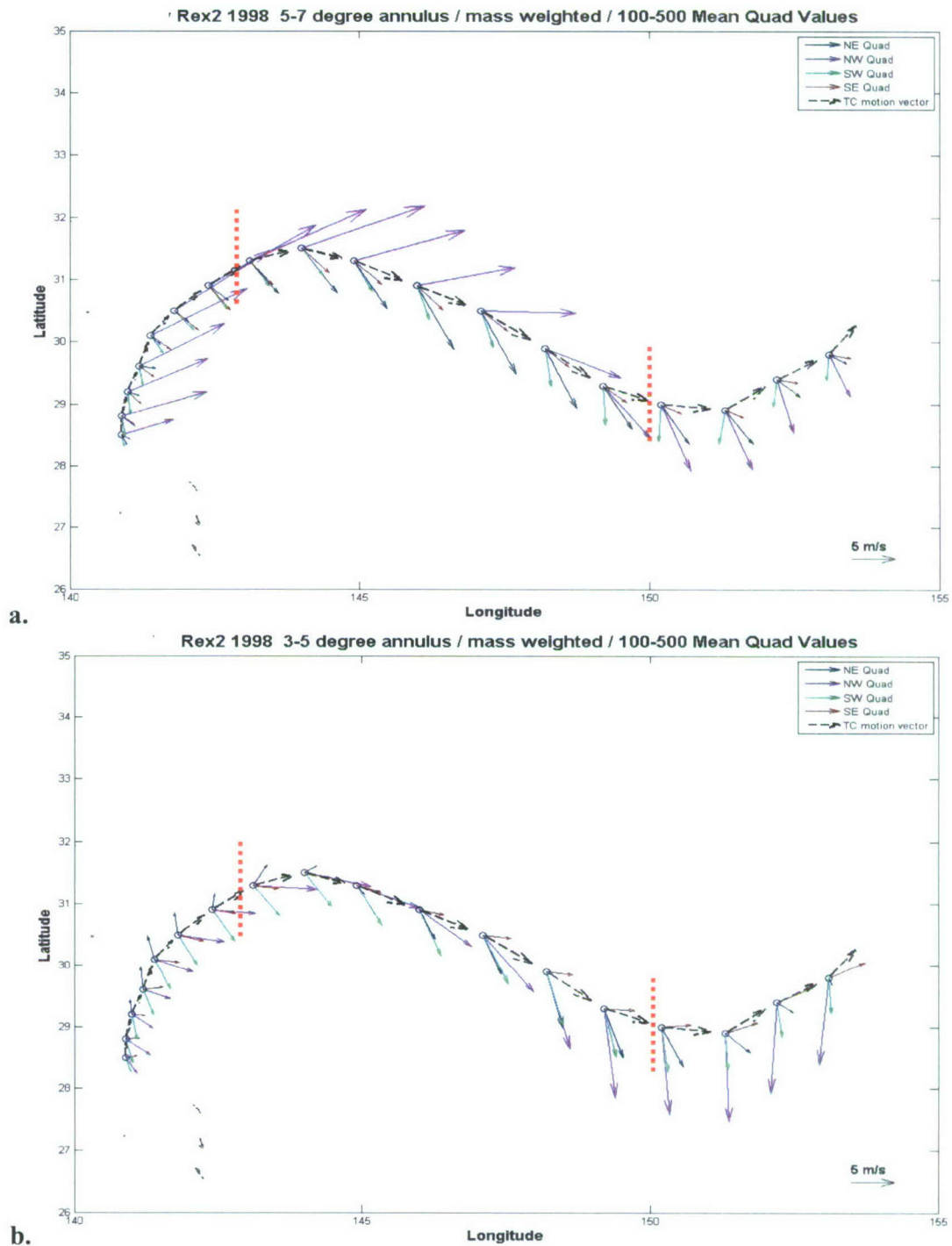
Figure 3.14 Four-quadrant mean wind field analysis of the upper layer for Rex2. Vectors are scaled to the average speed of the TC between each 6 hourly time step. Vectors point in the mean radial direction for (a) the 5°-7° and (b) the 3°-5° radial bands. Red dotted lines mark the interaction start (00Z-06Z 31 August) and end points (18Z 31 August– 00Z 1 September 1998).
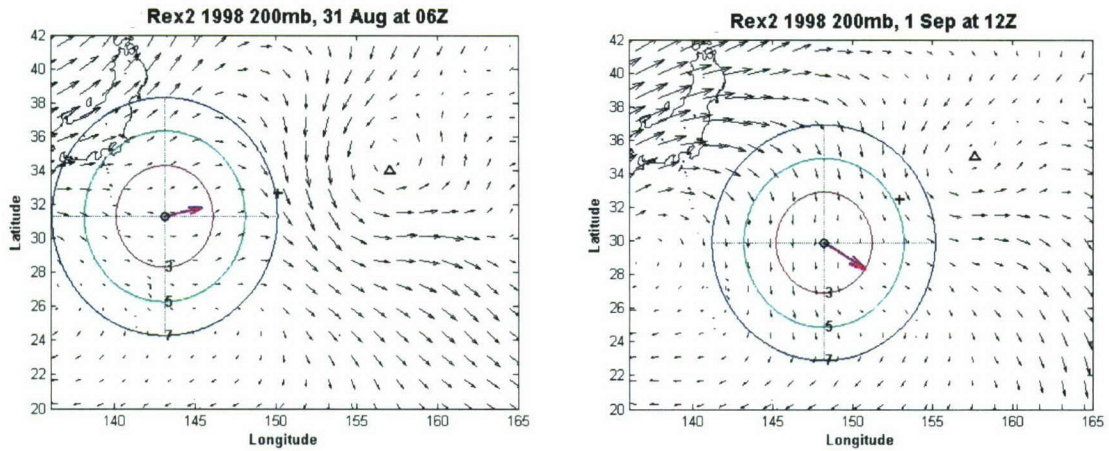
Figure 3.15 Rex2 200 hPa wind field analysis at 06Z 31 August 1998 (on left and near the interaction start point) and 12Z 1 September 1998 (on right and late into the interaction period). The "o" represents the Best Track low-level center of Rex2. The "+" represents the centroid of the two circulations. The "Δ" represents the approximate 200 hPa TUTT cell circulation center. The red, green and blue circles represent the approximate 3°, 5° and 7° radii, respectively, and are divided into quadrants. The pink arrow represents the TC's trajectory.

Rex2 1998 5-7 degree annulus / mass weighted
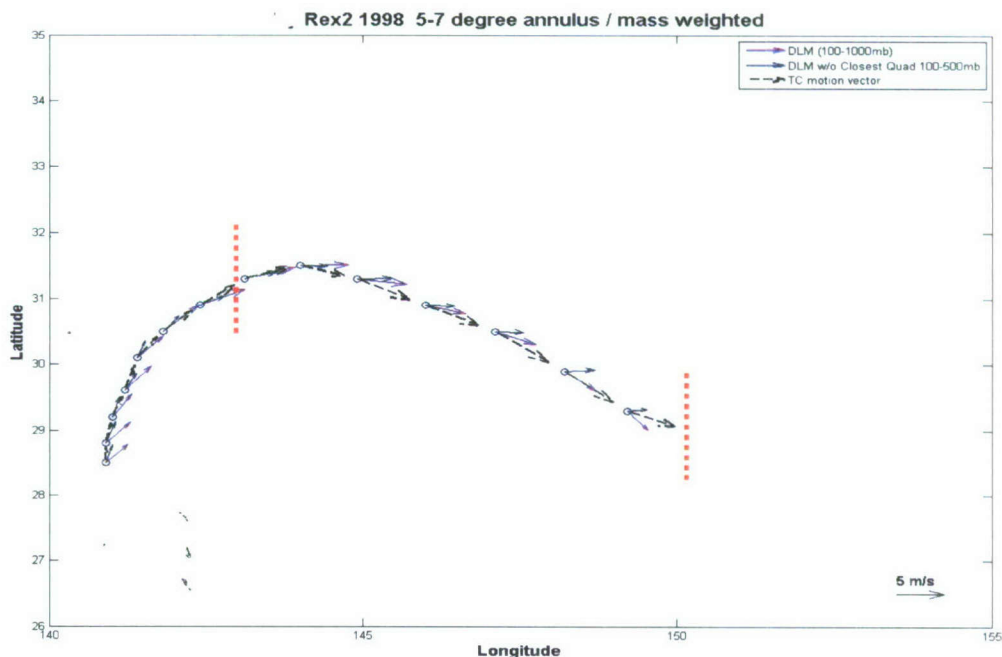
Figure 3.16 The original mass-weighted DLM and the new mass-weighted DLM with the upper layer quadrant closest to the TUTT cell removed for Rex2. Vectors are scaled to the average speed of the TC between each 6 hourly time step. Vectors point in the mean radial direction for the 5°-7° radial band.   Red dotted lines mark the interaction start (00Z-06Z 31 August) and end points (18Z 31 August– 00Z 1 September 1998). The TC's track stops at the interaction end point as the TUTT cell's 200 hPa circulation center dissipates.
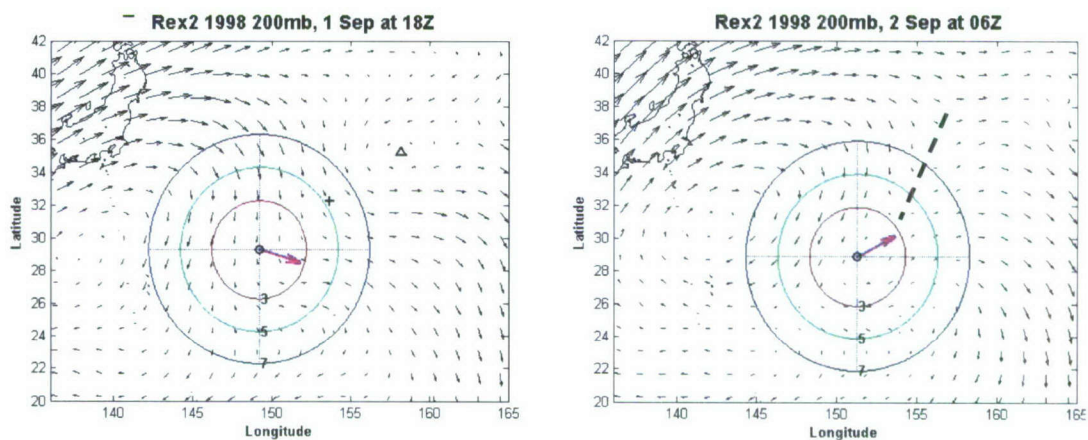
Figure 3.17 As in Figure 3.15 except at 18Z 1 September 1998 (left) and 06Z 2 September 1998 (right) at the interact end point. The dashed line represents a trough as indicated in the ERA-40 wind field due to the loss of a closed TUTT cell circulation center.
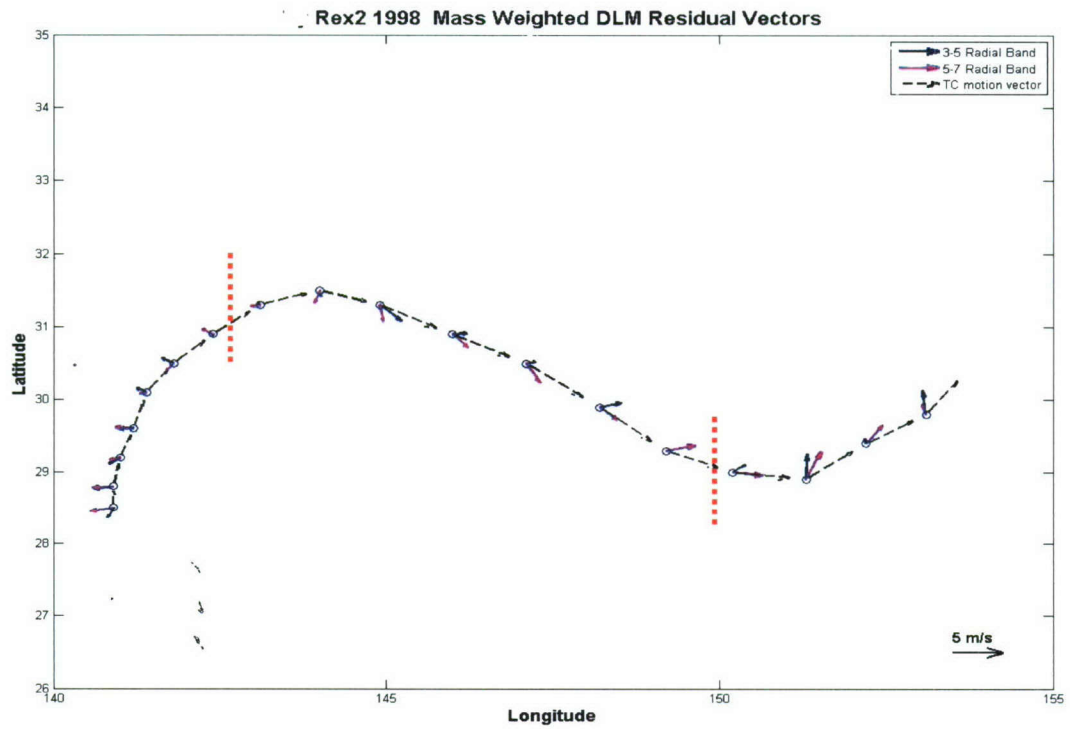
Figure 3.18 Mass-weighted DLM residual vector analysis for Rex2. Vectors are scaled to the average speed vector (dashed line) of the TC between each time step. Vectors point in the mean radial direction at different radial bands. Red dotted lines mark the interaction start (00Z-06Z 31 August) and end points (18Z 31 August– 00Z 1 September 1998).
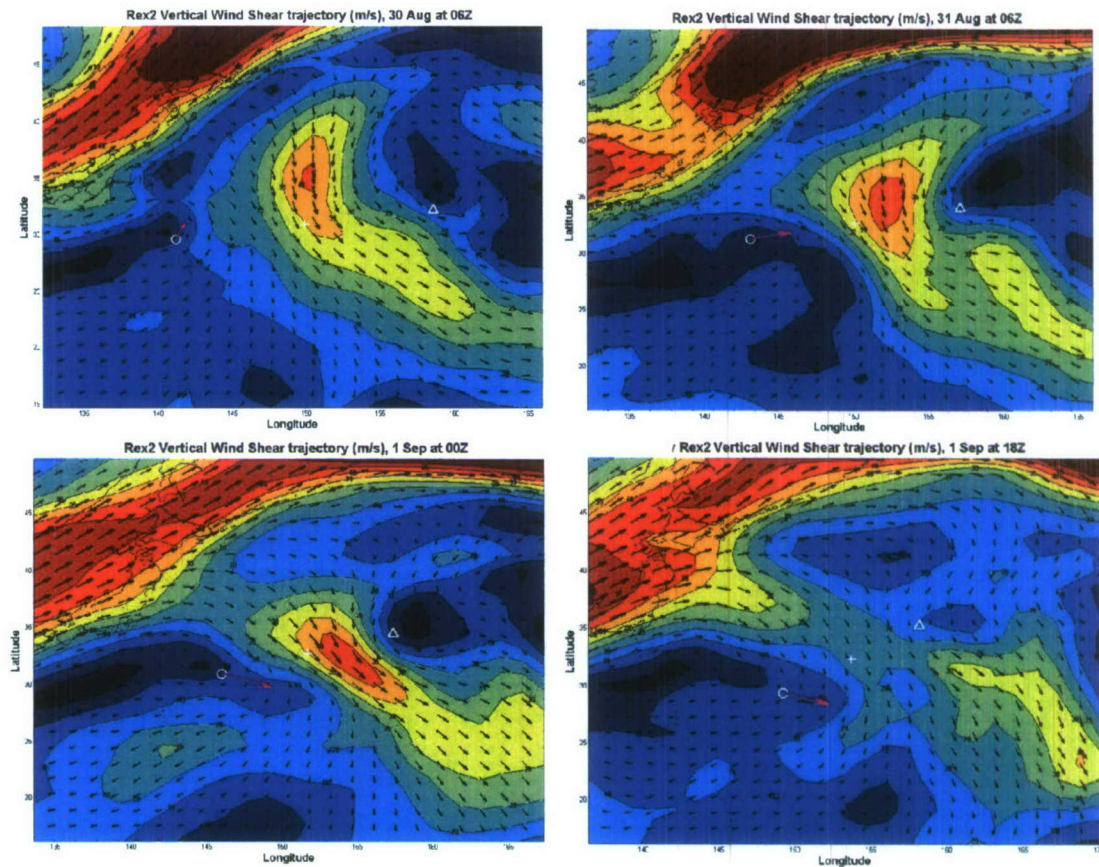
Figure 3.19 Rex2 vertical shear of the horizontal wind fields (200 hPa – 850 hPa) in m s⁻¹ for four time steps: (upper left) pre-interaction period at 12Z 29 August 1998, (upper right) interaction start point at 06Z 31 August 1998, (lower left) middle of the interaction period at 00Z 1 September 1998 and (lower right) just prior to the end point of the interaction period at 18Z 1 September 1998. The white "o" represents the TC center, the white "+" is the centroid and the white "Δ" is the approximate 200 hPa TUTT cell center of circulation. The pink arrow represents the TC's trajectory.

Figure 3.20 (a) Best Track and inset for Babs (20W) from the 1998 JTWC ATCR. Best Track intervals are at 6 hours. Annotation is in the form **DDHH S WW**, where **DD** = day of the month, **HH** = GMT (Zulu) hour, **S** = TC's forward speed in knots and **WW** = TC's maximum 1 minute averaged sustained wind speed in knots (1 knot = 0.514 m s^{-1}). (b) A graphical depiction of both the TC (pink) and TUTT cell (dark blue) tracks at 6-hourly intervals. The black arrow indicates general direction of TC motion. The red dotted lines indicate the start (between 12Z-18Z 17 October 1998) and end (between 12Z-18Z 19 October 1998) points of the TUTT cell interaction period.

Figure 3.21 GMS-5 water vapor (left) and infrared (right) satellite imagery of Babs at (a) 18Z 17
October 1998, just prior to the start of the interaction period, and at (b) 00Z 1 October 1998, near
the end of the interaction period.   The dashed red line approximately connects the centers of the
two circulations as defined by this study.   The white dashed line approximates the flow around
the TUTT cell center.
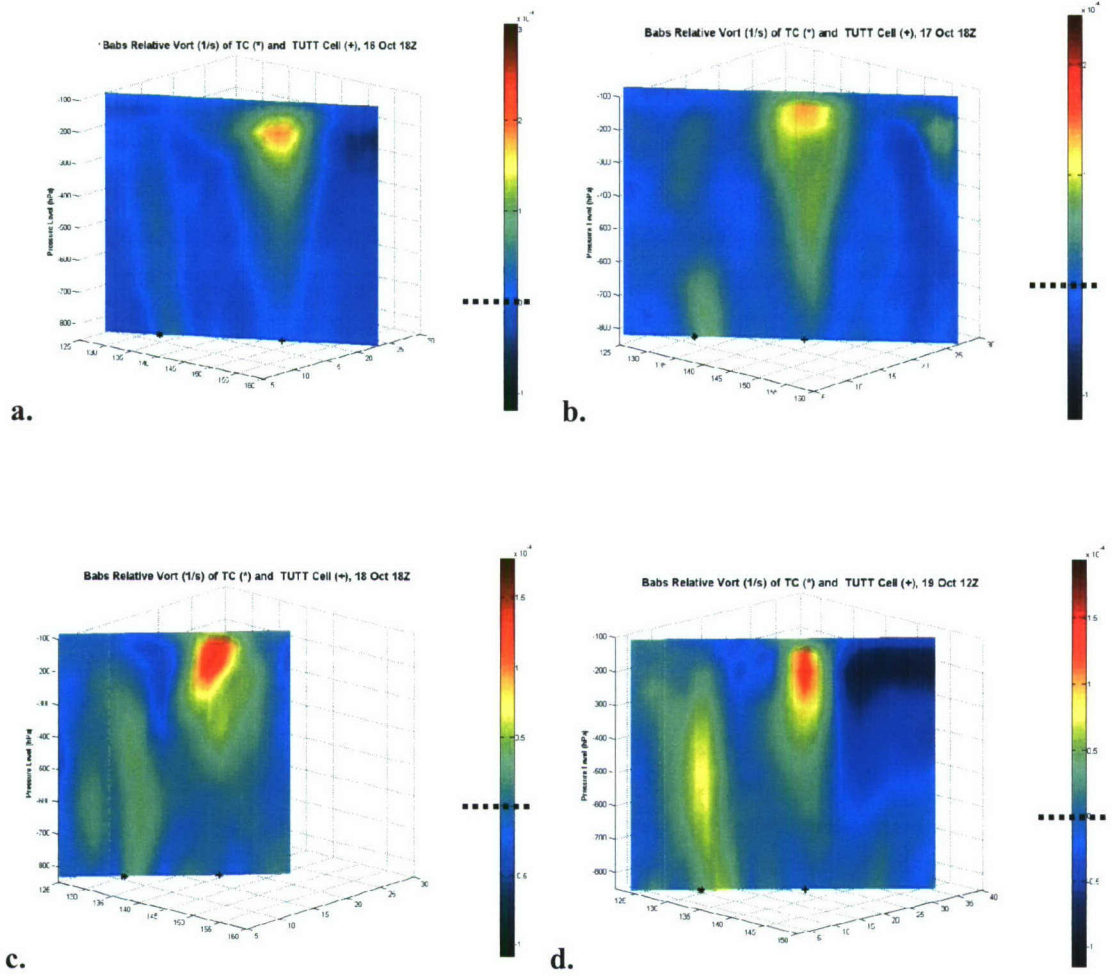
Figure 3.22 Relative vorticity (10^{-4} s^{-1}) cross-sections from 100 hPa down to 850 hPa for Babs at (a) 18Z 16 October 1998 (24 hours prior to the interaction start point), (b) 18Z 17 October 1998 (near the interaction start point), (c) 18Z 18 October 1998 (middle of the interaction period) and (d) 12Z 19 October 1998 (near the interaction end point). Deeper yellow and red colors represent greater *positive* relative vorticity. The black dotted line represents $\zeta_r = 0$.

Figure 3.23 (a) Centroid relative motion using a 2-point running average (black line running through the green and dark blue dots) between Babs and the associated TUTT cell. The red dotted lines indicate the start (between 12Z-18Z 17 October 1998) and end (between 12Z-18Z 19 October 1998) points of the TUTT cell interaction period. The black arrows indicate the general direction of motion. (b) LH93's Mac and Nancy (1979) centroid relative motion.

Figure 3.24 Babs 12-72 hour forecast errors for NOGAPS* (top left), CLIPER (top right) and the JTWC (bottom). *Note: some 72 hour forecast data was missing from JTWC records.

- 126 -

Figure 3.25 Babs forecast tracks at 6 and 12 hour intervals for NOGAPS (upper left), CLIPER (upper right) and the JTWC (bottom). The black arrow indicates general direction of TC motion. The red dotted lines indicate the start (between 12Z-18Z 17 October 1998) and end (between 12Z-18Z 19 October 1998) points of the TUTT cell interaction period.
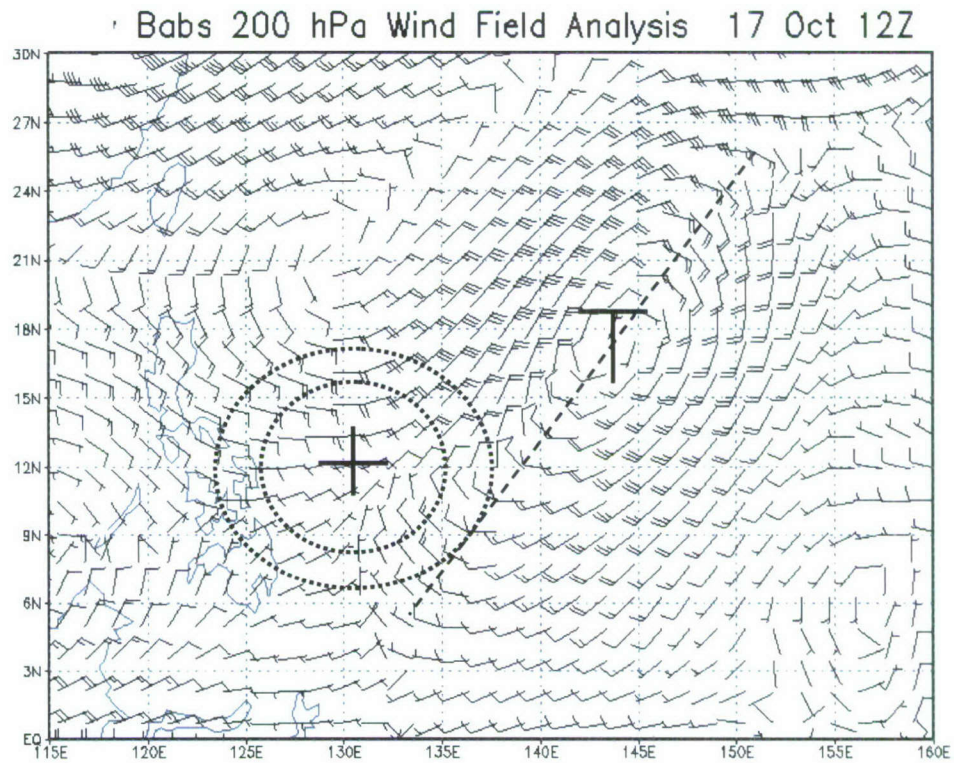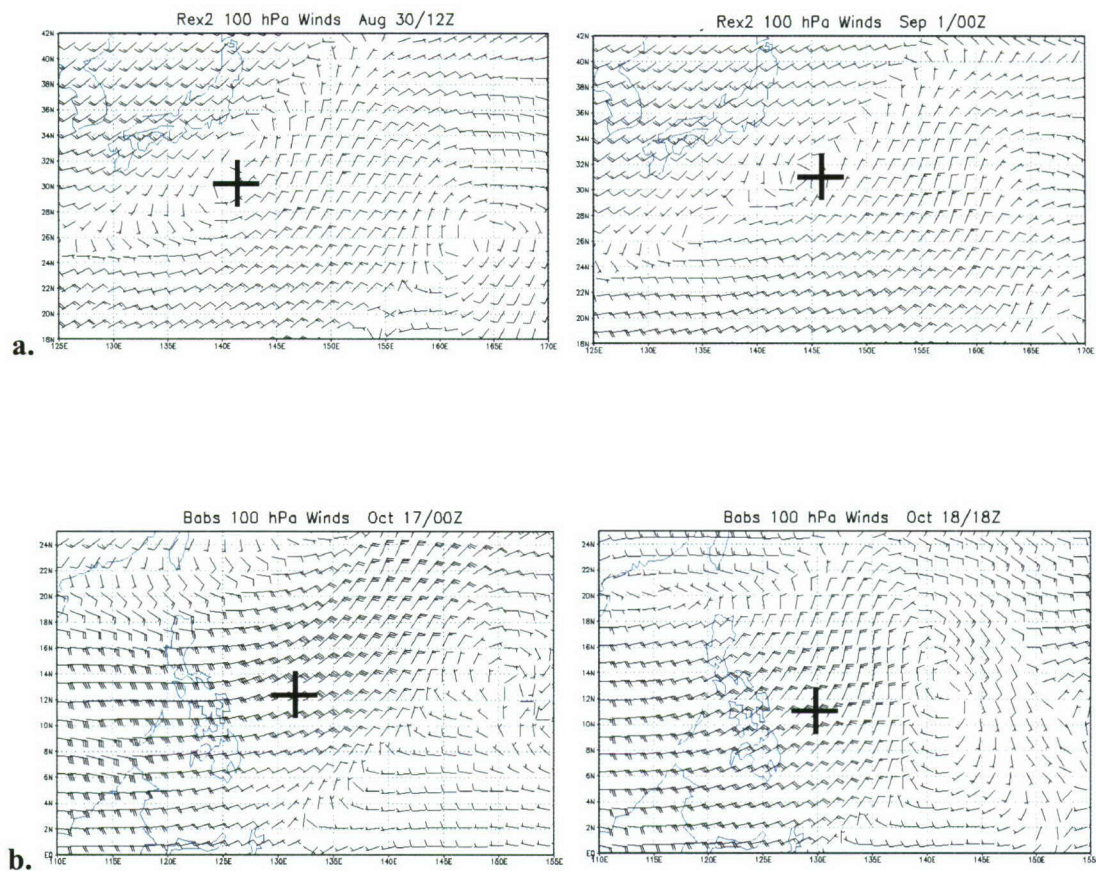
Figure 3.26   200 hPa wind field analysis at 12Z 17 October 1998 just prior to the start of the interaction period. The "+" represents the Best Track low-level center of Babs. The "T" represents the approximate 200 hPa TUTT cell center of circulation. The two dashed circles represent the approximate the 5° and 7° radial bands. A full wind barb equals 5 m s^{-1}. A half barb equals 2.5 m s^{-1}. For scaling purposes, the dashed straight line through the TUTT cell is approximately 2800 km.
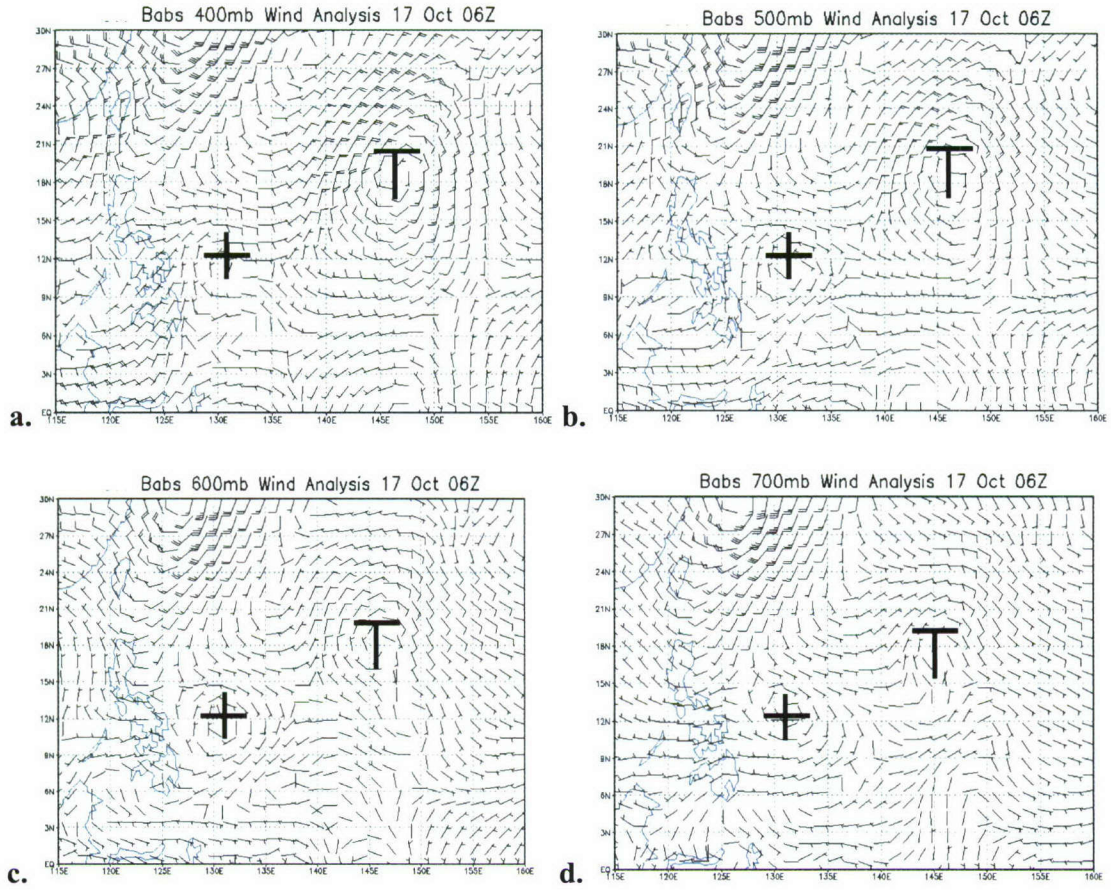
Figure 3.27 (a) 400 hPa, (b) 500 hPa, (c) 600 hPa and (d) 700 hPa wind field analysis at 06Z 17 October 1998 just prior to the start of Babs interaction period. The "+" represents the Best Track low-level center of Babs. The "T" represents the approximate TUTT cell center of circulation at each level. A full wind barb equals 5 m s^{-1}. A half barb equals 2.5 m s^{-1}.

Babs 1998 5-7 degree annulus / mass weighted

a.

Babs 1998 3-5 degree annulus / mass weighted
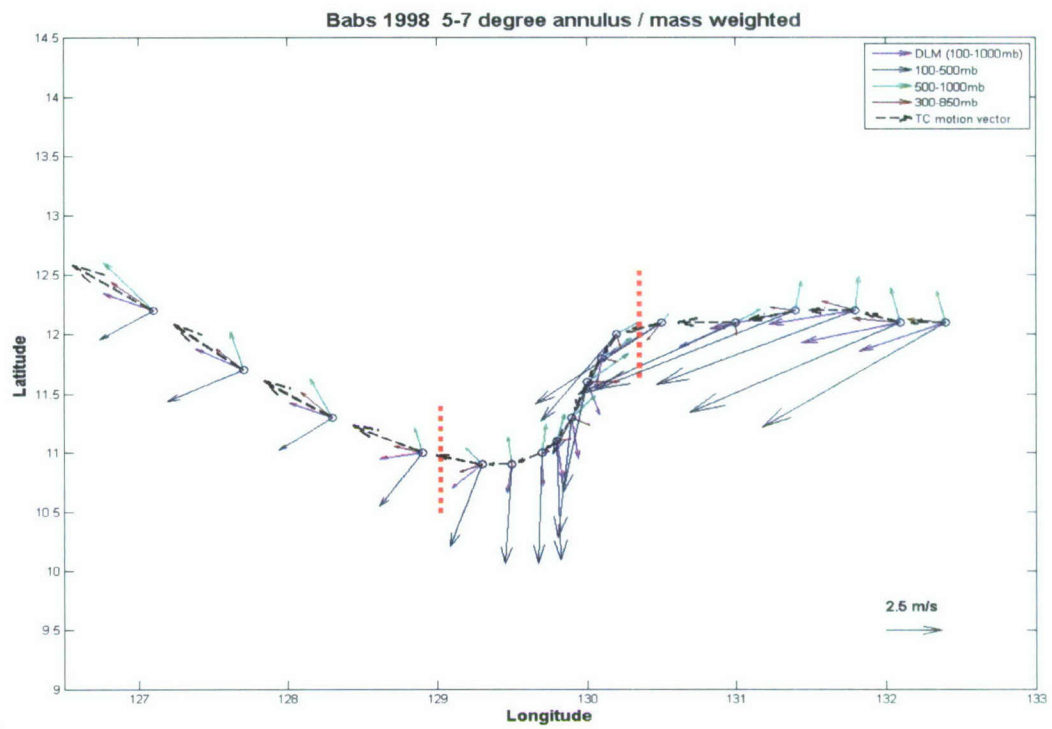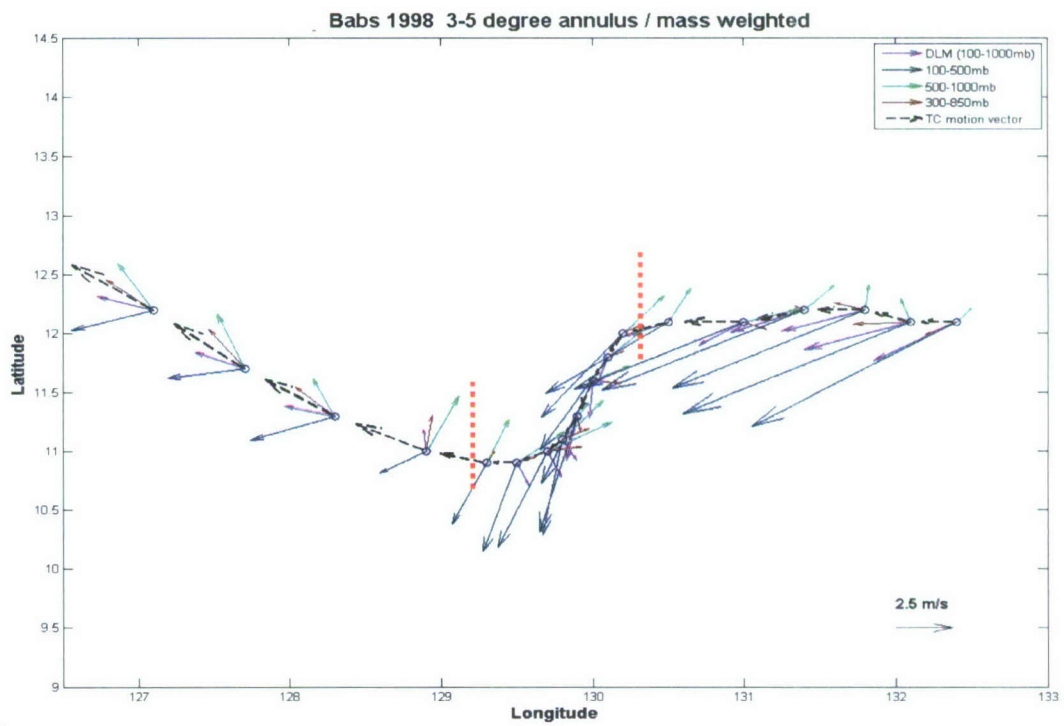
b.
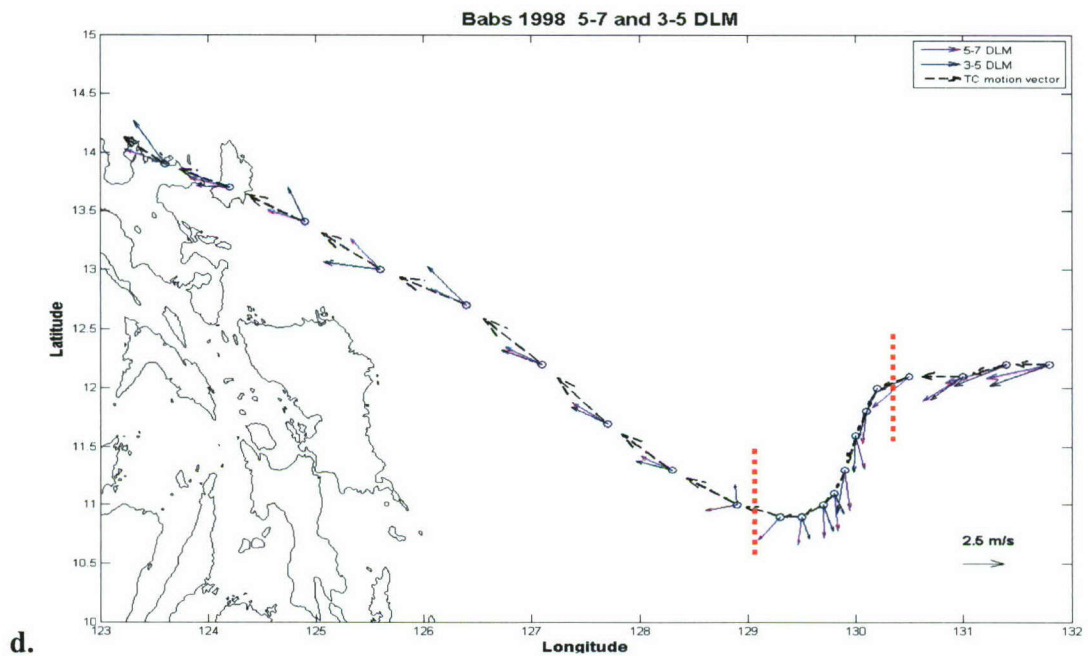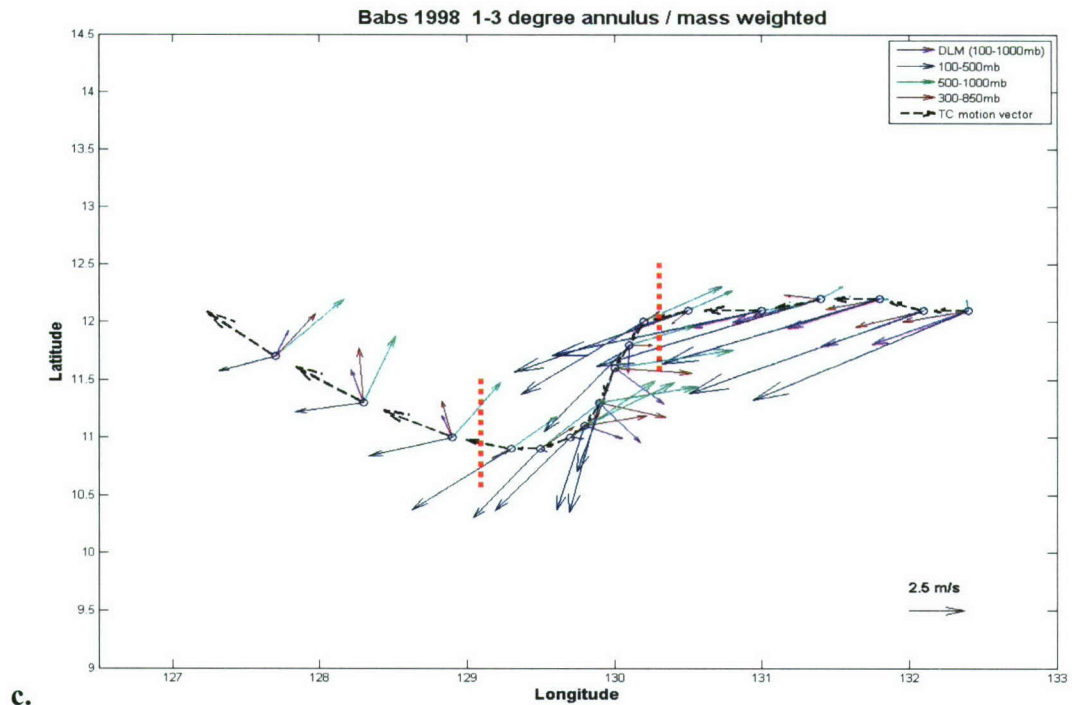
Figure 3.28 Babs' four-layer mean wind field analysis for the (a) 5°-7° (b) 3°-5° (c) 1°-3° radial bands and (d) an extended 5°-7° and 3°-5° DLM comparison. Vectors are scaled to the average speed of the TC between each 6 hourly time step. The red dotted lines indicate the start (between 12Z-18Z 17 October 1998) and end (between 12Z-18Z 19 October 1998) points of the TUTT cell interaction period.
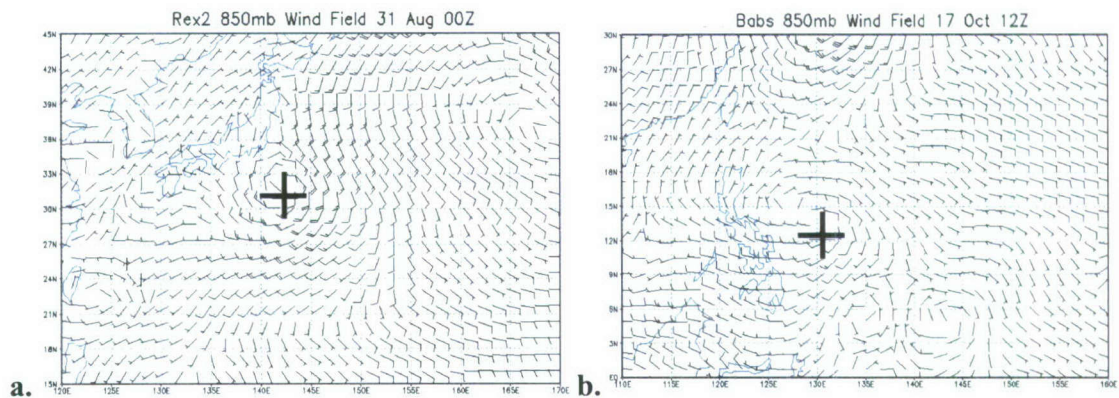
Figure 3.29 **850 hPa wind field analysis for (a) Rex2 and (b.) Babs just prior to the start of each TC's respective interaction period. The "+" represents the Best Track low-level center of the two TCs. A full wind barb equals 5 m s^{-1}. A half barb equals 2.5 m s^{-1}.**

a.

Babs 1998 3-5 degree annulus / mass weighted / 100-500 Mean Quad Values

Babs 1998 1-3 degree annulus / mass weighted / 100-500 Mean Quad Values
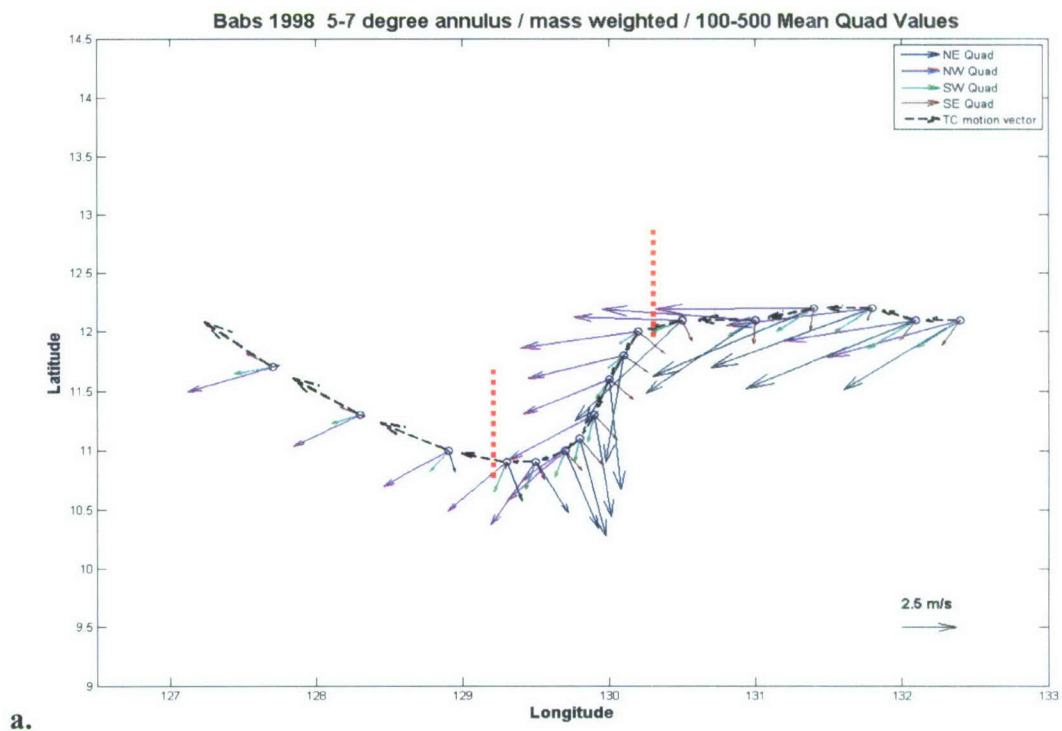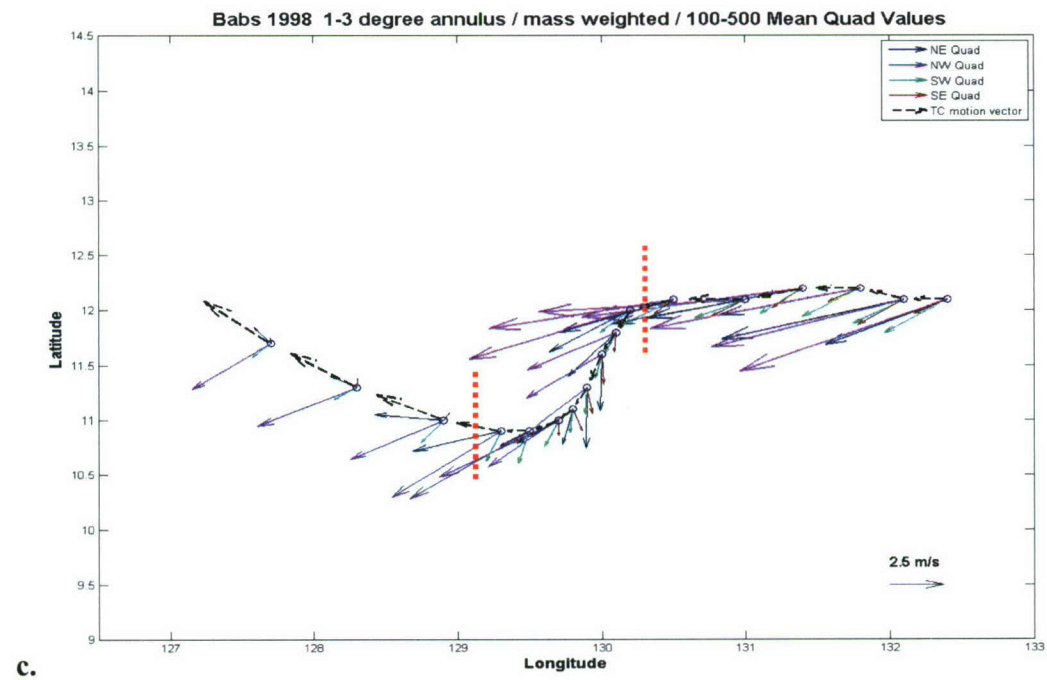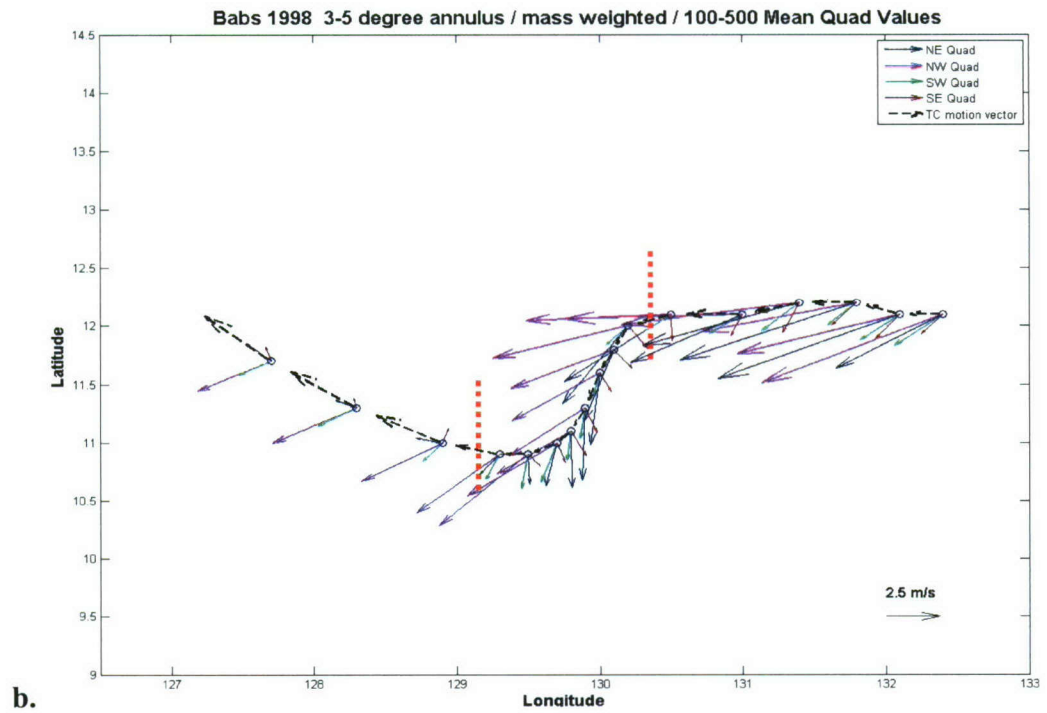
Figure 3.30 Four quadrant mean wind field analysis for Babs. Vectors are scaled to the average speed of the TC between each 6 hourly time step. Vectors point in the mean radial direction for (a) the 5°-7° (b) 3°-5° and (c) 1°-3° radial bands. The red dotted lines indicate the start (between 12Z-18Z 17 October 1998) and end (between 12Z-18Z 19 October 1998) points of the TUTT cell interaction period.

- 133 -
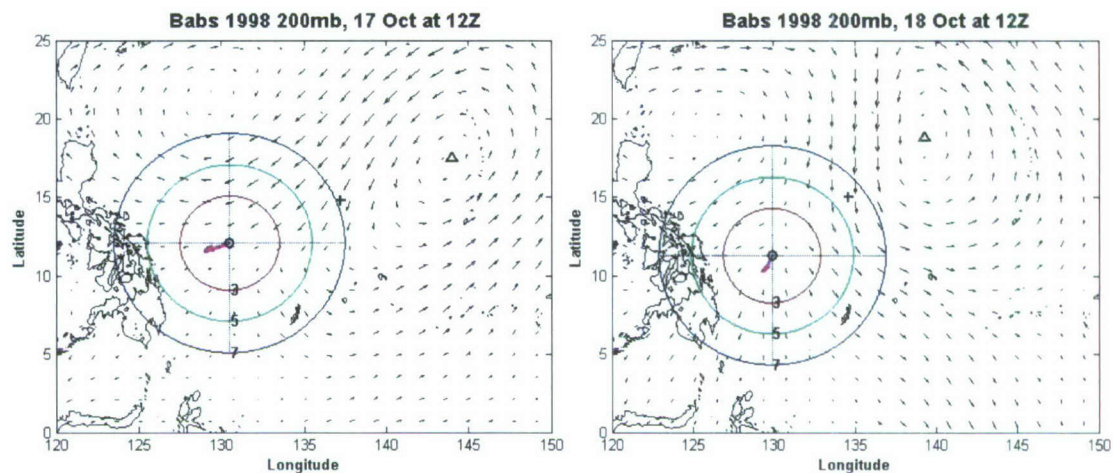
Figure 3.31 Babs 200 hPa wind field analysis at 12Z 17 October 1998 (left) and 12Z 18 October 1998 (right). The "o" represents the Best Track low-level center of Babs. The "+" represents the centroid of the two circulations. The "Δ" represents the approximate 200 hPa TUTT cell center of circulations. The red, green and blue circles represent the approximate 3°, 5° and 7° radial bands and are divided into quadrants. The pink arrow represents the TC's trajectory. Notice the TUTT cell's northerly flow initially covers the TC's NE quadrant in the image on the left (start of interaction period) but has begun to spread into the TC's NW quadrant by the image on the right (24 hours into the interaction period).

- 134 -

Babs 1998 5-7 degree annulus / mass weighted

a.

Babs 1998 3-5 degree annulus / mass weighted

b.
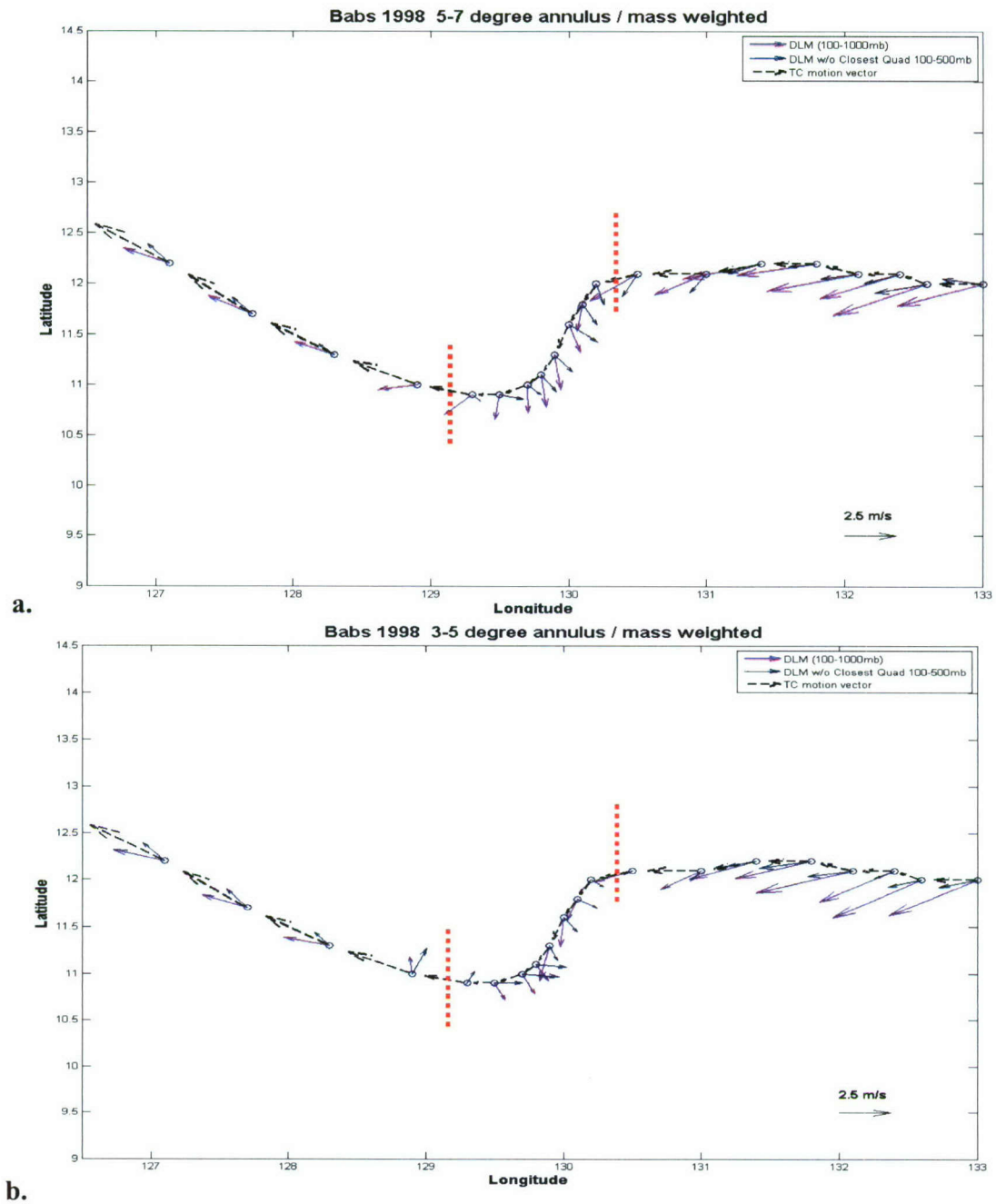
Figure 3.32   The original mass-weighted DLM (with TUTT cell flow) and the new mass-weighted DLM with the upper layer quadrant closest to the TUTT cell (much of its wind field) removed for Babs. Vectors are scaled to the average speed of the TC between each 6 hourly time step. Vectors point in the mean radial direction for (a) the 5°-7° and (b) the 3°-5° radial bands.   The red dotted lines indicate the start (between 12Z-18Z 17 October 1998) and end (between 12Z-18Z 19 October 1998) points of the TUTT cell interaction period.

- 135 -
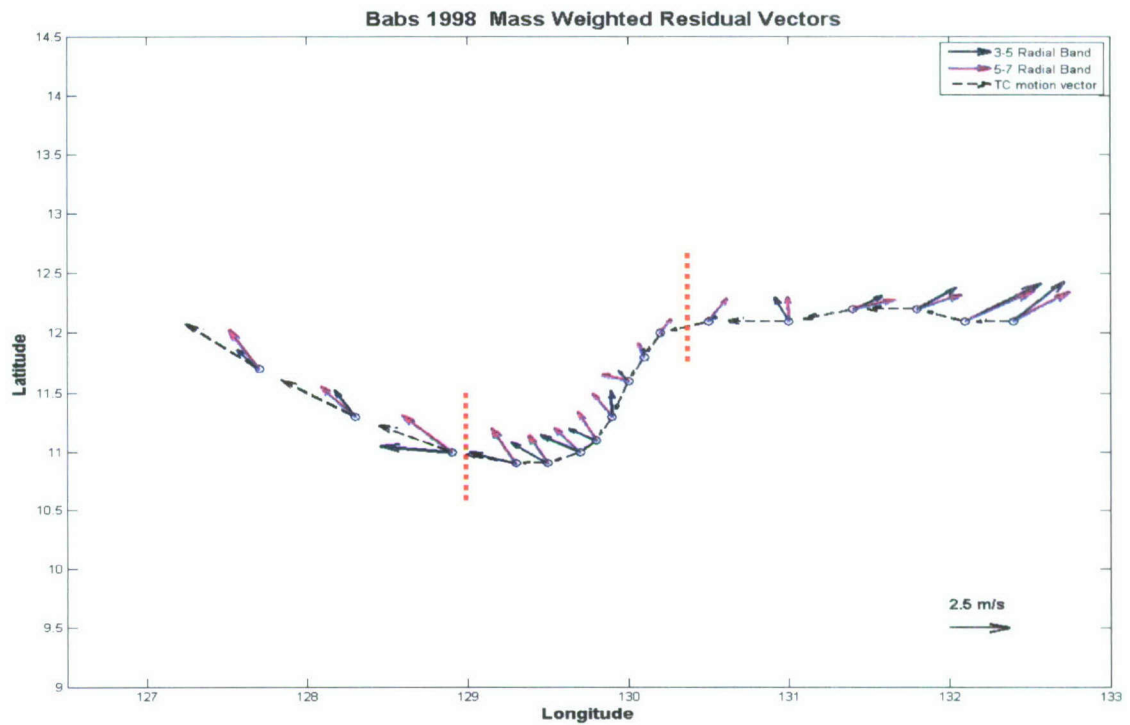
Figure 3.33 Mass-weighted DLM residual vector analysis for Babs. Vectors are scaled to the average speed vector (dotted line) of the TC between each time step. Vectors point in the mean radial direction at different radial bands. The red dotted lines indicate the start (between 12Z-18Z 17 October 1998) and end (between 12Z-18Z 19 October 1998) points of the TUTT cell interaction period.

Figure 3.34 The 100 hPa wind field analysis for (a) Rex2 at 12Z 30 August 1998 (left) just prior to the interaction period then 00Z 1 September (right) in the middle of the interaction period and (b) Babs at 00Z 17 October 1998 (left) just prior to the interaction period then at 18Z 18 October 1998 (right) in the middle of the interaction period. The "+" represents the JTWC Best Track low-level center of the two TCs. A full wind barb equals 5 m s^{-1}. A half barb equals 2.5 m s^{-1}. Notice the well-developed anticyclone over Rex2 while Babs reveals southwestward flow. The 200 hPa analysis (not shown) for the same times indicate either a weaker anticyclonic pattern for Rex2 or northeasterly flow over top the TC's center for Babs. Only Rex2 indicates a cyclone/anticyclone couplet which was theorized to cause a left-of-VWS bias in TC motion.
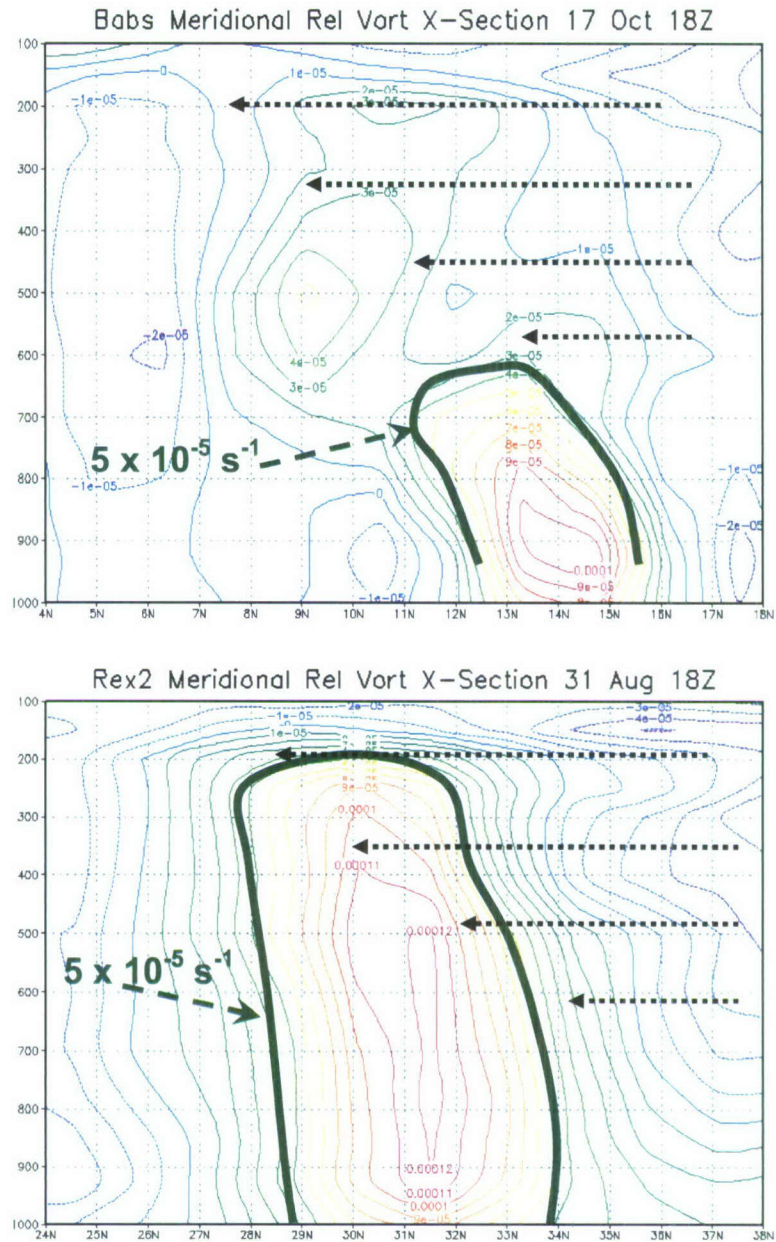
Figure 3.35 Meridional vertical cross sections of relative vorticity for Babs (top), a 25 m s^{-1} TC, and Rex2 (bottom), a 50 m s^{-1} TC, near their respective interaction start points. Approximate TUTT cell induced upper layer winds are superimposed with black dotted arrows. The TUTT cell characteristics for each case are very similar. Notice the dissimilar structure between the two TCs, including Babs lack of vertical extent and greater downshear tilt compared to Rex2.
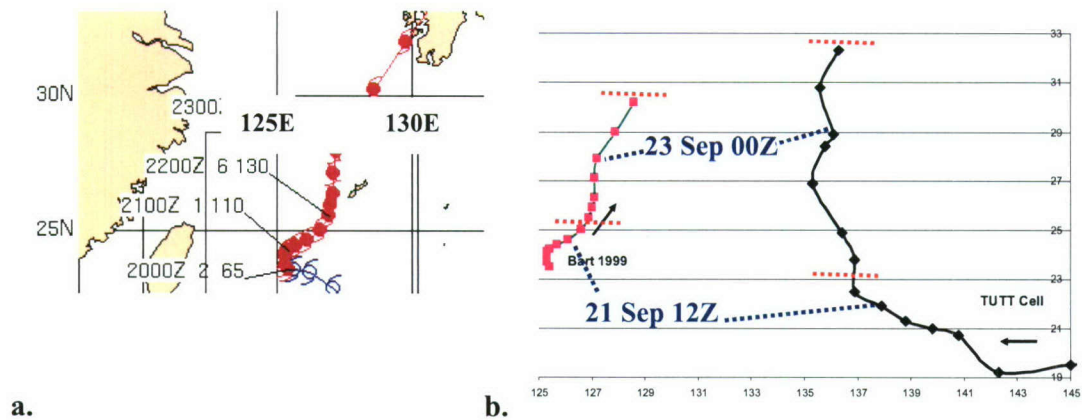
Figure 3.36 (a) Best Track for Bart (24W) from the 1999 JTWC ATCR. Best Track intervals are at 6 hours. Annotation is in the form DDHH S WW, where DD = day of the month, HH = GMT (Zulu) hour, S = TC's forward speed in knots and WW = TC's maximum 1 minute averaged sustained wind speed in knots (1 knot = 0.514 m s^{-1}). (b) A graphical depiction of both the TC (pink) and TUTT cell (blue) tracks at 6-hourly intervals. The red dotted lines indicate the start (between 18Z 21 September – 00Z 22 September 1999) and end (between 12Z-18Z 23 September 1999) points of the TUTT cell interaction period.
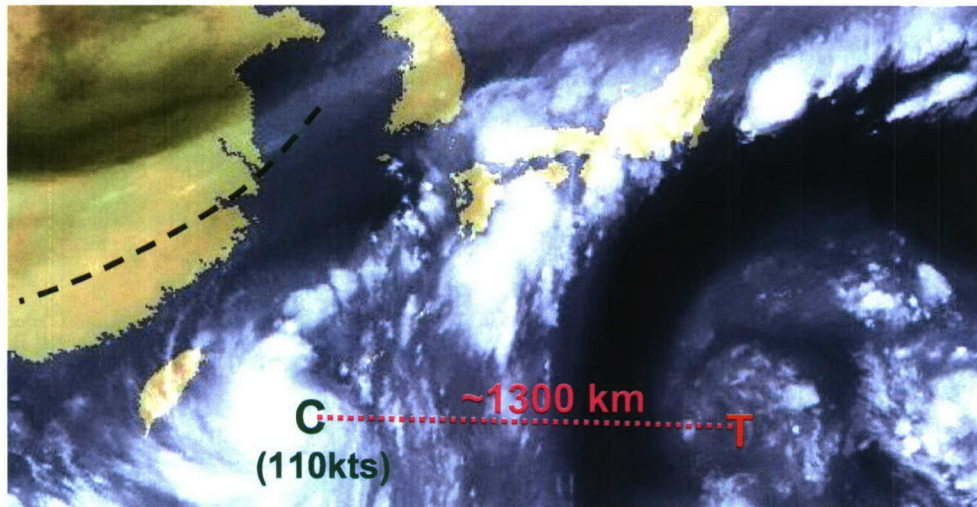
Figure 3.37. GMS-5 water vapor imagery for 06Z 21 September 1999, about 12 hours prior to the interaction start point. The "T" represents the approximate 200 hPa TUTT cell center and the "C" the center of Bart. The JTWC Best Track intensity for the TC is below the TC center. The approximate distance between the two circulations is annotated in purple. A weak, mostly stationary upper level mid-latitude trough is annotated by the dashed line (based on the 200 hPa wind field from the ERA-40 dataset) discussed in section 2.3.1.1.

- 139 -

Bart Relative Vort (1/s) of TC (*) and TUTT Cell (+)

300 hPa Streamline Analysis for Bart 21 Sep at 06Z

a.

Bart Relative Vort (1/s) of TC (*) and TUTT Cell (+)

300 hPa Streamline Analysis for Bart 22 Sep at 00Z

b.
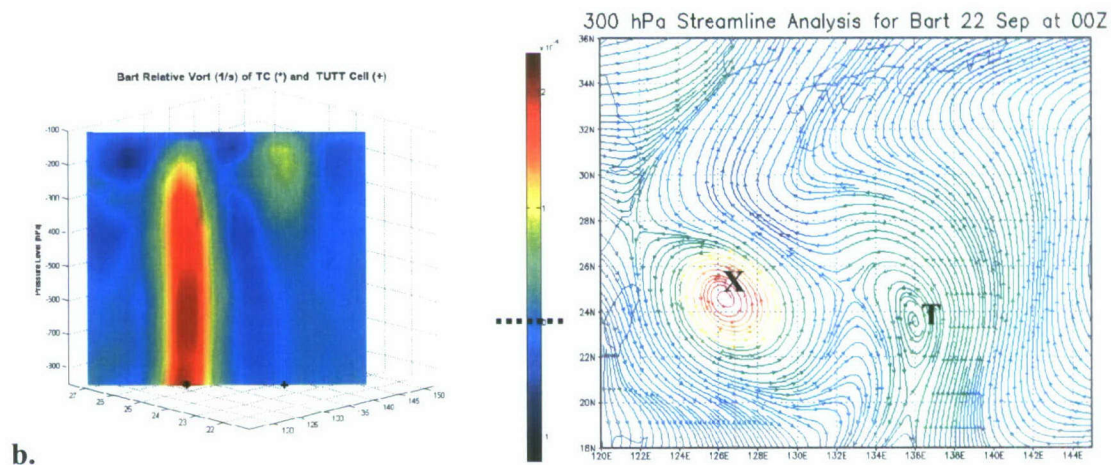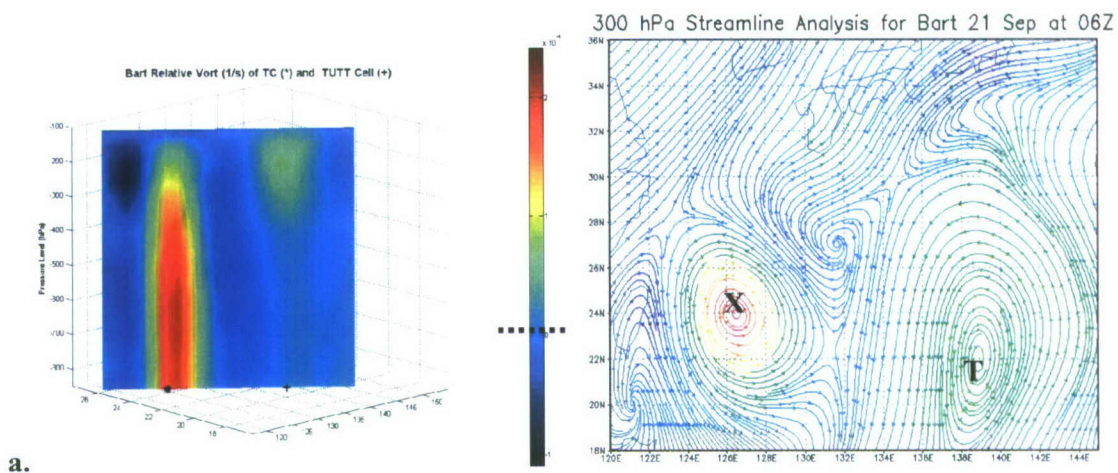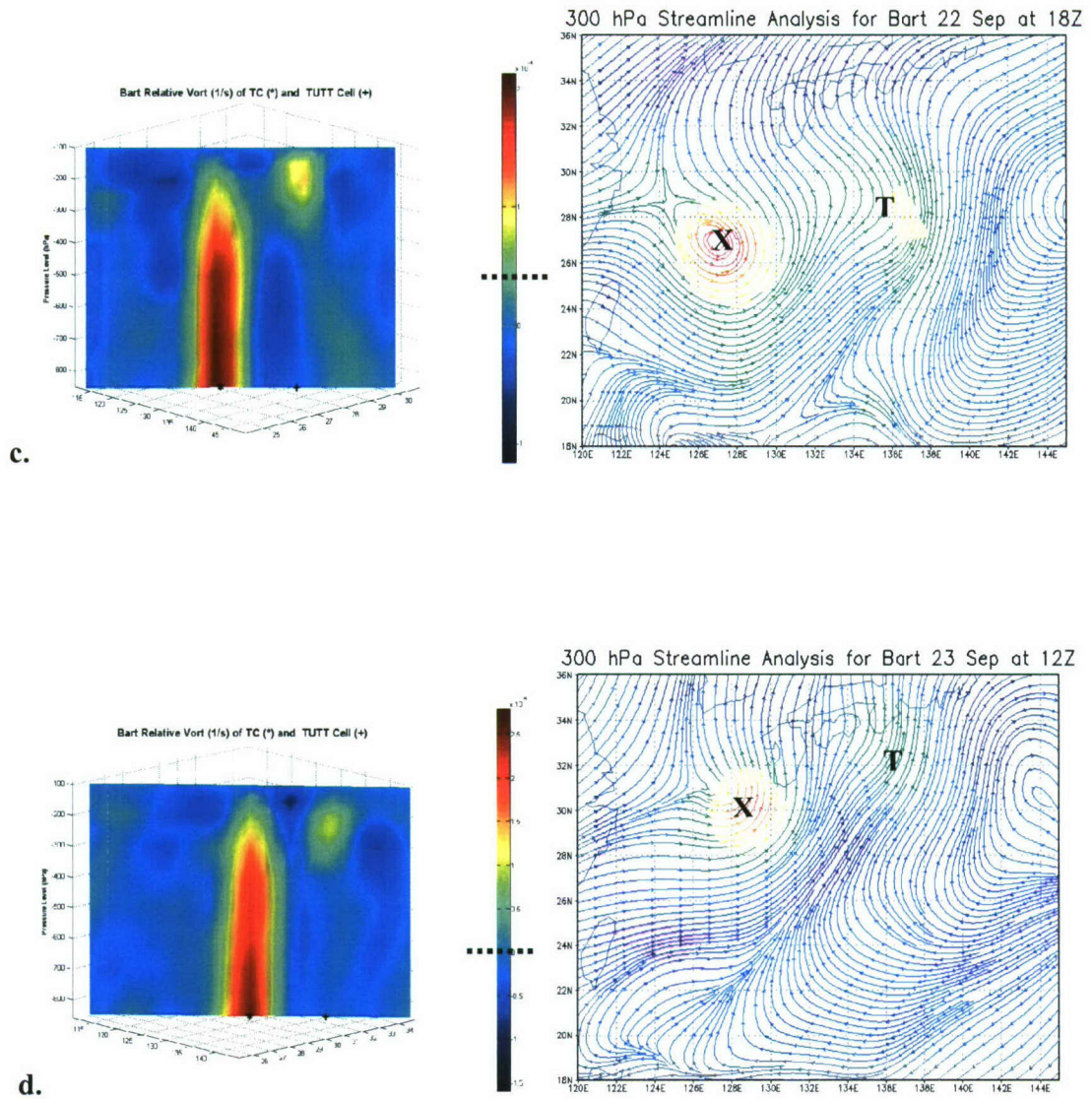
Figure 3.38 Relative vorticity (10^{-4} s^{-1}) cross-sections from 100 hPa down to 850 hPa (left) and 300 hPa streamline analysis with relative vorticity shading (right) for Bart at (a) 06Z 21 September 1999 (prior to interaction period), (b) 00Z 22 September 1999 (at interaction start point), (c) 18Z 22 September 1999 (within interaction period) and (d) 12Z 23 September 1999 (near interaction end point). The color bar provides ζ_r values for the vertical profile on the left where black dotted line represents $\zeta_r = 0$. For the streamline analysis, deeper yellow and red colors represent greater *positive* relative vorticity values. Deeper blues and purples represent *negative* relative vorticity values. The black 'X' represents the approximate surface center of the TC. The black 'T' represents the approximate 200 hPa center of the TUTT cell.
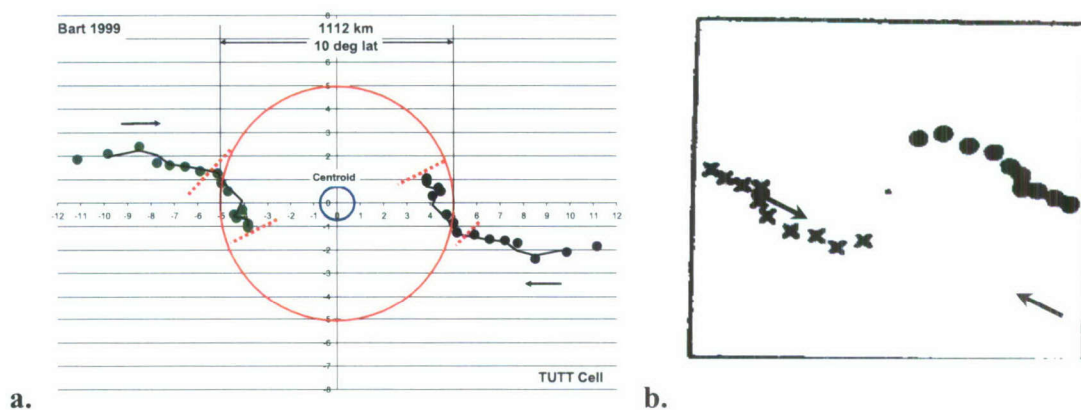
Figure 3.39a,b (a) Centroid relative motion using a 2-point running average (black line running through the green and dark blue dots) between Bart and the associated TUTT cell. The red dotted lines indicate the start (between 18Z 21 September – 00Z 22 September 1999) and end (between 12Z-18Z 23 September 1999) points of the TUTT cell interaction period. The black arrows indicate the general direction of motion. (b) LH93's Mary and Nadine (1974) centroid relative motion.
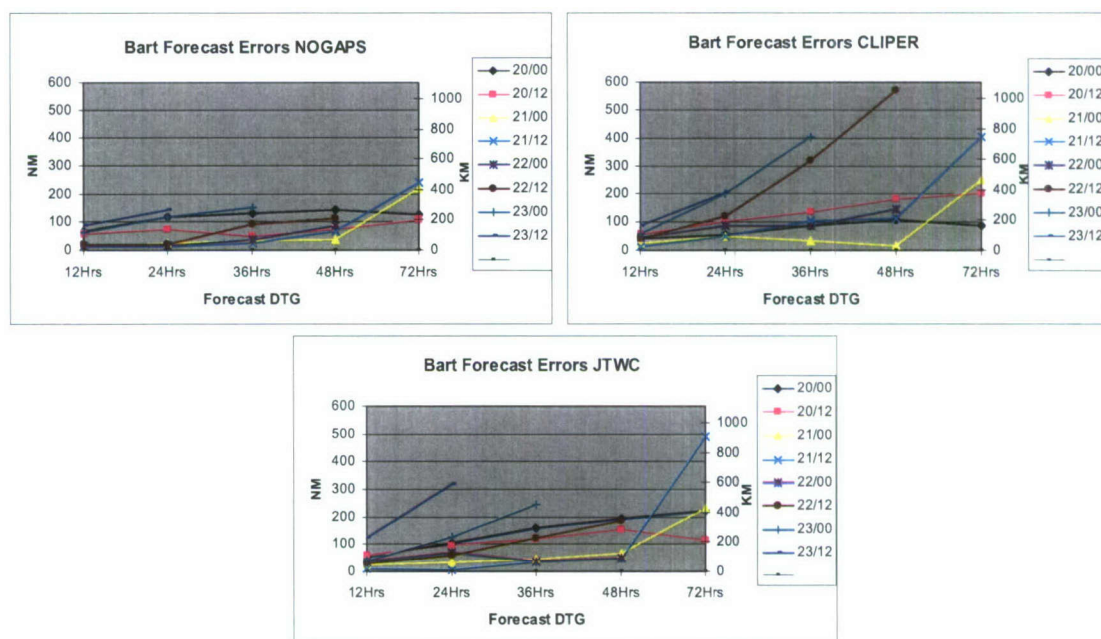
Figure 3.40 Bart 12-72 hour forecast errors for NOGAPS* (top left), CLIPER* (top right) and the JTWC* (bottom). *Note: some 72 hour forecast data was missing from records.
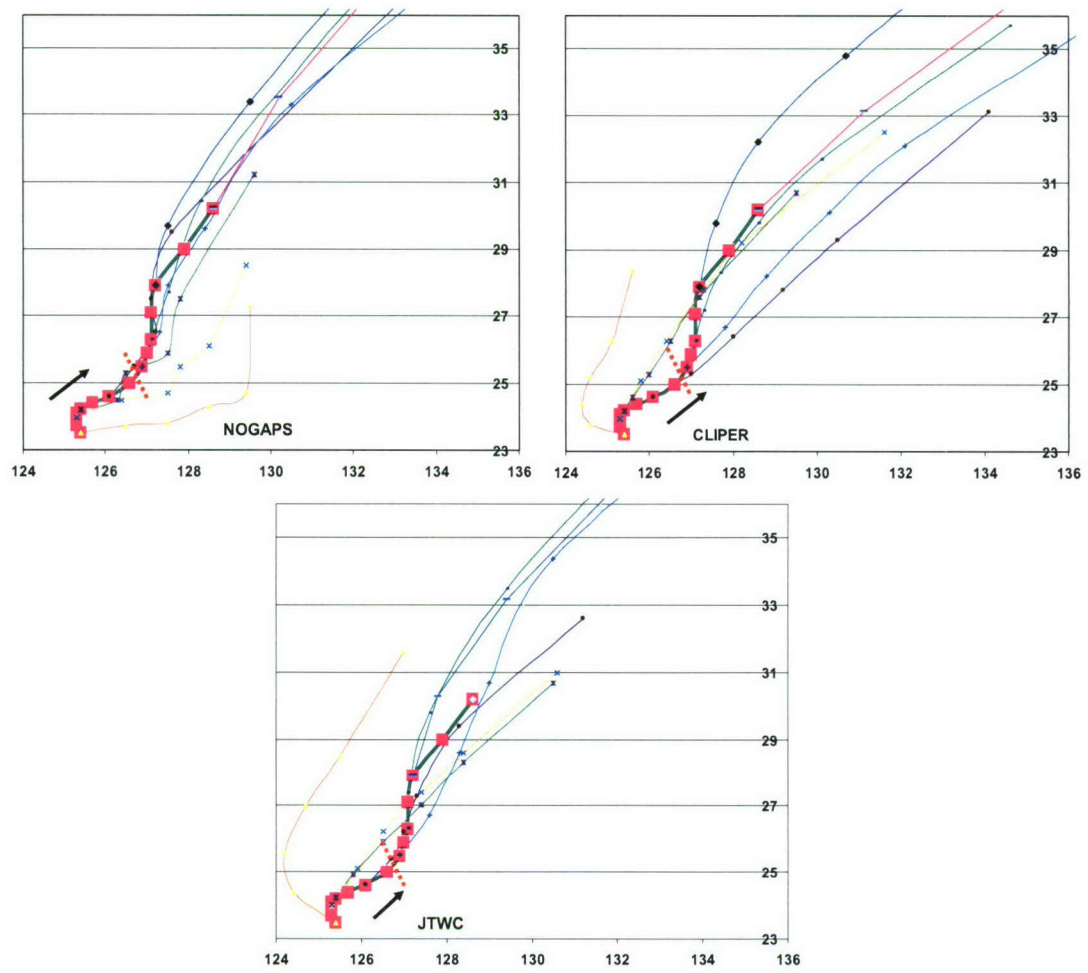
Figure 3.41 Bart forecast tracks (6-hourly intervals) at various intervals for NOGAPS (upper left), CLIPER (upper right) and the JTWC (bottom). The black arrow indicates general direction of TC motion. The red dotted lines indicate the start (between 18Z 21 September – 00Z 22 September 1999) and end (between 12Z-18Z 23 September 1999) points of the TUTT cell interaction period. The track ends at the point the TUTT cell's closed 200 hPa circulation dissipated.
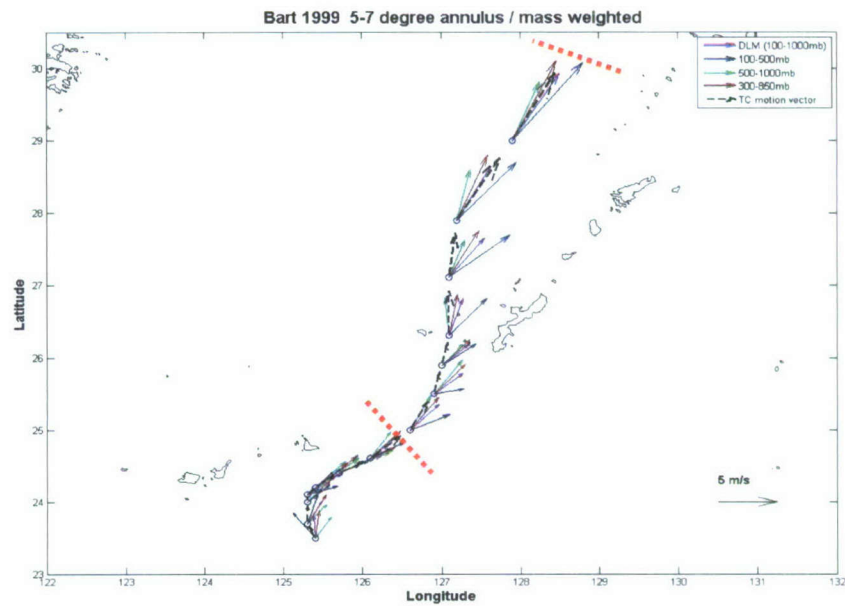
Figure 3.42 Four-layer mean wind field analysis for Bart. Vectors are scaled to the average speed of the TC between 6 hourly time steps. Vectors point in the mean radial direction for the 5°-7° radial band.   The red dotted lines indicate the start (18Z 21 September 1999 –00Z 22 September 1999) and end (12Z-18Z 23 September 1999) points of the TUTT cell interaction period.

Bart 1998 200mb, 21 Sep at 12Z

Bart 1998 200mb, 22 Sep at 00Z

Bart 1998 200mb, 22 Sep at 12Z

Bart 1998 200mb, 23 Sep at 00Z

a.
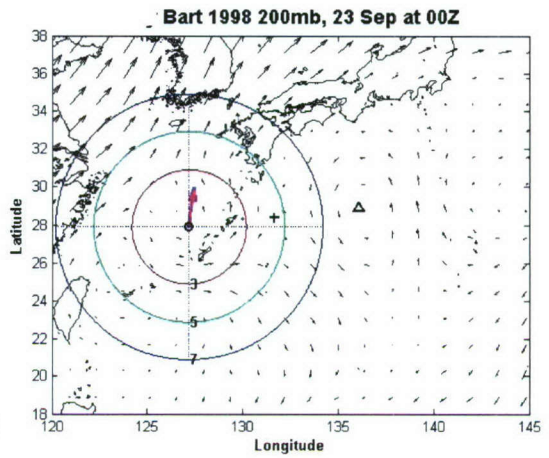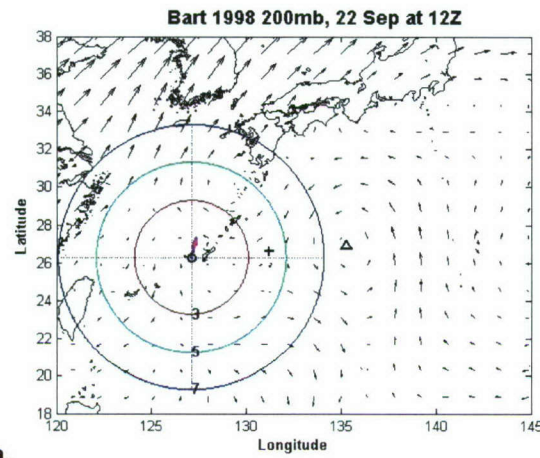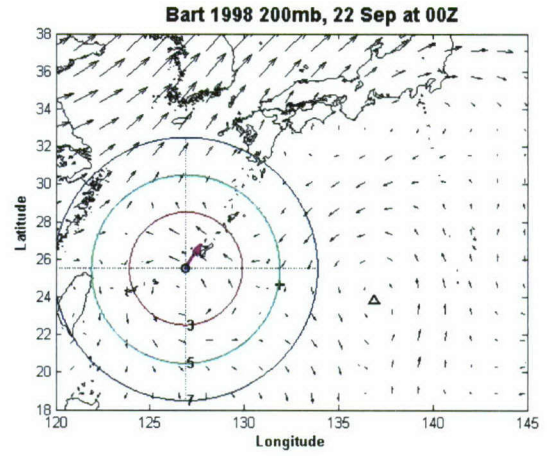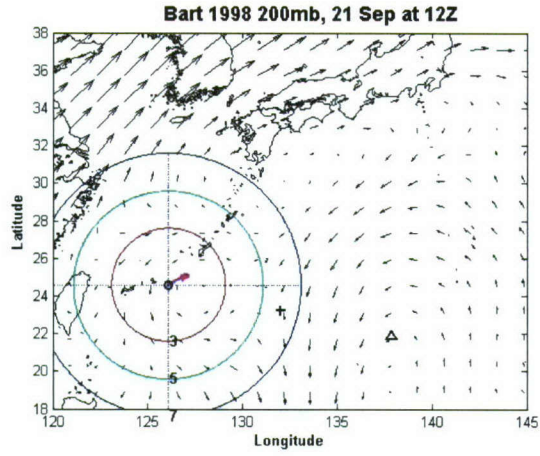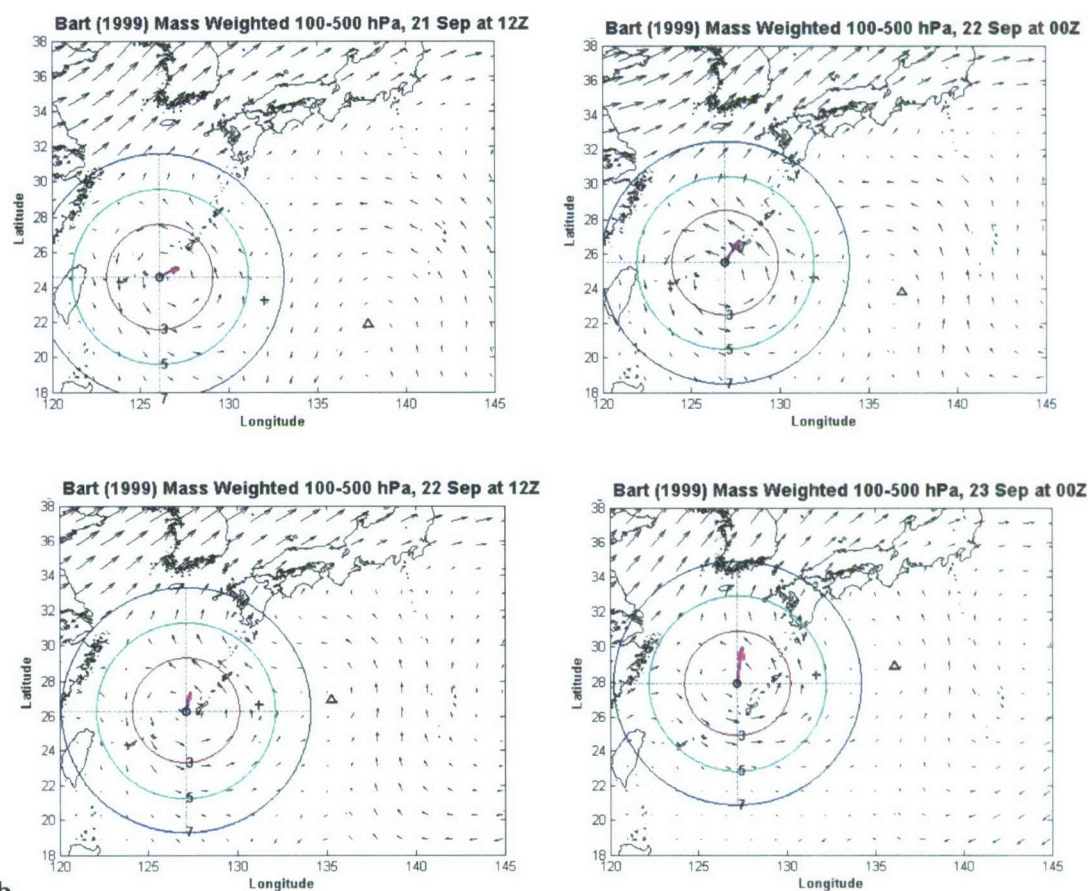
Figure 3.43 Bart (a) 200 hPa and (b) mass-weighted 100 hPa to 500 hPa wind fields at 12-hourly intervals for time steps starting just prior to the interaction start point at 12Z 21 September (upper left) and ending 00Z 23 September 1999 (lower right) just prior to the dissipation of the TUTT cell. The "o" represents the Best Track low-level center of Bart. The "+" represents the centroid of the two circulations. The "Δ" represents the approximate 200 hPa TUTT cell center of circulations. The red, green and blue circles represent the approximate 3°, 5° and 7° radial bands and are divided into quadrants. The pink arrow represents the TC's trajectory.
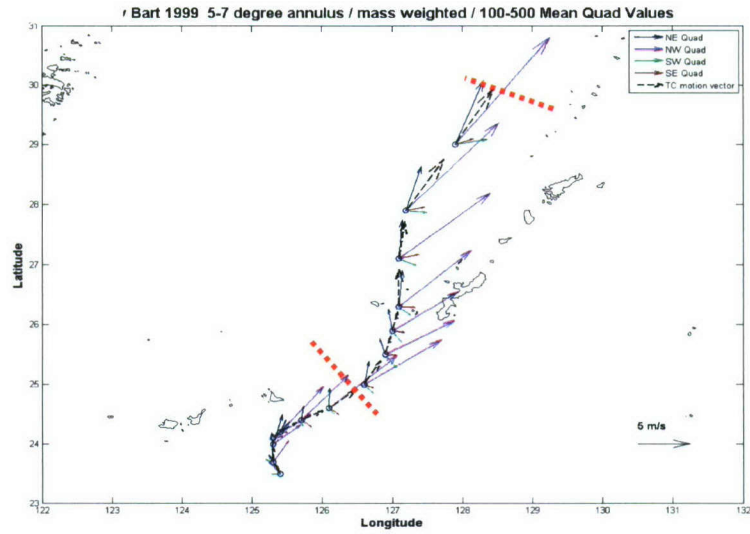
Figure 3.44 Four quadrant mean wind field analysis for Bart. Vectors are scaled to the average speed of the TC between 6 hourly time steps. Vectors point in the mean direction for the 5°-7° radial band.   The red dotted lines indicate the start (18Z 21 September – 00Z 22 September 1999) and end (between 12Z-18Z 23 September 1999) points of the TUTT cell interaction period.
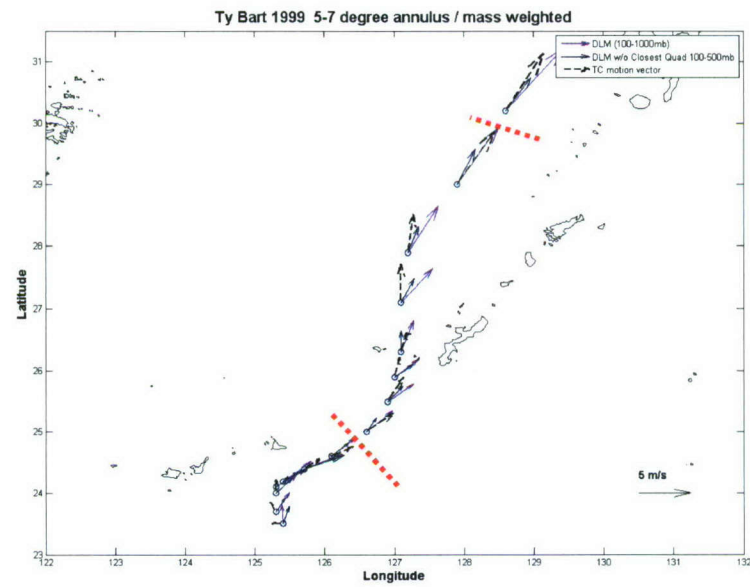

Figure 3.45 The original mass-weighted DLM and the new mass-weighted DLM with the upper layer quadrant closest to the TUTT cell removed for Bart. Vectors are scaled to the average speed of the TC between each 6 hourly time step. Vectors point in the mean direction for the 5°- 7° radial bands. The red dotted lines indicate the start (18Z 21 September – 00Z 22 September 1999) and end (between 12Z-18Z 23 September 1999) points of the TUTT cell interaction period.

Bart 1999 Mass Weighted DLM Residual Vectors
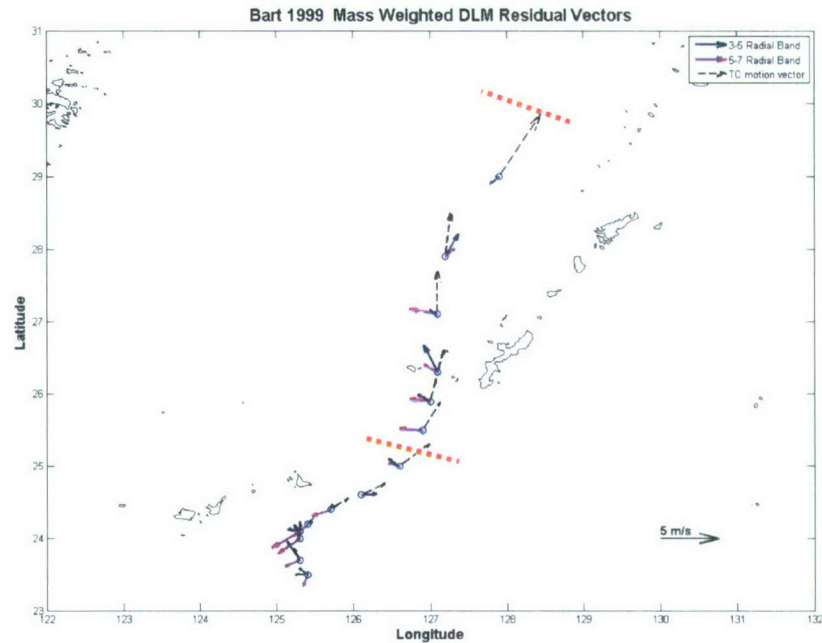
Figure 3.46 Mass-weighted DLM residual vector analysis for Bart. Vectors are scaled to the average speed vector (dotted line) of the TC between each time step. Vectors point in the mean radial direction. The red dotted lines indicate the start (18Z 21 September – 00Z 22 September 1999) and end (between 12Z-18Z 23 September 1999) points of the TUTT cell interaction period.
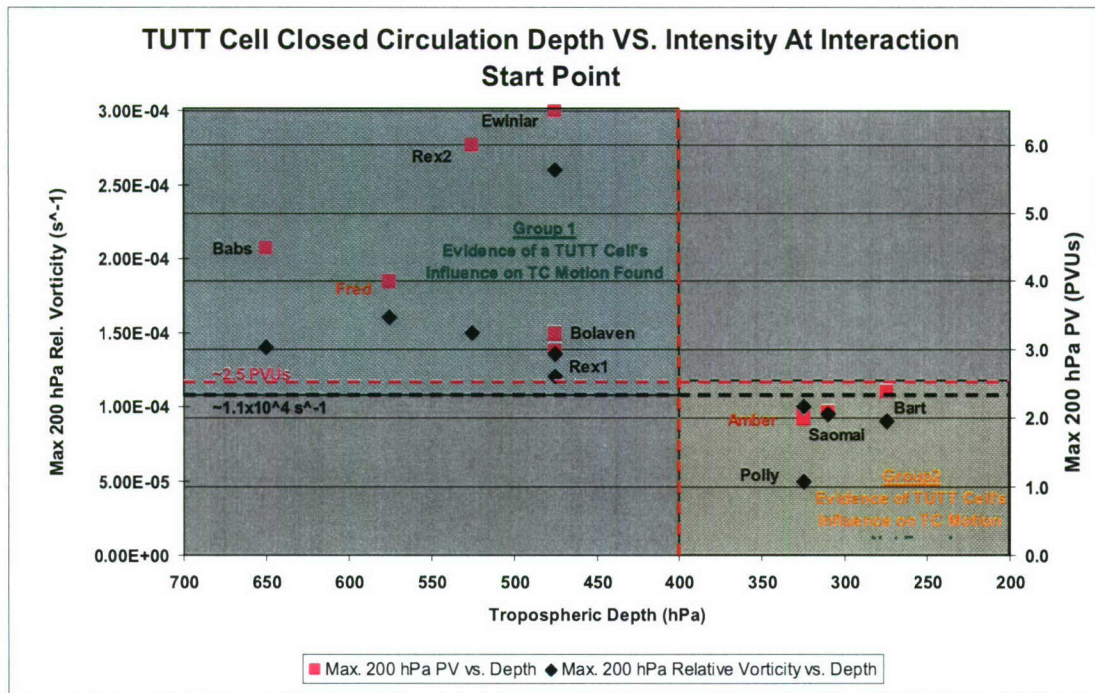
Figure 3.47 Maximum depth of the TUTT cell closed circulation for each case versus intensity (the maximum associated 200 hPa PV (purple, the right Y axis) and relative vorticity (blue, the left Y axis)). Cases are labeled near the two intensity values (aligned vertically). Group one (shaded green) yielded evidence of a TUTT cell's influence on TC motion found. Group two (shaded yellow) did not. Outliers are highlighted in red (Amber and Fred). Approximate intensity and maximum depth values separating the two groups are annotated.
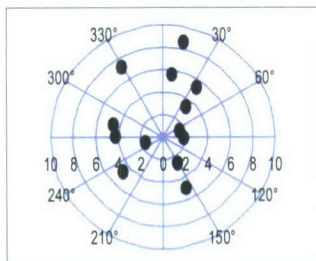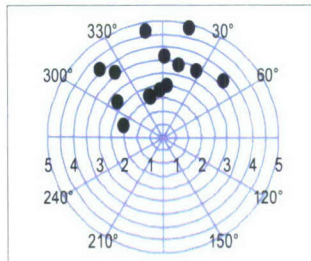
Ewiniar 28°N   Bolaven 23°N   Amber 16°N
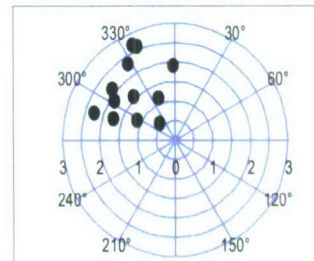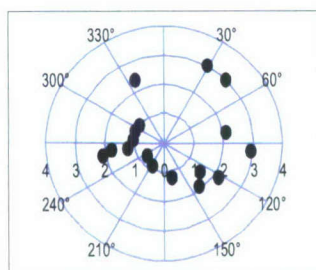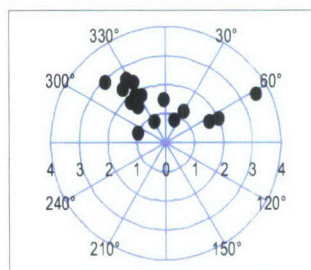
Rex2 30°N   Babs 12°N   Rex1 25°N
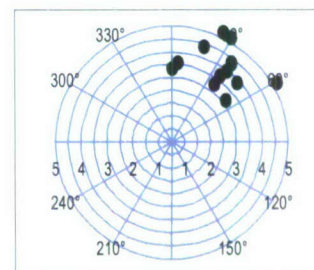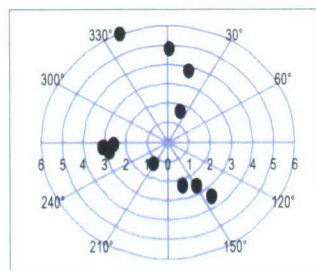
Saomai 15°N   Fred 18°N   Bart 27°N

Polly 22°N

a.

Ty Amber 1997 Mass Weighted DLM Residual Vectors
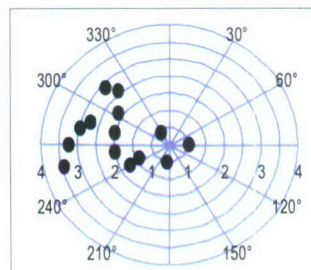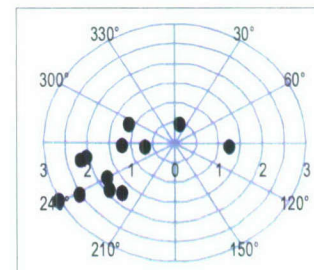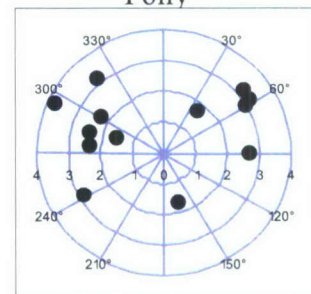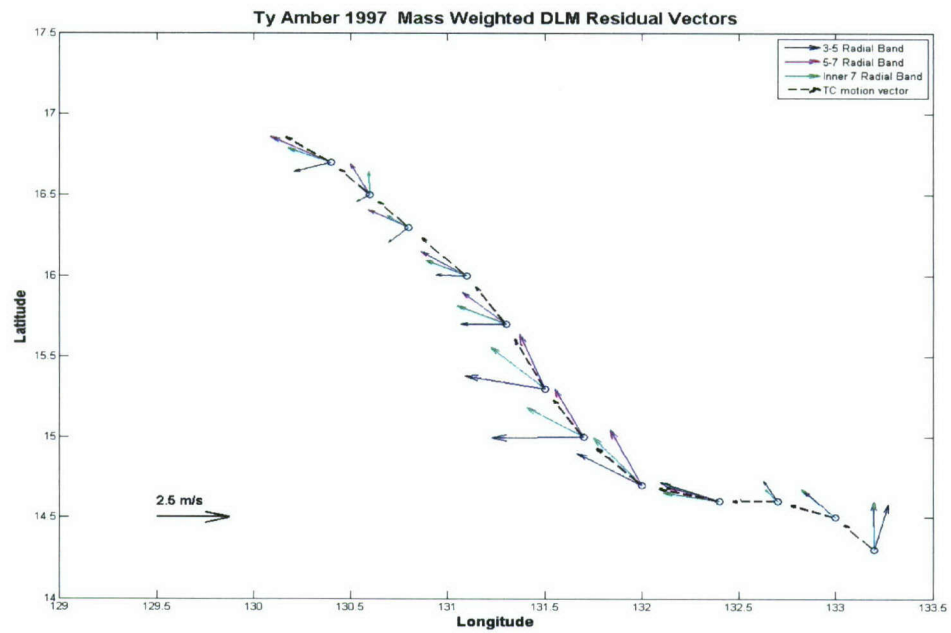
b.

Figure 3.48 (a) Polar projections of all cases mass-weighted 5°-7° DLM residual vectors. Speeds are in m s⁻¹. 360° is due north. TC mean latitudes are provided next to the TC's name. (b) Mass-weighted DLM residual vector analysis for Amber. Vectors are scaled to the average speed vector (dotted line) of the TC between each time step. Vectors point in the mean radial direction.
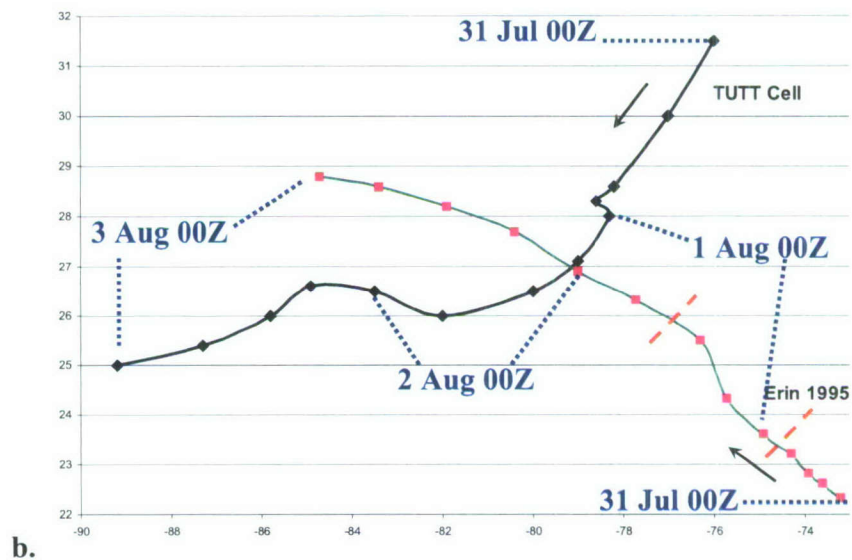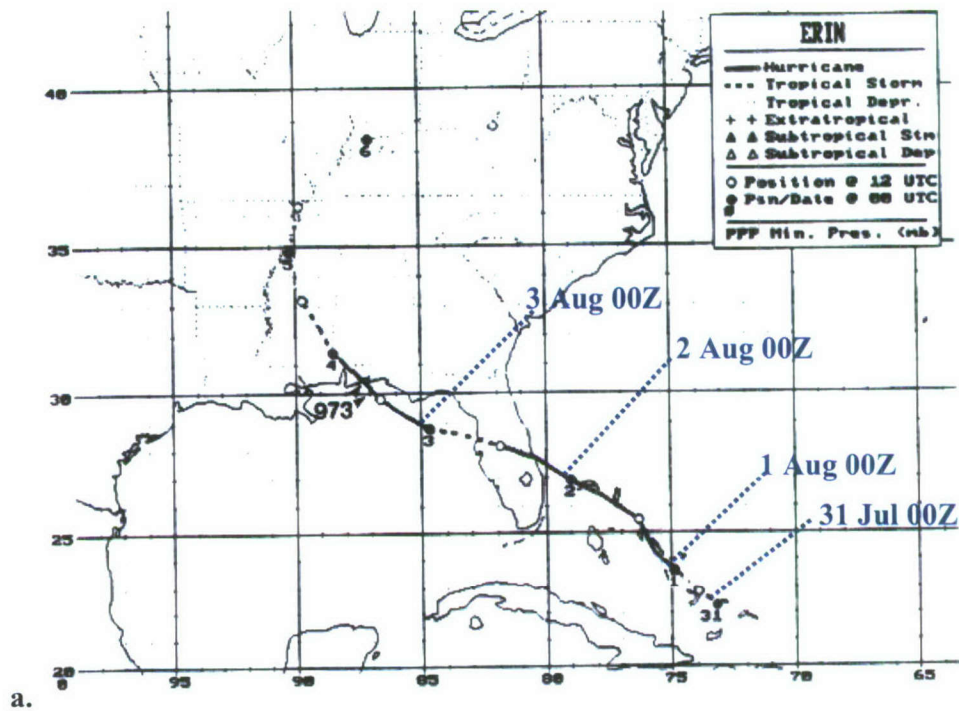
- 151 -

Figure 3.49 (a) The NHC track of Erin (1995) and a (b) generic graphic of both circulations at the same 6-hourly intervals. Hurricane Erin is annotated in red dots and the associated TUTT cell in dark blue dots. The black arrows indicated the general direction of motion. The red dotted lines indicate the estimated start (between 18Z 31 July and 00Z 1 August 1995) and end (12-18Z 1 August 1995) points of the TUTT cell interaction period.
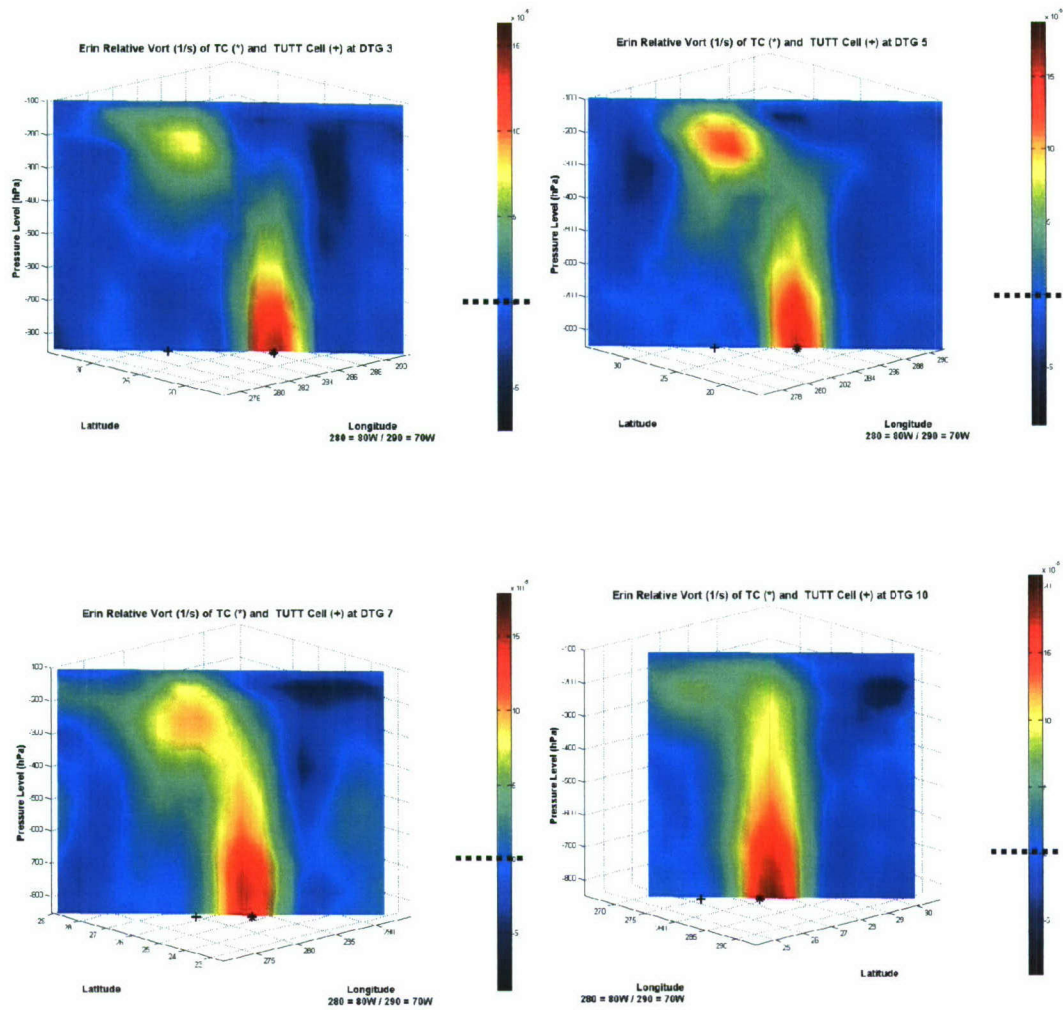
Figure 3.50 Relative vorticity (10^{-5} s^{-1}) cross-sections from 100 hPa down to 850 hPa for Erin at (a) 12Z 31 August 1995 (12 hrs prior to interaction period), (b) 00Z 1 September 1995 (at interaction start point), (c) 12Z 1 September 1995 (near interaction end point) and (d) 06Z 2 September 1995 (12 hrs after interaction end point). Deeper yellow and red colors represent greater *positive* relative vorticity. The black dotted line represents $\zeta_r = 0$.
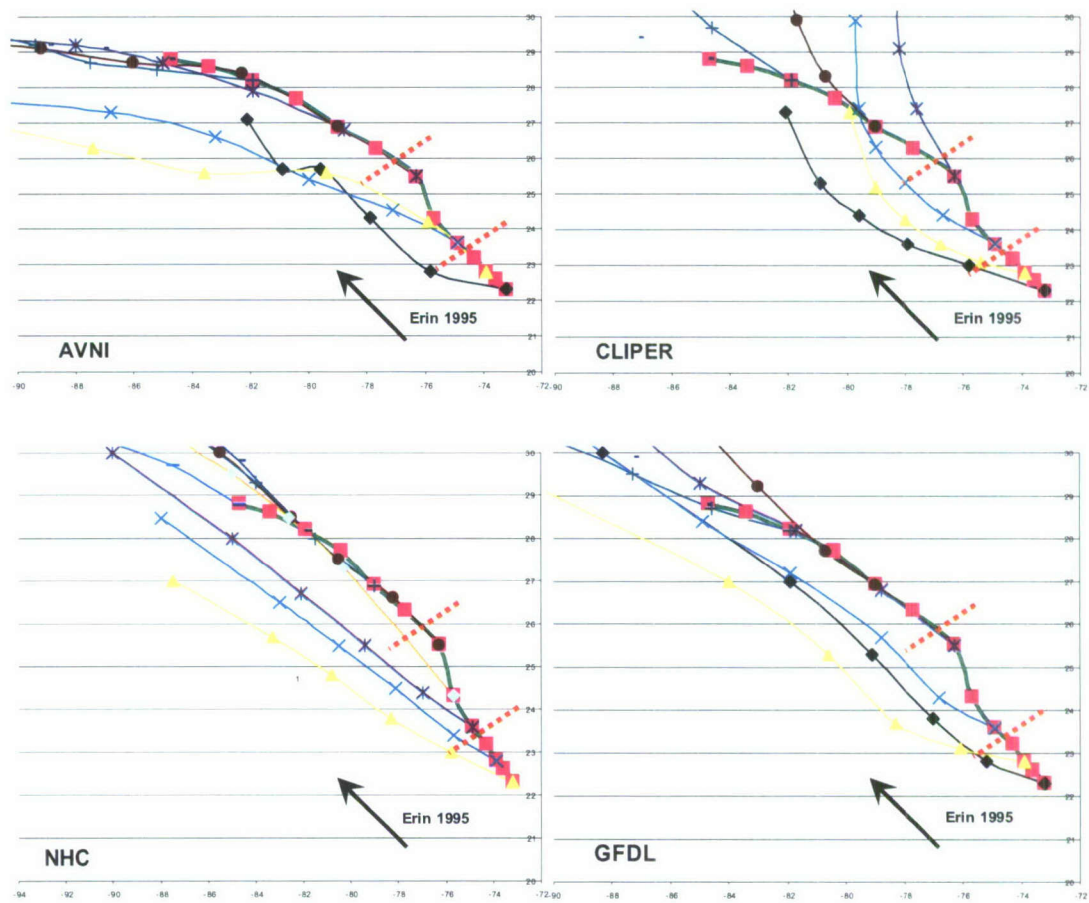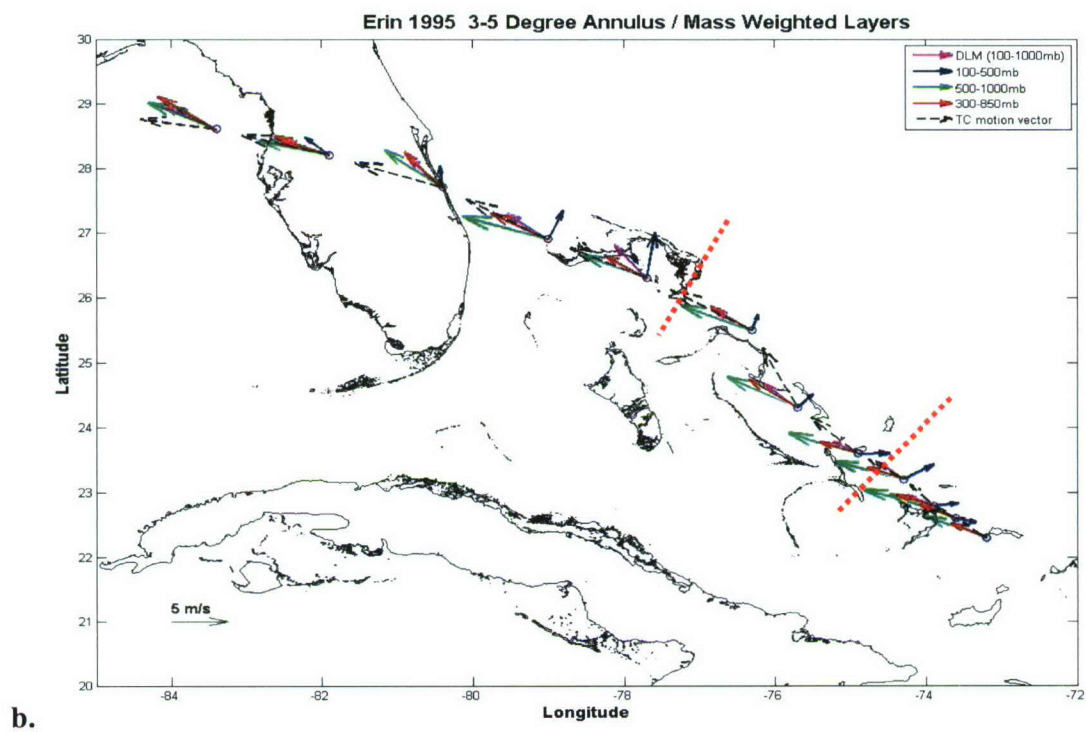
Figure 3.51 Erin forecast tracks at 6 and 12 hour intervals for AVNI (upper left), CLIPER (upper right), NHC (bottom left) and GFDL (bottom right). Black arrow indicates the general direction of TC motion. The red dotted lines indicate the estimated start (between 18Z 31 July and 00Z 1 August 1995) and end (12-18Z 1 August 1995) points of the TUTT cell interaction period.

Erin 1995 5-7 Degree Annulus / Mass Weighted Layers

a.

Erin 1995 3-5 Degree Annulus / Mass Weighted Layers

b.

Erin 1995 1-3 Degree Annulus / Mass Weighted Layers
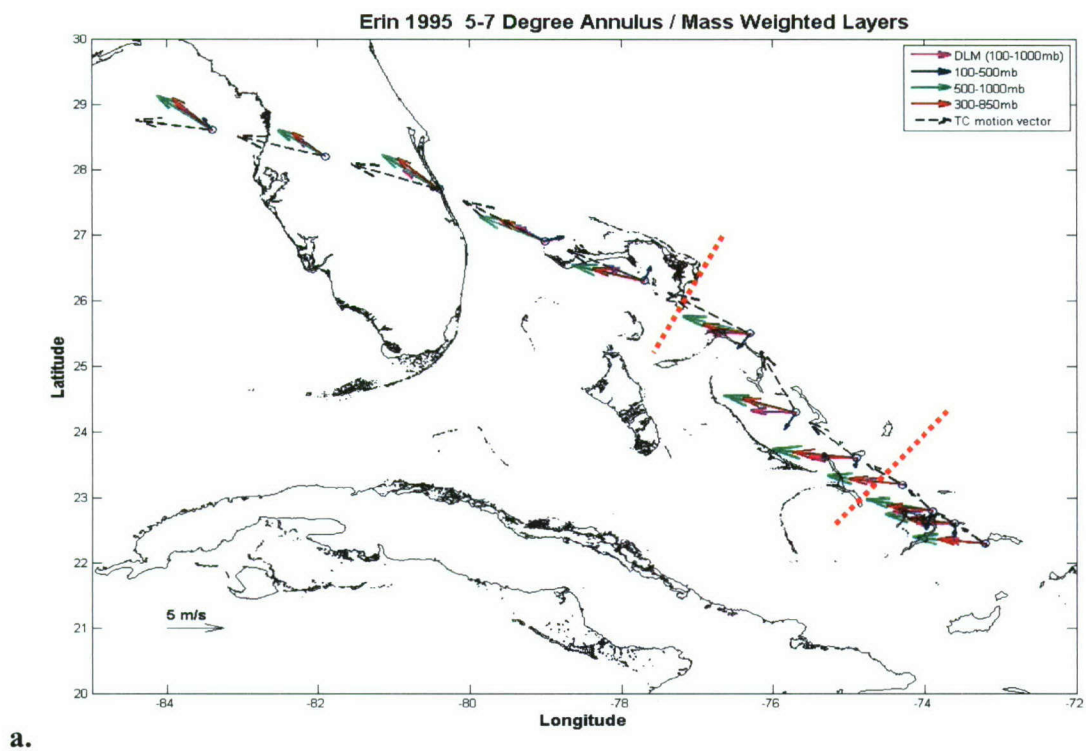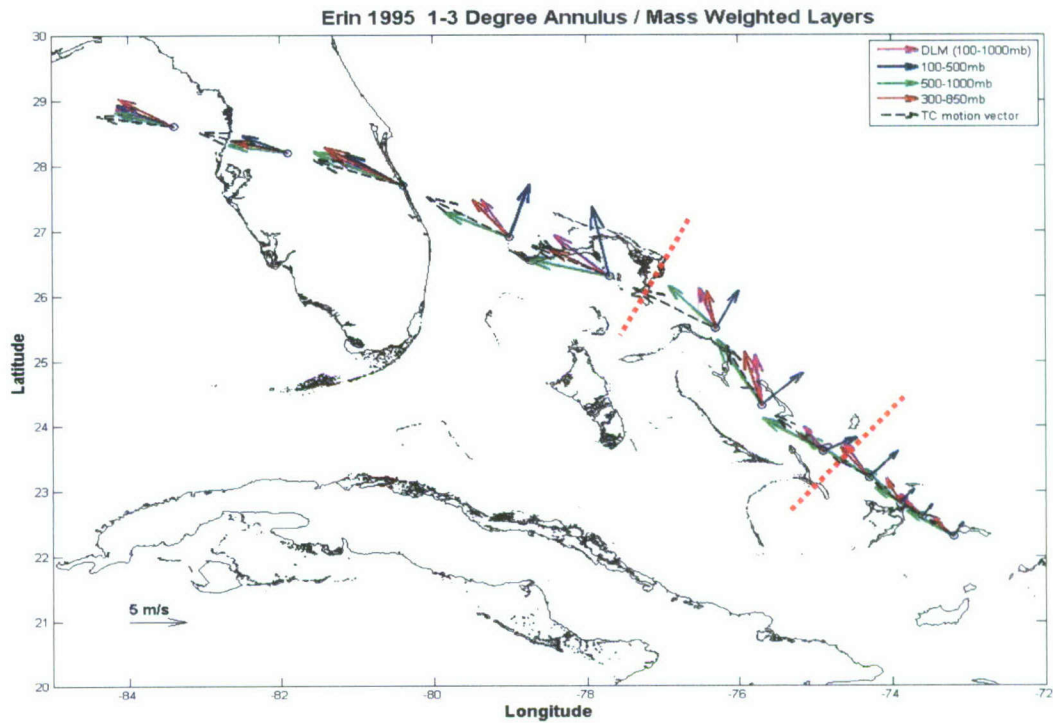
c.

Figure 3.52   Four-layer mean mass-weighted wind field analysis for Erin. Vectors are scaled to the average speed of the TC between each 6 hourly time step. Vectors point in the mean radial direction for (a) the 5°-7° (b) 3°-5° and (c) 1°-3° radial bands.   The red dotted lines indicate the estimated start (between 18Z 31 July and 00Z 1 August 1995) and end (12-18Z 1 August 1995) points of the TUTT cell interaction period.

- 156 -

a.

b.

Erin 1995 1-3 Degree Annulus / Mass Weighted / 100-500 hPa Mean Quadrant Values
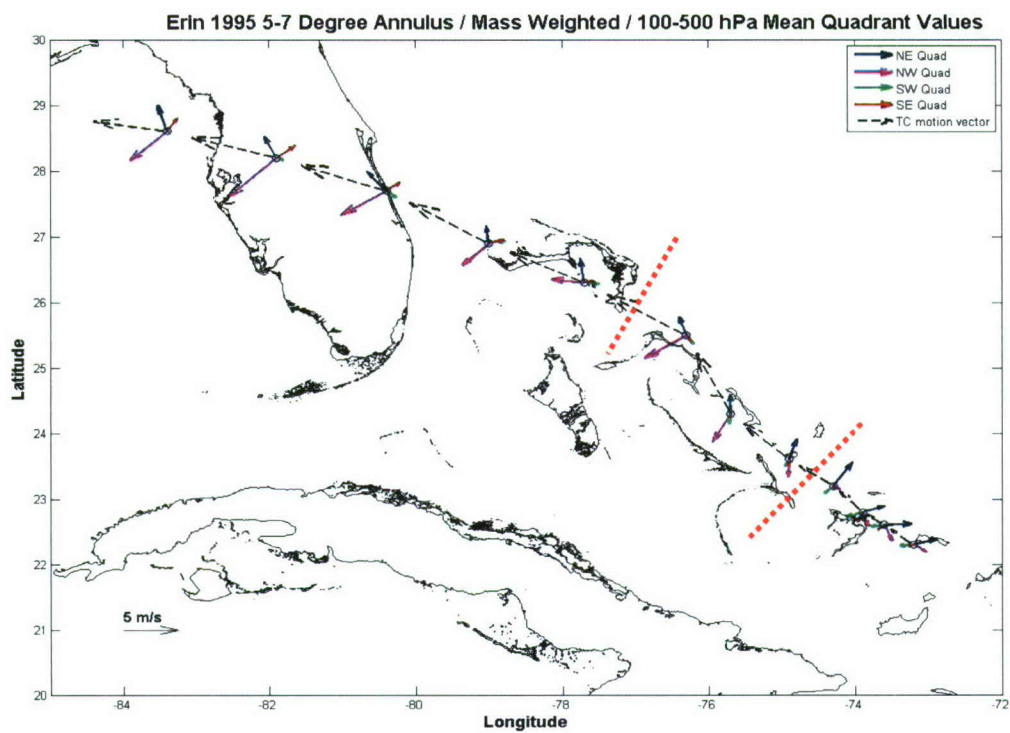
c.

Figure 3.53 Four quadrants of the mass-weighted upper layer mean wind field analysis for Erin. Vectors are scaled to the average speed of the TC between each 6 hourly time step. Vectors point in the mean radial direction for (a) the 5°-7° (b) 3°-5° and (c) 1°-3° radial bands. The red dotted lines indicate the estimated start (between 18Z 31 July and 00Z 1 August 1995) and end (12-18Z 1 August 1995) points of the TUTT cell interaction period.
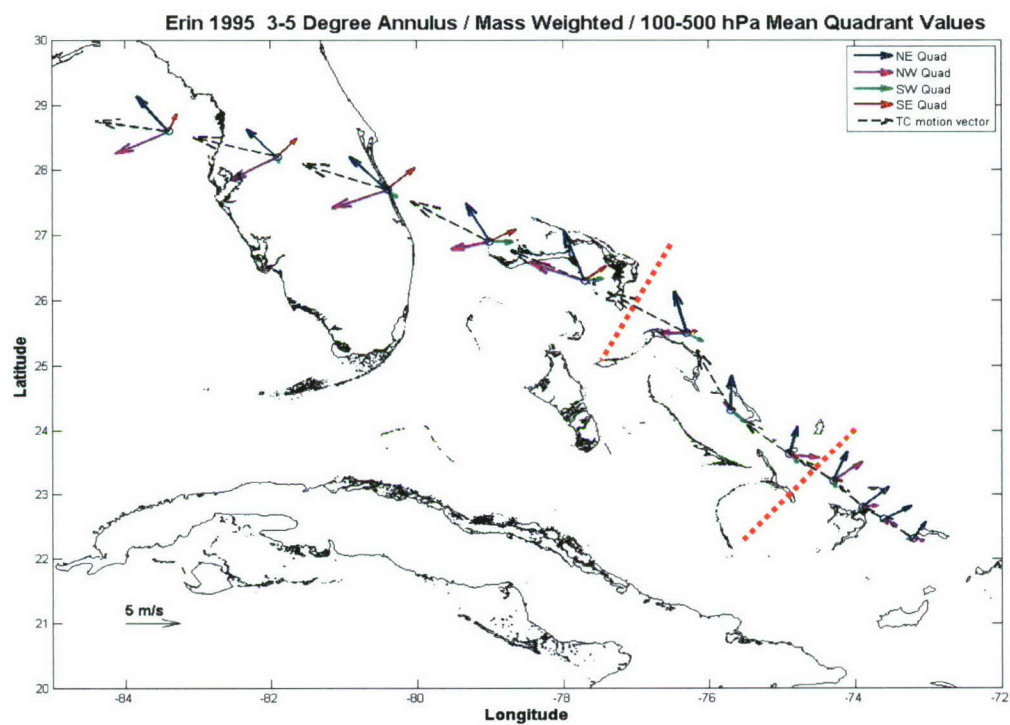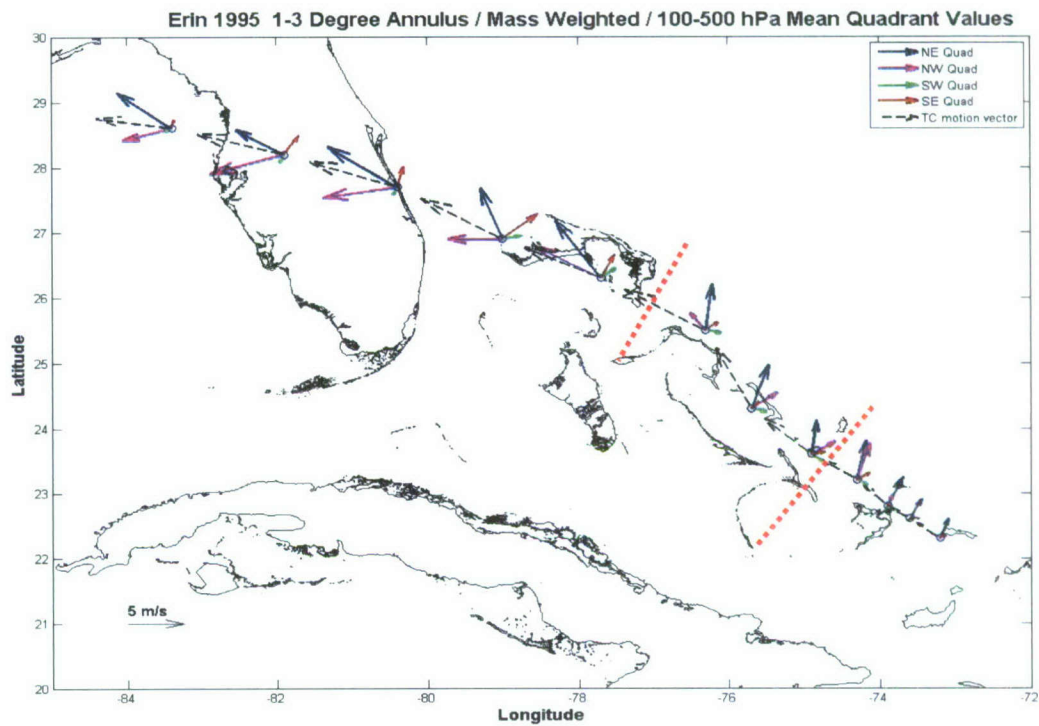
- 158 -
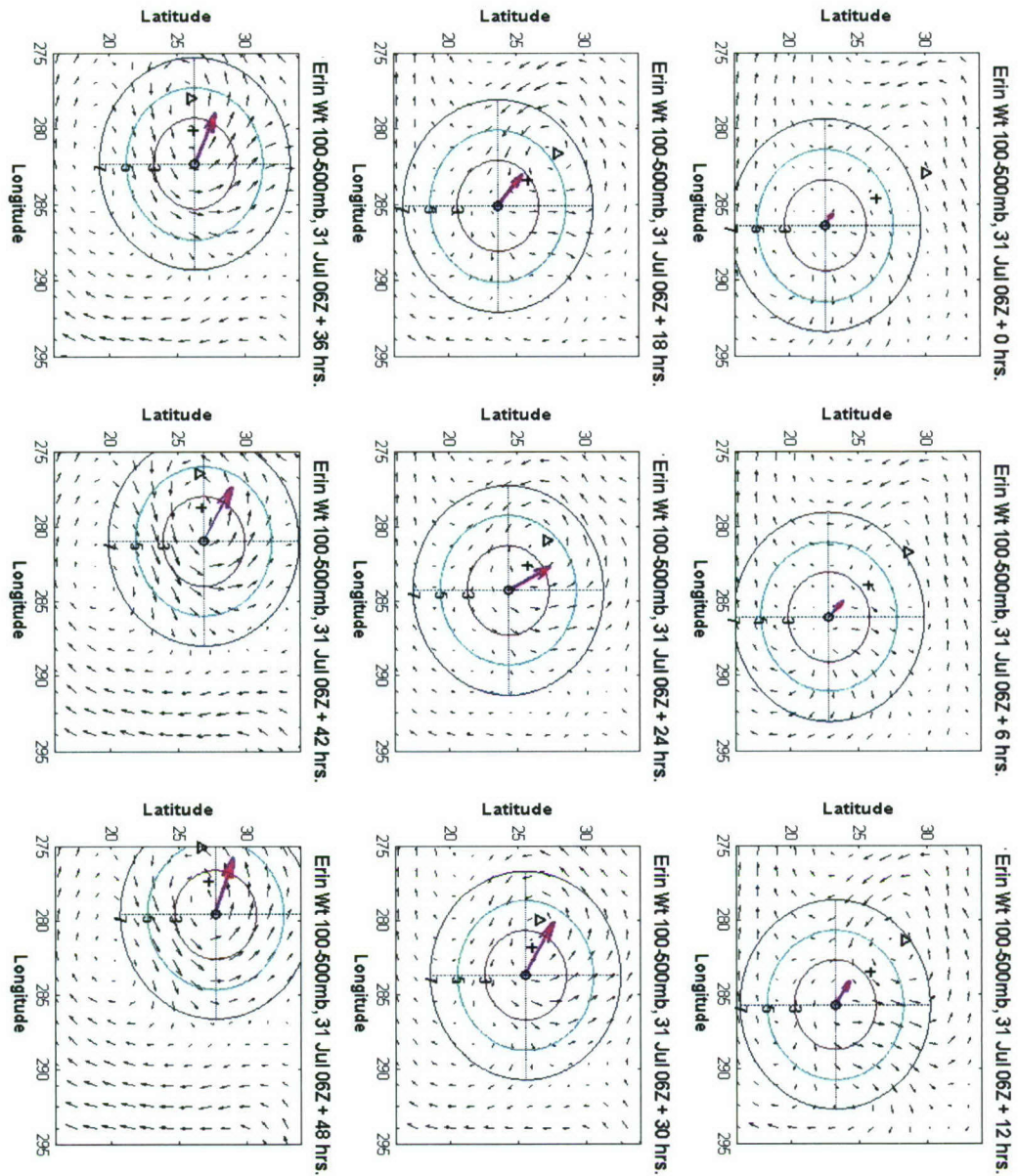
Figure 3.54   Erin's mass-weighted 100 hPa to 500 hPa (upper layer) wind fields at 6-hourly intervals for time steps around the interaction period starting 06Z 31 July 1995 (upper left when rotated) and ending 06Z 2 August 1995 (lower right when rotated). The "o" represents the NHC Best Track low-level center of Hurricane Erin. The "+" represents the centroid of the two circulations. The "Δ" represents the approximate 200 hPa TUTT cell center of circulations. The red, green and blue circles represent the approximate 3°, 5° and 7° radial bands and are divided into quadrants. The pink arrow represents the TC's trajectory. The interaction period began between 18Z 31 July (+12) and 00Z 1 August 1995 (+18) and ended 12Z-18Z 1 August 1995 (+30 - +36).

- 159 -

Erin 1995 5-7 degree annulus / mass weighted

Erin 1995 3-5 degree annulus / mass weighted

Erin 1995 1-3 degree annulus / mass weighted
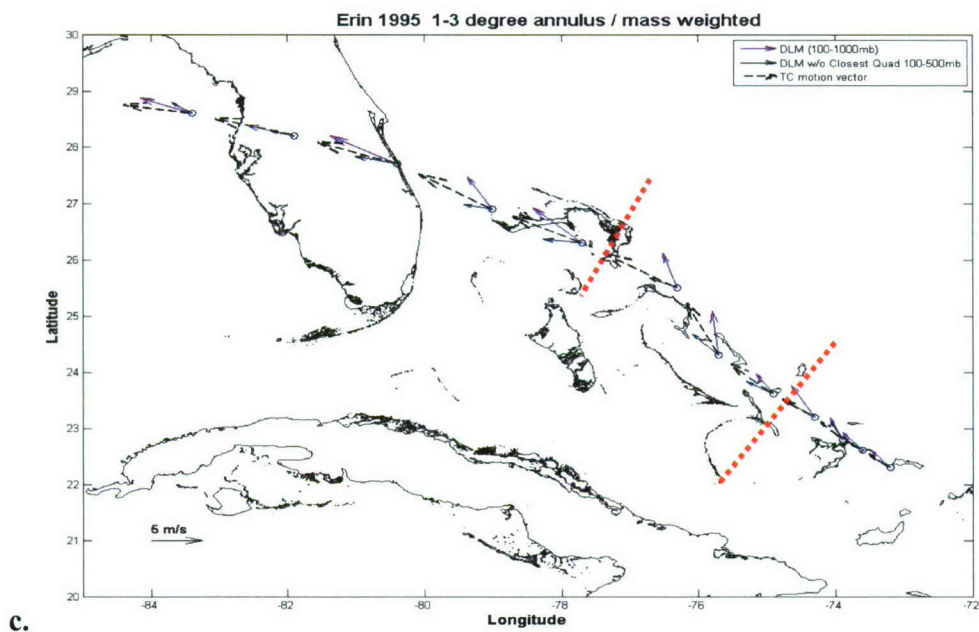
Figure 3.55 The original mass-weighted DLM and the new mass-weighted DLM with the upper layer quadrant closest to the TUTT cell removed for Erin. Vectors are scaled to the average speed of the TC between each 6 hourly time step. Vectors point in the mean radial direction for (a) the 5°-7° (b) the 3°-5° and (c) the 1°-3° radial bands.   The red dotted lines indicate the estimated start (between 18Z 31 July and 00Z 1 August 1995) and end (12-18Z 1 August 1995) points of the TUTT cell interaction period.
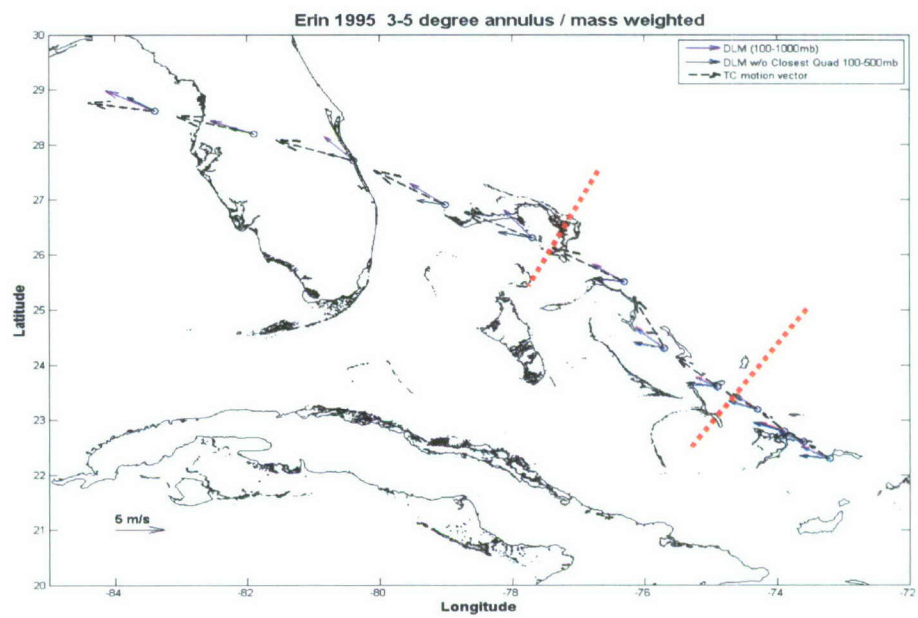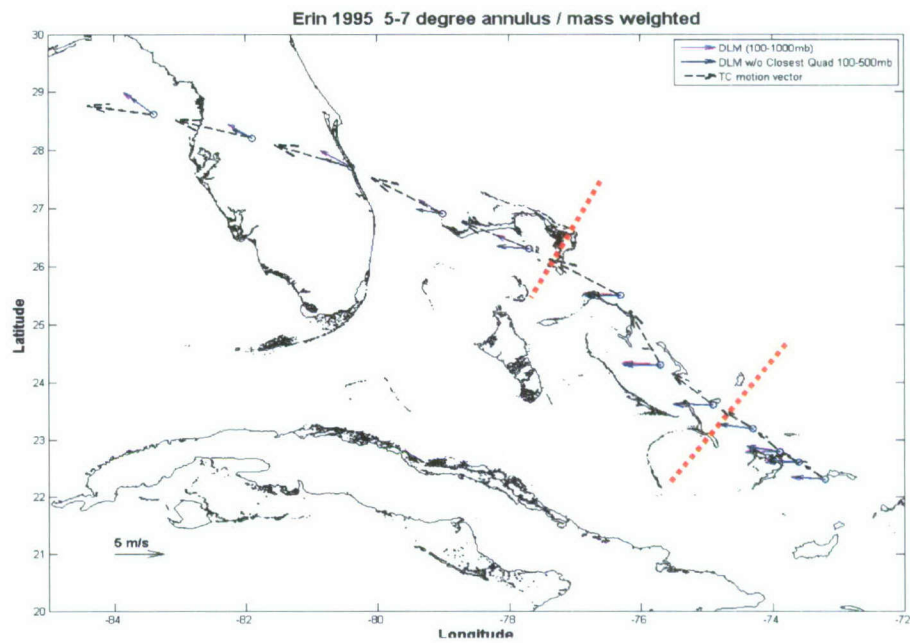
Case	Tracks	UW Centroid-Relative Motion

Rex2
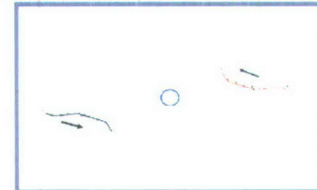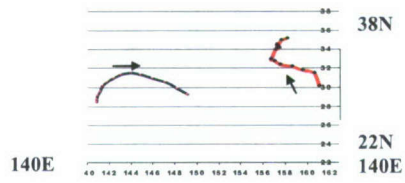
Babs
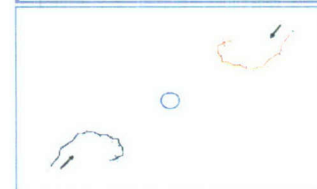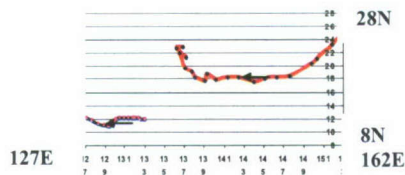
Rex1
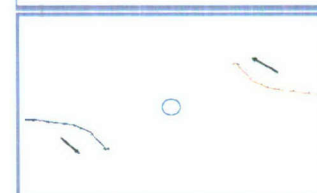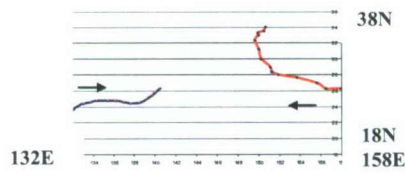
Ewiniar
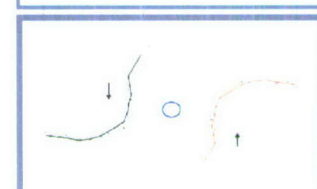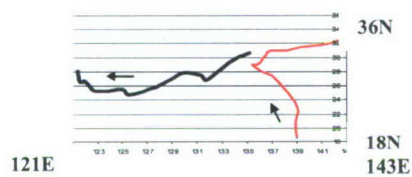
Bolaven

Amber

Fred

Saomai

- 162 -

Case	Tracks	UW Centroid-Relative Motion

Bart

Polly

Erin
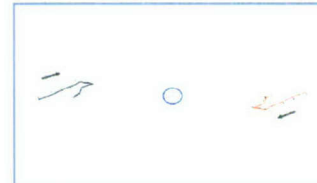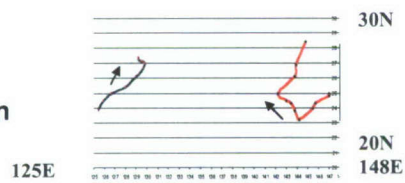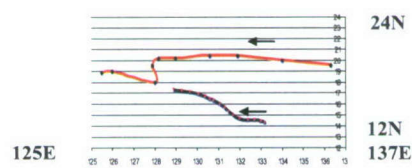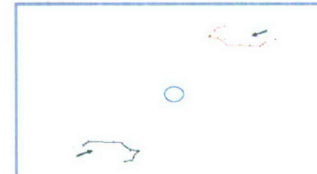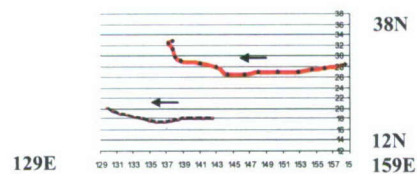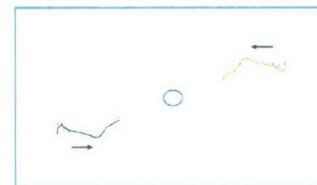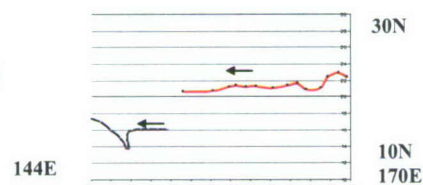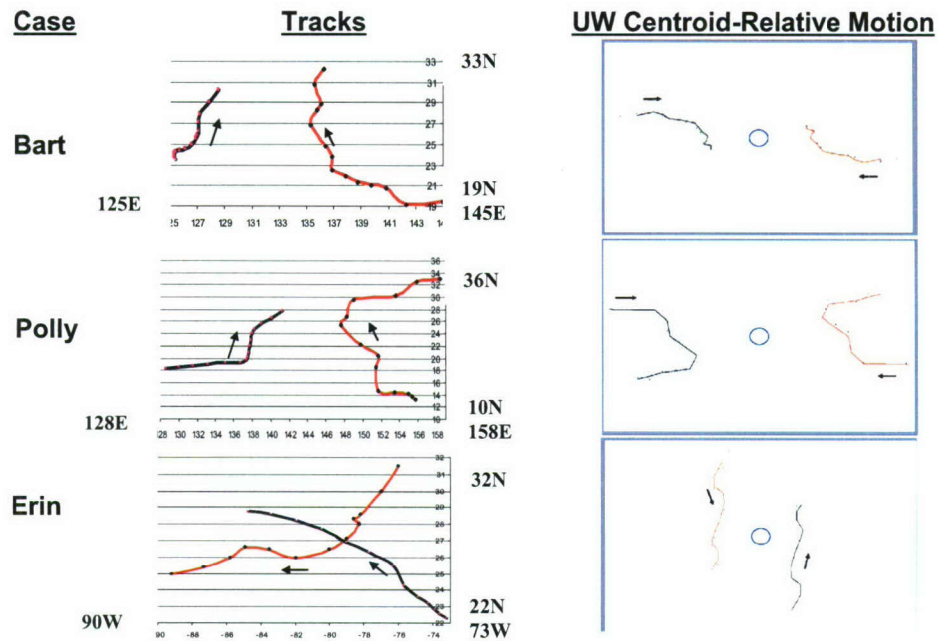
Figure 4.1 Actual TC and TUTT cell tracks (left side) and their unweighted centroid-relative motion depictions (right side) for all case's TC (blue) and associated TUTT cell (red) where 6-hourly time steps are equal. The latitudinal and longitudinal extremes of each case's domain are listed at the sides of each "tracks" image. Notice the anticyclonic unweighted centroid relative motion early on in TCs Bolaven, Fred and Saomai.

Rex1 25 Aug 98 at 06Z   200 hPa Wind Field

a.

Ty Rex1 26 Aug 98 at 06Z   200 hPa Wind Field
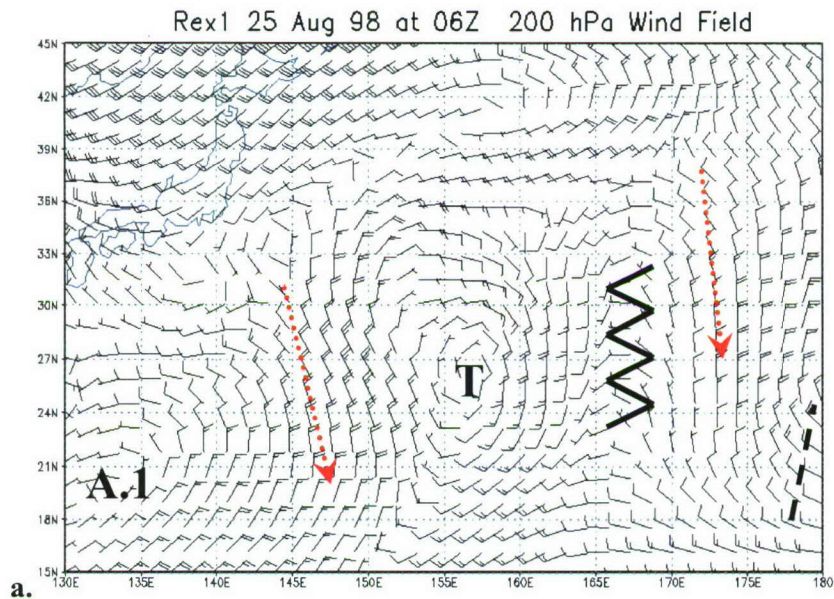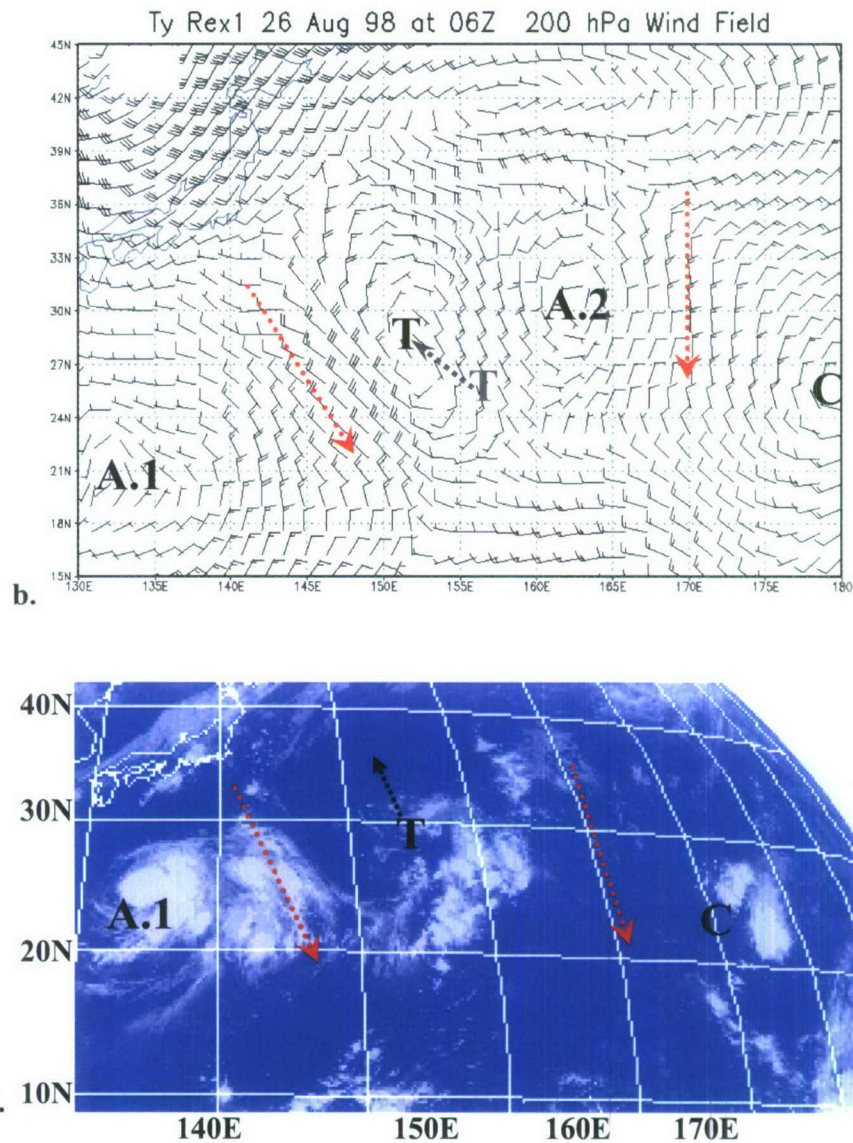
Figure 4.2 200 hPa wind field analysis for the TUTT cell associated with Rex1 at (a) 06Z 25 August and 24 hours later at (b) 06Z 26 August 1998. The "T" represents the approximate 200 hPa TUTT cell center of circulation and the grey "T" the previous position. The "A" and "C" marks represent the approximate center of nearby upper tropospheric anticyclones and cyclones, respectively, and are numbered to help identify between images. For example, A.1 is the anticyclone associated with the TC. The zig-zag line represents ridging while the dashed line represents a trough. The red dotted lines indicated general direction of flow to either side of the TUTT cell. A full wind barb equals 5 m s⁻¹. A half barb equals 2.5 m s⁻¹. (c) A GMS-5 infrared satellite image at 18Z 25 August 1998 (between the a. and b. dates/times) with the same annotation and approximate centers for each circulation. Even though the environmental flow at 200 hPa around the TUTT cell is predominantly toward the south, the cell propagates northward. It would appear the induced ridge and eventual closed upper tropospheric anticyclone helped in this steering.
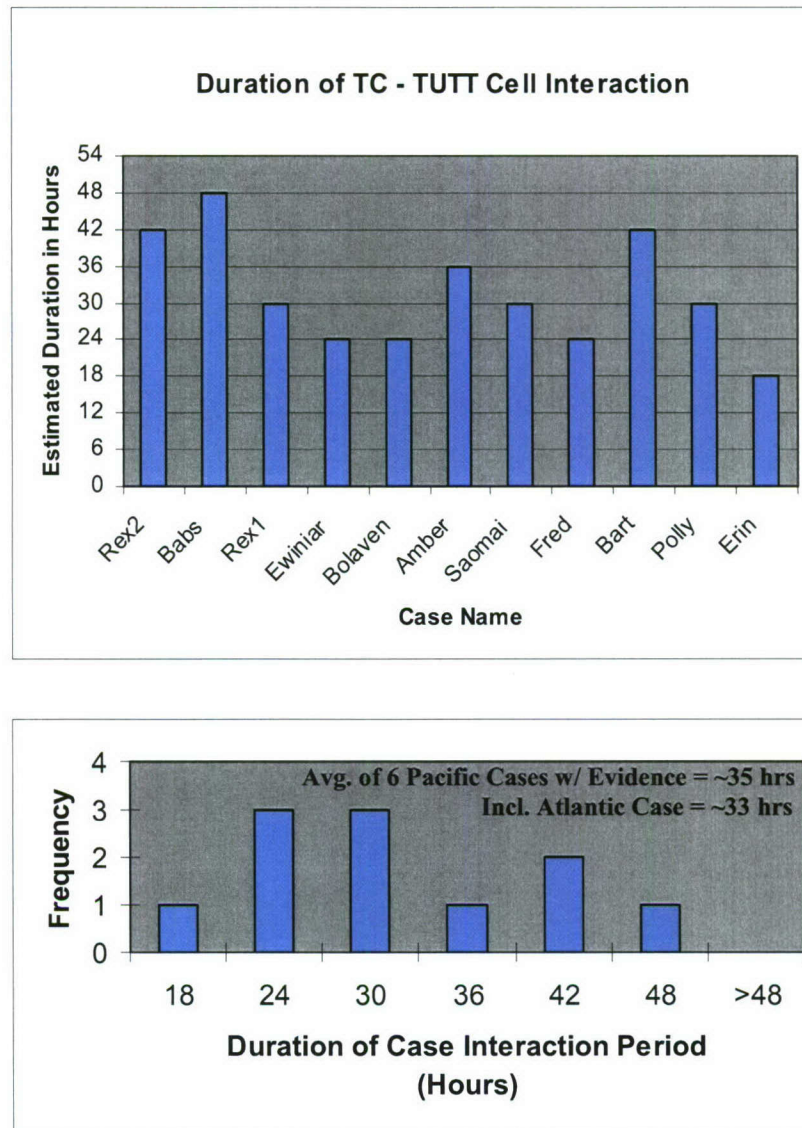
Figure 4.3 A bar graph (top) and histogram (bottom) representing the estimated TC – TUTT cell interaction period for each case, including Hurricane Erin from the Atlantic. Averages are provided in the upper right of the lower histogram.
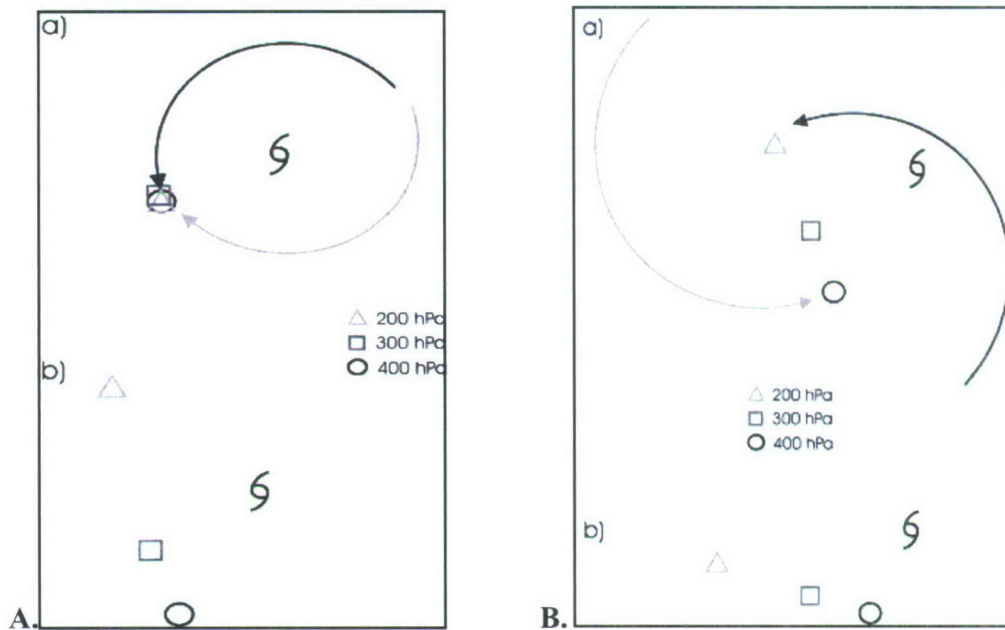
Figure 4.4 A.) From KE02, a schematic illustrating the stretching process. Three centers of the upper-level low are indicated by a triangle (200 hPa), square (300 hPa), and circle (400 hPa). The center of the vortex is indicated by a tropical cyclone symbol. The light arrow indicates the hurricane's anticyclonic outflow, the darker arrow corresponds to the lower-level cyclonic hurricane circulation. (a) The initially vertically stacked upper-level low located to the southwest of the vortex, and (b) after some time, the hurricane circulations stretch the upper-level low.   **B.)** A schematic illustrating the rotation process. The dark arrow indicates the cyclonic flow around the lower center of the low, the lighter arrow corresponds to the cyclonic flow around the upper center of the low. (a) The initially north–south-oriented upper-level low, and (b) after some time, the low has rotated counter-clockwise to a more east–west-oriented position.
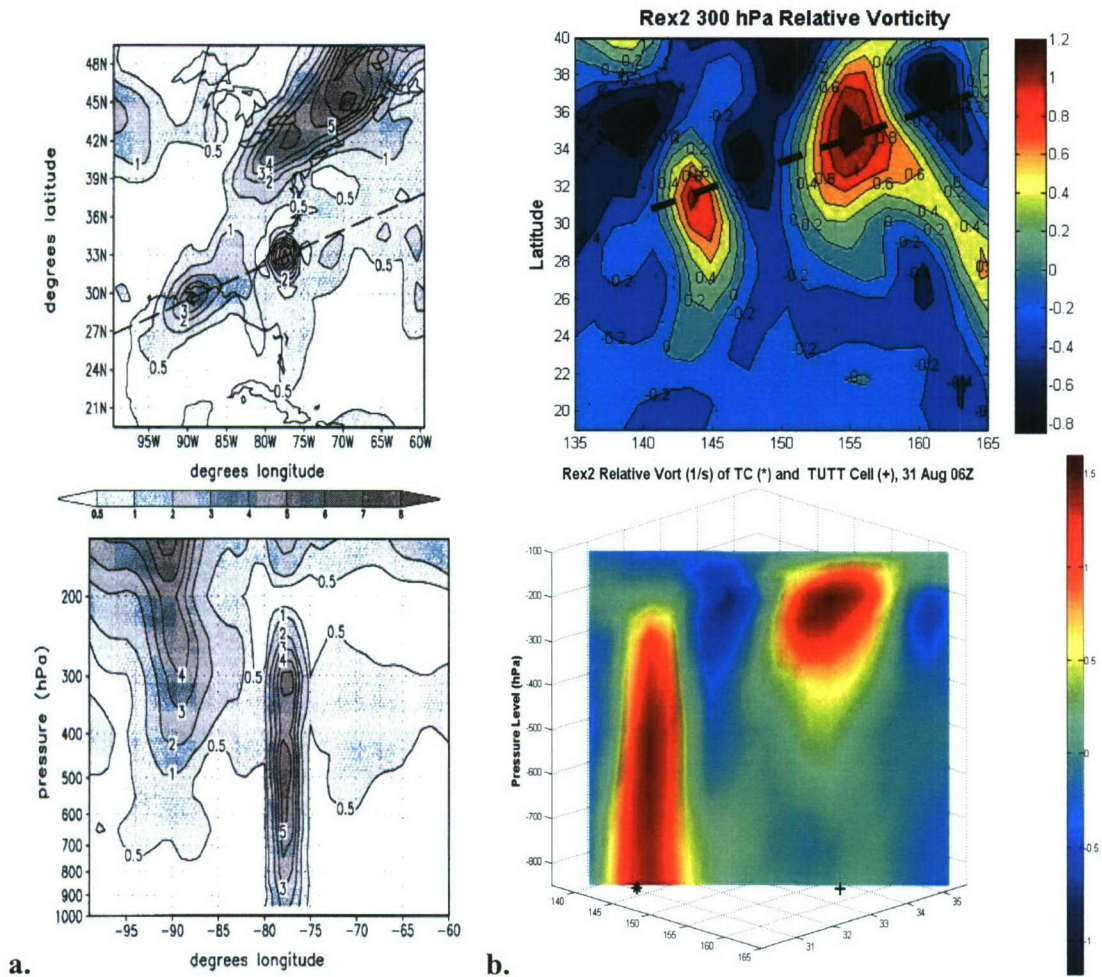
Figure 4.5 (a) From KE02, the 300 hPa PV (in PVUs) field of Hurricane Dennis and an upper-level low to its southwest at 06Z 30 August 1999 at 300 hPa (upper). A vertical cross- section (lower) follows along the dashed line shown in the upper. (b) As in (a) except for Rex2 and the associated TUTT cell's relative vorticity (s⁻¹) at 06Z 31 August 1998. The TUTT cell is to the east-northeast of the Ty Rex2, the reverse of KE02's case.

Rex2 TUTT Cell and TC Center Positions
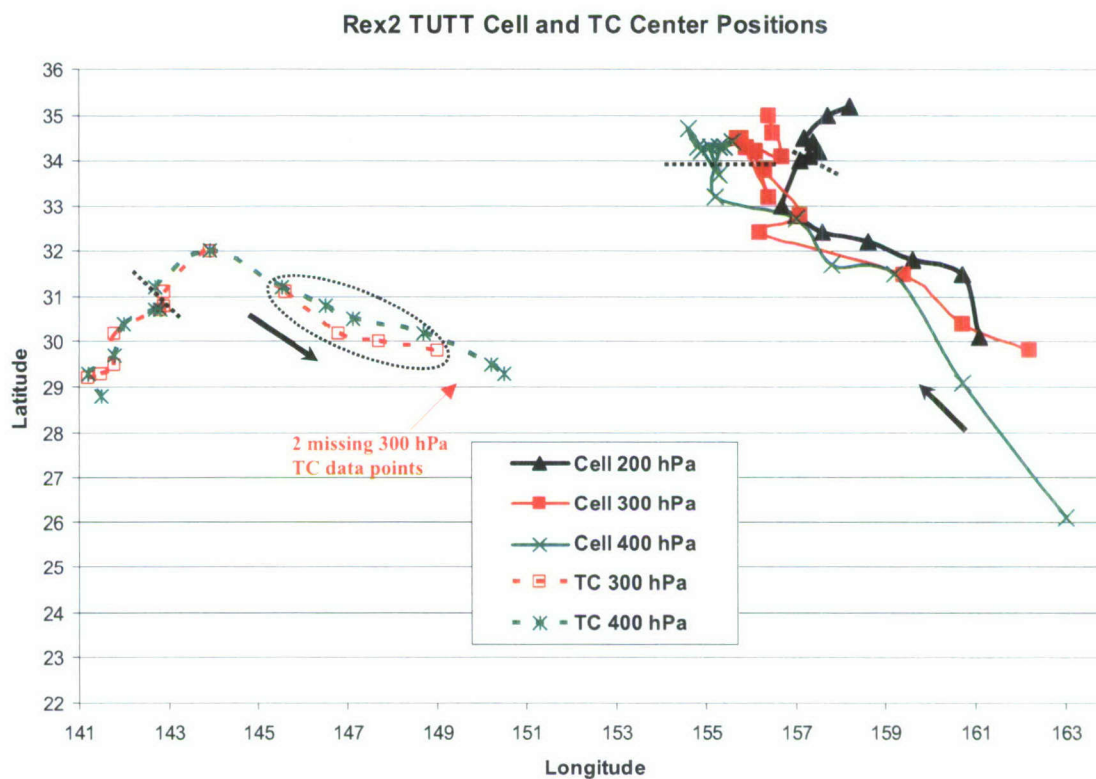
Figure 4.6 Graphic of circulation centers for Rex2 (300 and 400 hPa) and TUTT cell (200, 300 and 400 hPa) for 36 hours prior to the interaction and for 36 hours into the interaction period. The black dotted lines indicate the interaction start points. Arrows indicate general direction of circulation motion. Each time step is separated by 6 hours and is evenly matched between the two circulations except for TC at 300 hPa where the last two time steps are missing (no closed circulation). The dotted black oval indicates the area of disconnect between the TC's 300 hPa and 400 hPa circulation centers in the ERA-40 data set.

SCENARIO 1
CELL DIRECTLY AHEAD
Guidance: Bias to right of ensemble. No speed bias.

TUTT Cell (200mb)

SCENARIO 2
CELL AHEAD AND TO RIGHT
Guidance: Bias to the right of ensemble with a slower speed bias.

TUTT Cell (200mb)

SCENARIO 3
CELL TO RIGHT
Guidance: Bias to the left of ensemble with a slower speed bias.

TUTT Cell (200mb)

SCENARIO 4
CELL AHEAD AND TO LEFT
Guidance: Bias to the right of ensemble with a faster speed bias.

TUTT Cell (200mb)

SCENARIO 5
CELL TO LEFT
Guidance: Bias to the left of ensemble with a faster speed bias.

TUTT Cell (200mb)

JTWC TDO QUESTIONS (values +/- ~10%)

1. Is the 200 mb TUTT cell center within 900 nm (~15°) of the TC? **Y / N**

2. Is the TC and TUTT cell separation distance decreasing? **Y / N**
Expect decreasing influence as separation distance begins to increase.

3. Is the TUTT cell's 200 mb winds field (> 25 kts) within 430 nm (~7°) of the TC's center? *(use satellite winds, model analysis)* **Y / N**

4. Has the TUTT cell maintained* a maximum 200 mb intensity of either:
   4a. Potential Vorticity $\geq$ 2.5 PVUs (3 x 10-6 m^2 K s^{-1} kg^{-1}) or
   4b. Relative Vorticity $\geq$ 11 x 10-5 s^{-1} ? **Y / N**
Monitor 200 mb analysis every 6-hours to maintain continuity

5. Has the TUTT cell had a *closed* circulation at or below 400 mb? **Y / N**
6. Is the TC at tropical storm intensity* or greater? **Y / N**

If an interaction is believed to be already occurring, go directly to the section below. If not and you answered "N" to *any* of the Y / N questions, there is *currently* a low likelihood the TUTT cell will have a significant influence on the TC's motion. Note: *The influence of other environmental features on TC motion must also be considered. Guidance is based the orientation of the two circulations at each independent time step of forecast development, from the analysis time forward to each forecast DTG. Adjust the scenarios accordingly based on forecast motion and orientation of both circulations.*

REFERS TO SCENARIO SECTION
Which scenario (1-5) best describes the orientation between your TC and the TUTT cell? (Ensemble = Model Ensemble) **1 - 6** → ____

Forecast Adjustment: Scenarios depict the general orientation between the two circulations relative to the TC. Examples are provided. The suggested forecast track bias is indicated within the Model Ensemble field (trapezoid). Green (G) areas represents a likely bias of the TC's forecast track and the red (R) an unlikely bias. The forecaster is urged to bias (i.e. nudge) their forecast TC track towards the green areas during the expected interaction period once the initial forecast (which excluded this guidance) is completed. Reconsider the scenario and associated track bias at each forecast time step.

Persistence: Once an expected bias in TC motion occurs, consider greater persistence (e.g., 12-24 hours) application during the next 24 hour of forecasts. Afterwards, reduce the weight of persistence back to normal.

Figure 5.1 Conceptual model designed for *operational* guidance at the JTWC. The forecaster initially analyzes the available fields, answers the questions on the upper right in units used by forecasters and decides whether an interaction is likely. If likely, the forecaster then identifies a similar scenario and applies the recommended TC track and persistence biases. The influence of other TC environmental features must also be incorporated into the decision making process.

REFERENCES

Brand, S., 1970: Interaction of binary tropical cyclones of the western north Pacific ocean. *J. Applied. Met.*, **9**, 433-441.

Carr, L. E. and R. L. Elsberry, 1990: Observational evidence for predictions of tropical cyclone propagation relative to environmental steering. *J. Atmos. Sci.*, **47**,542-548.

_____, and _____, 1994: Systematic and integrated approach to tropical cyclone track forecasting. Part I. Approach overview and description of meteorological basis. Tech. Rep. NPS-MR-94-002, Naval Postgraduate School, Monterey, CA, 273 pp. [Available from Naval Postgraduate School, Monterey, CA 93943-5114.].

_____, and _____, 1998: Objective diagnosis of binary tropical cyclone interactions for the western north Pacific basin. *Mon. Wea. Rev.*, **126**, 1734-1740.

_____, and _____, 2000a: Dynamical tropical cyclone track forecast errors. Part I: Tropical region error sources, *Wea. and Forecasting*, **15**, 641-661.

_____, and _____, 2000b: Dynamical tropical cyclone track forecast errors. Part II: Midlatitude circulation influences, *Wea. and Forecasting*,**15**, 662-681.

Carr, L.E., M. Boothe, and R. Elsberry, 1997: Observational evidence for alternative modes of track-altering binary tropical cyclone scenarios. *Mon. Wea. Rev.*, **125**, 2094-2111.

Chen, G., and L. F. Chou, 1994: An investigation of cold vortices in the upper troposphere over the western north Pacific during the warm season. *Mon. Wea. Rev.*, **122**, 1436-1448.

Chan, J. C. L., and R.T. Williams, 1987: Numerical studies of the beta effect in tropical cyclone motion. Part I: Zero mean flow. *J. Atmos. Sci.*, **44**, 1257-1265.

Chan, J. C. L., and R. H. F. Kwok, 1999: Tropical Cyclone Genesis in a Global Numerical Weather Prediction Model. *Mon. Wea. Rev.*, **127**, 611-624.

Chan, J. C. L., F. M. F. Ko and Y. M. Lei, 2002: Relationship between potential vorticity tendency and tropical cyclone motion. *J. Atmos. Sci.*, **59,** 1317-1336.

Chen, S., J. Knaff and F. Marks, 2006: Effects of Vertical Wind Shear and Storm Motion on Tropical Cyclone Rainfall Asymmetries Deduced from TRMM. *Mon. Wea. Rev.*, **134**, 3190-3207.

DeMaria, M, J.J. Baik and K. Kaplan, 1993: Upper-Level Eddy Angualr Momentum Fluxes and Tropical Cyclone Intensity Change. *J. Atmos. Sci.*, **50**, 1133–1147.

Dong, K. and C.J. Neumann, 1983: On the relative motion of binary tropical cyclones. *Mon. Wea. Rev.*, **111**, 945-953.

_____, and _____, 1986: The relationship between tropical cyclone motion and environmental geostrophic flows. *Mon. Wea. Rev.*, **114**, 115-122.

Eliassen, A., 1952: Slow thermally or frictionally controlled meridional circulation in a circular vortex. *Astrophys. Norv.*, **5**, 19-60.

Elsberry, R. L., 1995: Tropical cyclone motion. Global perspectives on tropical cyclones, R. L. Elsberry, Ed., WMO/TD-No. **693**, World Meteorological Organization, 106–197.

Figueroa, A. R., 2003: Environmental steering flow model analysis on central north Pacific tropical cyclones. M.S. thesis, Dept. of Meteorology, Univ. of Hawaii. 93 pp.

Fiorino, M., and R.L. Elsberry, 1989: Some aspects of vortex structure related to tropical cyclone motion. *J. Atmos. Sci.*, **46**, 975-990.

Fitzpatrick, P. J., J.A. Knaff, C.W. Landsea and S.V. Finley, 1995: Documentation of a systematic bias in the Aviation Model's forecast of the Atlantic tropical upper-tropospheric trough: Implications for tropical cyclone forecasting, *Wea. and Forecasting*, **10**, 433-446.

Flatau, M., W. Schubert and D. Stevens, 1994: The Role of Baroclinic Processes in Tropical Cyclone Motion: The Influence of Vertical Tilt. *J. Atmos. Sci.*, **51**, 2589-2601.

Frank, W. M., 1977b: The structure and energetics of the tropical cyclone II. Dynamics and energetics, *Mon. Wea. Rev.*, **105**, 1136-1150.

_____, 1977a: The structure and energetics of the tropical cyclone I. Storm structure, *Mon. Wea. Rev.*, **105**, 1119-1135.

Franklin, J.L., 1990: Dropwindsonde observations of the environmental flow of hurricane Josephine (1984): Relationship to vortex motion. Mon. Wea. Rev., 118, 2732-2744.

_____ 2006: 2005 National Hurricane Center Forecast Verification Report. NOAA/NWS/NCEP/Tropical Prediction Center report, 52 pp.

Fujiwhara, S., 1923: On the Growth and Decay of Vortical Systems. *Quart. J. Roy Meteor. Soc.*, **49**, 75-104.

George, J.E. and W.M. Gray, 1976: Tropical cyclone motion and surrounding parameter relationships. *J. Appl. Meteor.*, **15**, 1252-1264.

Hanley, D., J. Molinari, and D. Keyser, 2001: A composite study of the interactions between tropical cyclones and upper-tropospheric troughs. *Mon. Wea. Rev.*, **129**, 2570-2584.

Haurwitz, B., 1935: The height of tropical cyclones and the "eye" of the storm. *Mon. Wea. Rev.*, **63**, 45-49.

Hodanish, S., and W. M. Gray, 1993: An observational analysis of tropical cyclone recurvature. *Mon. Wea. Rev.,* **121,** 2665–2689.

Hogan, T.F., M.S. Peng, J.A. Ridout, and W.M. Clune, 2002: A description of the impact of changes to NOGAPS convection parameterization and the increase in resolution to T239L30. NRL Memorandum Report (NRL/MR/7530-02-52), 10 pp.

Holland, G. J., 1983: Tropical cyclone motion: Environmental interaction plus a beta effect, *J. Atmos. Sci*, **40**, 328-342.

_____, 1984: Tropical cyclone motion: A comparison of theory and observation. *J. Atmos. Sci.*, **41**, 68-75.

_____, and M. Lander, 1993: The meandering nature of tropical cyclone tracks. *J. Atmos. Sci.*, **50**, 1254-1266.

____, and G.S. Dietachmayer, 1993: On the interaction of tropical-cyclone-scale vortices. III: Continuous barotropic vortices. *Quart. J. Roy. Meteor. Soc.*, **119**, 1381-1398.

JTWC, 1994: Annual Tropical Cyclone Report, U. S. Naval Oceanography Command Center, Guam, Mariana Islands. 108 pp

_____, 1996: Annual Tropical Cyclone Report, U. S. Naval Oceanography Command Center, Guam, Mariana Islands. 101 pp

_____, 1998: Annual Tropical Cyclone Report, U. S. Naval Oceanography Command Center, Guam, Mariana Islands. 62 pp

_____, 1999: Annual Tropical Cyclone Report, U. S. Naval Oceanography Command Center, Guam, Mariana Islands. 63 pp

Kasahara, A., 1960: The numerical prediction of hurricane movement with two-level baroclinic model. *J. Meteor.*, **17**, 357-370.

Kelley, W. E., and D. Mock, 1982: A diagnostic study of upper tropospheric cold lows over the western north Pacific, *Mon. Wea. Rev.*, **110**, 471-480.

Kimball, S. K. and J. L. Evans, 2002: Idealized numerical simulations of hurricane-trough interaction. *Mon. Wea. Rev.*, **130**, 2210-2227.

Koteswaram, P., 1967: On the structure of hurricanes in the upper troposphere and lower stratosphere. *Mon. Wea. Rev.*, **95**, 541.564.

Lander, M.A. and G.J. Holland, 1993: On the interaction of tropical-cyclone-scale vorticies, I: Observations. *Quart. J. Roy. Meteor. Soc.*, **119**, 1347-1361.

Li, X and B. Wang, 1993: Barotropic Dynamics of the Beta Gyres and Beta Drift. J. Atmos. Sci., **51**, 746-756.

Merrill, R.T., 1988: Environmental Influence on Hurricane Intensification. *J. Atmos. Sci.*, **45**, 1678-1687.

Molinari, J., S. Skubis, and D. Vollaro, 1995: External influences on hurricane intensity: Part III. Potential vorticity structure. *J. Atmos. Sci.,* **52,** 3593-3606.

_____, S. Skubis, D. Vollaro, and F. Alsheimer, 1998: Potential Vorticity Analysis of Tropical Cyclone Intensification. *J. Atmos. Sci.*, **55**, 2632-2644.

Neumann, C. J., 1979: On the use of deep-layer-mean geopotential height fields in statistical prediction of tropical cyclone motion. *6th Conference on Probability and Statistics in Atmospheric Sciences. Amer. Meteor. Soc.*, Boston, 32-38.

_____, 1992: Final report, Joint Typhoon Warning Center (JTWC92) Model. SAIC Contract Rep. N 00014-90-C-6042 (Part 2), 83 pp.

Nieto F. R., and W. H. Schubert, 1999: On the role of tropical cyclones in the formation of tropical upper tropospheric troughs. *J. Atmos. Sci.*, **56**, 2891-2907.

Pike, A., 1985: Geopotential heights and thicknesses as predictors of Atlantic tropical cyclone motion and intensity. *Mon. Wea. Rev.*, **113**, 931-939.

Prieto, R., et al., 2003: A classification of binary tropical cyclone-like vortex interactions. *Mon. Wea. Rev.*, **131**, 2656-2666.

Ramage, C. S., 1959: Hurricane Development. *J. of Meteor.*, **16**, 227-237.

Ritchie, E. A. and G.J. Holland, 1993: On the interaction of tropical-cyclone-scale vorticies, II: Discrete vortex patches. *Quart. J. Roy. Meteor. Soc.*, **119**, 1363-1379.

Sadler, J. C., 1967: The tropical upper tropospheric trough as a secondary source of typhoons and primary source of trade wind disturbances. Final Report, Contract No. AF 19(628)-3860, Hawaii Institute of Geophysics, Report 67-12. 44 pp.

_____, 1975: The Upper Tropospheric Circulation Over the Global Tropics. Dept. of Meteorology, Univ. of Hawaii, UHMET-75-05.

_____, 1976: A role of the tropical upper tropospheric trough in early season typhoon development. *Mon. Wea. Rev.*, **104**, 1266- 1278.

_____, 1978: Mid-season typhoon development and intensity changes and the tropical upper tropospheric trough. *Mon. Wea. Rev.*, **106**, 1137–1152.

Sanders, F. and R.W. Burpee, 1968: Experiments in barotropic hurricane track forecasting. *J. Appl. Meteor*, **7**, 313-323.

Thorncroft, C.D., B.J. Hoskins, and M.E. McIntyre, 1993: Two paradigms of baroclinic-wave lifecycle behavior. *Q. J. Roy. Meteor. Soc.*, **119**, 17-55.

UCAR-DSS, cited 2006: ERA40 T85 analysis fields on pressure surfaces, created at NCAR. [Available online at *http://dss.ucar.edu/datasets/ds124.1/*]

Uppala, S. M. et al, 2005: The ERA-40 re-analysis. *Quart. J. R. Met. Soc.*, **131**, 2961-3012.

Velden, C.S., and L.M. Leslie, 1991: The basic relationship between tropical cyclone intensity and the depth of the environmental steering layer in the Australian region. *Wea. and Forecasting*, **6**, 244-253.

Wang, B., and X. Li, 1992: The beta-drift of three dimensional vortices: A numerical study. *Mon. Wea. Rev.*, **120**, 579-593.

Wang, Y, and G.J. Holland, 1995: On the interaction of tropical-cyclone-scale vortices, IV: Baroclinic vortices. *Quart. J. Roy. Meteor. Soc.*, **121**, 95-126.

Wang, Y, and G.J. Holland, 1996: The beta drift of Baroclinic vortices, Part I: Adiabatic Vortices. *J. Atmos. Sci.*, **53**, 411-423.

Wang, Y, and G.J. Holland, 1996: The beta drift of Baroclinic vortices, Part II: Diabatic Vortices. *J. Atmos. Sci.*, **53**, 3737-3755.

Weatherford C.L., and W.M. Gray, 1988: Typhoon structure as revealed by aircraft reconnaissance. Part I: Data analysis and climatology. *Mon. Weathar Rev.* **116**.1032–43.

Whitfield, M. B, and S. W. Lyons, 1992: An upper-tropospheric low over Texas during summer, *Wea. and Forecasting*, **7**, 89-106.

Willoughby, H. E., 1995: Mature structure and evolution. Global Perspectives on Tropical Cyclones, R. L. Elsberry, Ed., WMO/TD-No. **693**, World Meteorological Organization, 21–62.

Wong, M.L.M and J.C.L. Chan, 2004: Tropical cyclone intensity in vertical wind shear. *J. Atmos. Sci.*, **61**, 1859-1876.

Wu, C-C., and K. Emanuel, 1993: Interaction of a baroclinic vortex with background shear: Application to hurricane movement. *J. Atmos. Sci.*, **50**, 62-76.

_____, and Y. Kurihara, 1996: A numerical study of the feedback mechanisms of hurricane-environment interaction of hurricane movement from the potential vorticity perspective. *J. Atmos. Sci.*, **53**, 2264-2282.

_____, T.S. Huang, W.P,Huang, and K.H. Chou, 2003: A new look at the binary interaction: Potential vorticity diagnosis of the unusual southward movement of Tropical Storm Bopha (2000) and its interaction with Supertyphoon Saomai (2000). *Mon. Wea. Rev.*,**131**, 1289-1300.